1966

An investigation of the control of hydraulic fracturing through the inclusions of prefractures

William Joseph Kabeiseman

Department: Physics

AN INVESTIGATION OF THE CONTROL OF HYDRAULIC FRACTURING THROUGH THE INCLUSIONS OF PREFRACTURES

A dissertation

Presented to

the Faculty of the Graduate School

The University of Missouri

In Partial Fulfillment

of the Requirements for the Degree

Doctor of Philosophy

---

by

William Joseph Kabeiseman - 1933

July 1966

Doctor James J. Scott Dissertation Supervisor

ABSTRACT

Among the methods for determining the in-situ state of stress within the earth's crust, hydraulic fracturing has been and is receiving much attention. This method, in principle, measures stress directly with no delicate electronic equipment required nor knowledge of the elastic modulus of the material.

This dissertation investigates experimentally whether or not control of fracture orientation can be achieved by the introduction of circular and elliptical prefractures along with sand inclusions into cast hydrostone blocks which are hydraulically fractured. A mathematical model is presented and analytically solved for the stress condition associated with a circular crack containing fluid pressure with a superimposed biaxial or uniaxial confining load. An analysis and correlation is made between the experimental results and the mathematical expectations.

It is concluded that under restricted stress conditions, fracture orientation and control can be achieved; however, for a general state of stress, fracture orientation cannot be achieved such that the plane of the hydraulic fracture will turn so as to become perpendicular to the least compressive stress.

ACKNOWLEDGEMENTS

The author wishes to express his gratitude first to his wife and children, for without their patience and sacrifices this dissertation would not have been possible. He is especially indebted to Dr. James J. Scott, his dissertation supervisor, for his confidence, encouragement and guidance during the past two years. The writer wishes to acknowledge and express his thanks to the National Science Foundation for their Research Grant "NSF GP-3072" which provided financial assistance during the first year of this investigation and to Walter Lewis and John Chester of the United States Bureau of Mines in Minneapolis, Minnesota who were instrumental in the granting of the Bureau of Mines Research Fellowship which enabled the completion of the investigation. Thanks are given to Dr. George Clark and Professor Ralph Lee for their counsel and encouragement. A special thanks is given to Professor Sylvester Pagano for his critical reading and constructive criticism of the mathematical development.

TABLE OF CONTENTS

LIST OF TABLES

LIST OF FIGURES

LIST OF SYMBOLS

α, β, μ, ν = indices.

$\tau_{\alpha\beta}$ = shearing stresses.

σ_{α} = stresses.

τ_{o} = cohesive strength.

ϕ = coefficient of internal friction.

c = crack radius or length.

W = energy.

T = surface tension.

σ_{c} = critical stress.

ε = an increment.

σ_{m} = maximum stress.

ϕ, θ, ψ = angles.

P, Q, R = principal stresses.

σ_{t} = essential compressive stress.

S = uniaxial compressive strength.

G = modulus of rigidity.

ν = Poisson's ratio.

K_{p} = net tension.

P_{o} = internal pressure.

P_{i} = initiating pressure.

P_{f} = instantaneous shut in pressure.

ρ = density, ratio of radial displacement with crack radius.

g = gravitational attraction.

d = displacement.

X,Y,Z = cartesian coordinates.

PHC = circular prefracture.

PHE = elliptical prefracture.

PHS = sand inclusion.

HCZ = cylindrical zone.

psi = pounds per square inch.

c.c. = cubic centimeters.

$\Delta\sigma$ = stress difference.

r,ϕ,z = cylindrical coordinates.

$Z_\alpha^\beta, C_\alpha^\beta, S_\alpha^\beta$ = various Bessel combinations.

η = ratio of Y-displacement with crack radius.

$\vec{e}'_\alpha, \vec{e}''_\alpha$ = unit vectors in cylindrical coordinates.

$\vec{i},\vec{j},\vec{k}$ = unit vectors in rectangular cartesian coordinates.

$a_{\alpha\beta}$ = direction cosines.

S_1, S_2, S_3 = principal stresses.

$\Delta\theta$ = angular increment.

∇^2 = Laplacian operator in rectangular coordinates.

$\overline{\nabla}^2$ = Laplacian operator in cylindrical coordinates.

Θ = sum of the three normal components of stress.

Φ = arbitrary stress function.

$\lambda, \overline{G}$ = Lame constants.

J_ν = Bessel functions of order ν.

$\overline{f}(\S)$ = Hankel transform.

f = arbitrary function.

$G(\S,y)$ = zero order Hankel transform.

D = differential operator.

$\S$ = roots of auxillary equation, parameter.

A, B = arbitrary constants of integration.

R = a defined function of ρ and η.

E = Young's Modulus.

ζ, μ, p w = parameters.

u_x, u_y, u_z = displacements.

i = unit imaginary.

$\Gamma(m)$ = gamma function.

$p_\mu^\nu(z)$ = associated Legendre function.

CHAPTER I

INTRODUCTION

In the search for newer and better methods of stress determination in the earth's crust the technology of hydraulic fracturing has been and is receiving much attention. Although it has not yet been developed for stress determination, it appears to possess several important advantages when compared to the conventional methods of stress determination.

Most stress determination techniques are founded on the assumption that the rock is of an elastic nature. High stress concentrations develop at the wall around a hole the instant that it is created and produces inelastic deformation of the wall.

In hydraulic fracturing, depth is no limitation and the necessary equipment is already available in the petroleum industry. No delicate electronic equipment is required nor knowledge of the elastic modulus as the stresses are measured directly.

If hydraulic fracturing is to be a positive method of stress measurement several important areas of investigation must be made.

It is the purpose of this dissertation to investigate experimentally whether a fracture of prescribed orientation and shape can be initiated, extended and controlled by

hydraulic means and to present a mathematical model which describes this fracturing phenomena.

Hydrostone blocks were cast containing imbedded circular and elliptical prefractures along with blocks containing sand inclusions. These blocks were ground smooth and later subjected to an externally applied uniaxial or biaxial confining load and hydraulically fractured with a viscous oil. The nature and type of the fractured surfaces were noted and the breakdown pressures along with the fracture extension pressures recorded.

A mathematical model representing the experimental conditions is presented and solved with the aid of Hankel transforms. A number of selected interior points are chosen and stresses calculated from formulae developed from the mathematical model for the different loading conditions and fracturing pressures used in the experimental part of the investigation.

An analysis was made between the experimental results obtained and the corresponding theoretical expectations derived from the mathematical model given.

Several examples are given illustrating how a knowledge of the stress condition known at a point or region of the earth's crust might be used in the planning of a secondary oil recovery operation by means of hydraulic fracturing. Finally, conclusions and recommendations are given.

CHAPTER II

REVIEW OF LITERATURE

The problem of measuring stress in the earth's crust has become during recent years one of increasing interest to the mining, petroleum and civil engineers because it provides an earlier and more definite indication of ground-conditions than the measurement of rock displacement alone. The safety of mine excavations and the stability of massive structures which are being designed depend upon the properties and stresses in the rock. The magnitude and orientation of "in-situ" rock stresses can not in general be predicted theoretically and must therefore be determined in the final analysis by experimental means.

In the design of structures use is made of a "factor of safety" to compensate for a lack of knowledge which results in a waste of material and expenditures. In mining processes such as drilling, blasting, and comminution the "factor of safety" is used again by applying an excess of energy in which it has been estimated that up to 1000 times more energy is used than is actually required.

The petroleum engineer is interested in the direction and magnitude of the earth's stress in order to design secondary oil recovery operations. In formations with low vertical permeability, vertical fractures are superior to horizontal fractures in their ability to increase oil and

gas production; in other cases, horizontal fractures are to be preferred.

Governmental agencies have become interested in stress distribution associated with subsurface structures in relation to missile launching sites, underground shelters in case of nuclear attack, disposal of waste radio-active products deep within the earth's crust and subsurface nuclear detonations.

Fracture Theory

The term "fracture" denotes complete destruction of the cohesion of the material, resulting in the separation of a continuous body into two or more parts. Such separation is induced by the presence and secondary effects of the stresses which are generally classified as either shear fracture or tension fracture.

Shear fracture refers to separation resulting from the action of shear stresses, and it develops along the shear plane or shear trajectory; tension fracture or cleavage fracture refers to the fracture resulting from normal or tensile stress. These fractures can often be distinguished by the appearance of their fracture surfaces; the fracture surface due to tension always appears bright and granular, whereas the surface separated by shear gives the appearance of rough abrasion.

The criteria for failure of a material are established from the stress-strain relationship obtained from uniaxial tension and compression tests. During the last two centuries

a number of theories have been introduced to predict the condition of failure of a material under a given set of combined stresses. However, the failure or fracture phenomena of both ductile and brittle materials have not been clearly understood, these theories do not give an accurate method for determining to which type of failure the theories should be referred. All theories are based on the assumption that a material is homogeneous, isotropic, and follows Hooke's law. Some of the more interesting theories in historical order are:

1. Maximum stress theory
2. Maximum shear-stress theory
3. Maximum strain theory
4. Mohr's theory of failure
5. Theory of maximum distortion energy
6. Griffith's theory of rupture.

The validity of these theories has been discussed by Silverman (45)[1]. With the exception of Mohr's and Griffith's theories, the above theories are restricted to ductile materials whose strength in tension is the same as in compression.

Mohr's Theory. Mohr states that a material will fail either through plastic slip or by fracture when either (1) the shearing stress τ in the plane of slip has increased to

---

[1] A number in parenthesis and underlined refers to a number in the Bibliography.

a certain value or (2) the maximum tensile normal stress reaches a limiting value, these being dependent upon the properties of material.

In a general state of stress, Mohr's theory postulates that the intermediate stress has no influence on the failure such that it is sufficient to consider only the major principal stresses corresponding to the maximum and minimum normal stresses in the graphical representation of the limiting state of stress at a point. The shearing stress in a plane of slip depends only on the values of these two normal stresses, which act on the same plane and is given by the relationship

$$(1) \quad \tau = f(\sigma)$$

In the practical case the slope of the envelope is often assumed to be a straight line determined by the circles for uniaxial tension and compression. For brittle materials, the enveloping curve inclines to the σ axis and can be approximated by the equation

$$(2) \quad \tau = \tau_o + \sigma\tan(\phi)$$

where ϕ is the coefficient of internal friction and τ_o is the intersection of the envelope with the ordinate when the normal stress σ is zero and represents the cohesive strength of the material.

Because of the similarity of equation (2) to that given

by the Coulomb-theory, the theory of Mohr is modified to the so-called Coulomb-Mohr theory of failure.

The criterion of the Coulomb-Mohr theory is that fracture should occur when the shearing stress exceeds the sum of the cohesive resistance of the material and the friction resistance on the slip plane $\sigma\tan(\phi)$.

In practice, modifications of the theory are required to improve its accuracy. A major deficiency of the theory is that it does not describe the fracture phenomena, such as crack propagation, which occurs simultaneously when brittle materials fail.

Griffith's Theory of Rupture. An elastic body under stress undergoes rupture by a process involving a continuous decrease in potential energy in the system. The condition for fracture is reached when the increase in surface energy, resulting from a small extension of an internal crack, is balanced by the release of elastic energy in the body surrounding the crack.

Griffith evaluated the amount of energy by which the elastic (potential) energy decreased in the formation of an elliptic hole of length 2c and the surface energy of the newly formed surfaces per unit thickness of the strip. The amount of energy in the system W decreases by the difference between the elastic energy and the surface energy. The elliptical crack will increase its length if the decrease in energy W with respect to the crack length c becomes

analytically a minimum, i.e.,

$$(3) \quad \frac{\partial W}{\partial c} = 0$$

which gives in the case of plane stress

$$(4) \quad \sigma = \sqrt{\frac{2ET}{\pi c}}$$

where σ is the average normal stress acting on the crack surface, T is the surface tension of the solid, and c is the crack length.

Hypothetically, equation (4) is the sufficient condition for an elastic crack to propagate in brittle materials on plane surfaces under uniaxial load (35). At fracture, σ becomes the critical stress, σ_c, which is considered the tensile strength of a material.

Griffith also showed that the stress at the tip of the crack approached the molecular cohesion or theoretical strength of materials. He obtained for the maximum stress, σ_m, at the tip of the crack to be

$$(5) \quad \sigma_m = 2\sigma\sqrt{\frac{c}{\varepsilon}}$$

where ε is the notch radius at the crack tip. Since ε is extremely small, the maximum stress at the tip approaches the theoretical strength when the crack propagates. Under uniaxial compression, Griffith postulated that a large tensile stress existed around the crack tip if the crack was inclined at an angle ψ with respect to the direction of load.

Finally, at rupture, if the angle of failure is orientated in a combined stress field where P and Q are the principal stresses, such that

$$(6) \quad \cos(2\psi) = -\frac{1}{2}\frac{P - Q}{P + Q}$$

then the "essential tensile" state of stress, as given by Orowan (35), occurs if $P > Q$, so that $P - Q > 0$ and $3P + Q > 0$, and the condition of fracture is

$$(7) \quad P = \sigma_t$$

and

$$(8) \quad \psi = 0$$

where σ_t is the ordinary uniaxial tensile strength.

The "essential compressive" state of stress (35) occurs if $P - Q > 0$ and $3P + Q < 0$, when the fracture condition is

$$(9) \quad (P - Q)^2 + 8\sigma_t(P + Q) = 0$$

In simple uniaxial compression, $P = 0$, and $Q < 0$, the fracture condition, equation (9), becomes

$$(10) \quad |Q| = 8\sigma_t = S$$

where S is the uniaxial compressive strength of the material.

Orowan (35) also pointed out that even if P and Q are both compressive, fracture can occur from the tensile stress produced at the tip of the crack by the shear stress τ_{PQ} resulting from P and Q provided that τ_{PQ} reached the value

given by

$$(11) \quad 2\tau_m^2 = \sum \frac{(P + Q)}{2}$$

In summary, some of the important conclusions involved in the Griffith theory are:

(1) The Griffith theory can predict the tensile strength of a brittle material, if, and only if, the critical crack length, the surface energy, and the modulus of elasticity are known.

(2) The Griffith theory is based on the case of a straight rectilinear crack in an elastic infinite body under the influence of a homogeneous stress field. The theory excludes the effects of plasticity in the system.

(3) The distribution of the stresses and the configuration of the crack near its ends are approximated. The maximum stress occurs at the tip of the crack and is infinite; this value of stress is of little physical significance in practice.

(4) Griffith's theory assumes no shear stress acting upon the initial crack surfaces such that the theory is not valid if a shear stress is so acting.

(5) The theory does not include the cause of the initial crack or the time effect in breaking; nor does it predict the path of crack propagation.

Starr (49) determined the relationship of the shear stress which caused the crack to spread by using Griffith's

analysis under a special condition. He assumed that the solid was subjected to a uniform external shear stress with requisite uniform shear over the surface of the crack. Thus, for a very thin crack, the shearing stress required to spread the crack is given by

$$(12) \quad \tau = \left[\frac{GT}{\pi c(1-\nu)}\right]^{\frac{1}{2}}$$

where G is the modulus of rigidity, T is the surface tension of the solid, c is the crack length, and ν is Poisson's ratio.

Some Methods of Determining Stress in Rock

"In-situ" measurement of stress is only possible through its effects. On this basis, investigators have tried to measure rock deformation associated with stress and from these deformation measurements determine the absolute value of the stress field.

To determine absolute stress by means of strain measurements it is necessary to completely relieve the stress at the point under consideration and to measure the strains associated with the relief of stress. From the theory of elasticity the stress may be computed from a knowledge of the relationship between stress and strain for the material. If a change in stress only is required, the principle of superposition permits the change in stress to be calculated from the strains which occured during the interval of interest.

Most of the methods used for the measurement of "in-situ"

stresses are based on the stress relieving principle and require underground access, usually a tunnel, mine roadway or bore hole. Also, in these methods, the determination of rock properties is necessary and are quite variable from one location to another.

The determination of the stresses on the surface of an underground excavation is a two-dimensional stress problem and strain measurements in three directions will give the required information. However, to determine the stresses within a rock body becomes a three-dimensional problem and six strain measurements will have to be made in order to obtain the necessary information.

Numerous experimental techniques have been developed over the last thirty years for the determination of "in-situ" stresses. Comprehensive analysis of the types of stress measuring devices and instruments in use today have been published in the literature (22), (25), (26). There is no single stress measuring technique that is the best under all circumstances; each instrument has capabilities, advantages and limitations which must be scrutinized carefully before a particular instrument is chosen. Also, the response of a device under realistic conditions must be known before a valid interpretation of the instrument readings in terms of actual rock stresses can be made.

Direct measurements of stress may be made by instruments incorporating electrical resistance strain gauges in their

construction. The use of these gauges depend upon the fact that certain alloys show a linear relationship between applied strain and electrical resistance, so that if a wire constructed from one of these alloys is fixed to the surface of an object subject to variable strain, the change of resistance in the wire will be a measure of the change of strain in the object.

Three distinct types of borehole strain measuring instruments have so far been developed. Leeman (25) classifies them as: (1) borehole deformation strain cells, (2) borehole inclusion stressmeters, (3) borehole strain gauge devices.

In the borehole deformation strain cells and the borehole inclusion stressmeters the stresses are determined by measuring changes in the dimensions of one or more diameters of a borehole by stress relieving the hole and using formulae developed by means of the theory of elasticity. In the borehole strain gauge devices the deformation of a rock core cut out from the bottom of the hole is directly measured by strain gauges secured onto the face at the bottom of the hole. The stresses are then calculated from the measured core deformation.

A method of determining stress in rock which is not based upon the measurement of strains in boreholes is the hydraulic jack method which measures the absolute stress by a stress relieving technique. Two types of hydraulic jacks

are in use today: (1) flat jacks (36), (38), and (2) curved jacks (22).

In the flat jack method a slot is cut in the rock nearby the point in which the stress is to be determined. A flat jack, a thin square or rectangular hydraulic-pressure cell, is cemented into the slot and pressure applied to the hydraulic fluid in the cell until the displacement created by cutting the slot is cancelled by the pressure in the flat jack. The pressure in the cell required to cancel this deformation in the rock is assumed to be equal to the stress in the rock before the slot was cut. To obtain the stresses in a biaxial field two flatjacks orientated at right angles are used.

Curved jacks (22) installed in boreholes are used to obtain more information than obtainable from flat jacks. A borehole is drilled to the depth at which it is desired to determine the rock stress and in a direction parallel to one of the principal stresses. Two curved jacks are fitted into the annular groove of the bore hole. The pressure in the jacks is raised to some value P and then overcored and the relief of pressure is noted due to the overcoring. Another pair of curved jacks is then inserted in the annular groove resulting from overcoring. The pressure P is restored in the first set of jacks and this procedure is repeated with the first set of jacks rotated through an angle of 90°. By using formulae derived from the theory of elasticity the stress may then be determined.

In the stress relief technique it is assumed that the stress relieved from overcoring is equal in magnitude to the stress in the in-situ rock but in opposite direction. Also, the rock is assumed to obey the laws for perfectly elastic, homogenous, isotropic media subject to plane stress or strain and that the values of the elastic constants can be accurately determined by laboratory methods. While in the flat jack method it is assumed that the strain or displacement produced by pressure in the flat jacks is equal in magnitude to that in the instrumented points which was caused by the cutting of the slot and the pressure in the cell is equal to the stress in the rock before the slot was cut.

The flat jack method has the advantage that the relationship between stress and strain in the rock need not be linear; however, the strain in the rock caused by making the slot must follow the same relationship as the strain caused by the pressure applied by the flat jack, whether this relationship is linear or not. Major disadvantages of the flat jack method is that it is very time consuming and is restricted essentially to the wall of the opening. The borehole stress-relief methods have the advantage that stress determination is relatively fast and can be used with relative ease up to 20 feet or more from the opening; however, the rock must core well, be reasonable elastic and cannot contain many defects.

The photostress method (41), (43) use the principles of

photoelasticity to determine changes in stress on the surface of a rock. The surface of the rock is made reflective to light either by polishing it or spraying it with a reflective paint and then coating it with a layer of special transparent photoelastic plastic. The surface is then illuminated with polarized light such that when the stress in the rock changes, the strain on the rock surface is transmitted to the plastic coating and a photoelastic fringe pattern develops in the plastic which will be related to the change in stress on the surface of the rock. Methods thus far developed, measure changes in stress and are not as precise as electrical resistance wire strain gauges and are not satisfactory for absolute stress determinations.

The sonic method (43) of determing rock stress has been used to determine the absolute stress in pillars in underground workings. From the theory of elasticity the compression wave travels faster than the shear wave and their velocities can be expressed in terms of the modulus of elasticity, Poisson's ratio and the density of the rock. If any of these elastic properties change with changes in stress, then the stress in the rock can be determined by measuring the velocity of propagation of either the compression or shear wave through it.

Investigations are presently being carried on by L. A. Panek (36) of the United States Bureau of Mines to develop a hydraulic cell to measure stress. In this method a thin

walled copper diaphragm is placed in the base of a borehole and encased in a cement or epoxy grout. The cell is pre-stressed by pumping a suitable fluid into the diaphragm which makes it responsive to changes in stress perpendicular to the plane of the diaphragm. The change in pressure on the cell is shown on a bourbon tube pressure gauge at the surface of the borehole. However, this only records changes in stress and does not measure absolute stress values.

Hydraulic Fracturing as a Stress Measuring Device

Hydraulic fracturing is a technique which was introduced to the petroleum industry in a paper by J. B. Clark (3) of the Stanolind Oil and Gas Company in 1948 to stimulate oil production from depleted oil wells. In this process a section of the oil well is sealed off with packers and fluid pressure is applied to the interval between the packers and the pressure is increased until a crack or fracture develops at the wall; the crack or fracture is then extended by the pressurized fluid which is continually being pumped into the well hole.

Hydraulic fracturing for the purpose of increasing well productivity is now generally accepted as a regular completion and workover practice. Numerous articles have appeared in the literature discussing the various techniques and theories of hydraulic fracturing (38). In general, three basic types of formation fractures are recognized today: (1) the horizontal fracture, (2) the vertical fracture, (3) and fractures

along natural planes of weakness in the formation.

There has been some controversy in the literature (20), (16) on the ability to predict the nature of the induced fractures; however, it is generally agreed, that the compressive stress in the rock at the time of fracture will tend to control the orientation of the fracture. Numerous other factors may enter into the problem such as porosity, pore pressure, tectonic conditions, tensile and shear strength of the rock, bedding planes, intrinsic fractures and the type of fracturing fluids used--penetrating or non-penetrating. Normally horizontal fractures are created at shallow depths with injection pressures equal to or greater than the overburden pressure and vertical fractures formed at deeper depths with injection pressures less than the overburden pressure. Fraser and Pettitt (11) developed an inflatable formation packer enabling them to obtain in-situ data about the orientation of the initiated fracture; however, no definite conclusions can be made about the direction of propagation of the fracture after initiation.

From theoretical considerations supported by experimental observations, fractures tend to propagate in a direction perpendicular to the direction of least stress. Theoretical models based on the principles of elasticity have been developed describing the fracturing phenomena. Some of the more interesting papers on this subject have been presented by Hubbert and Wills (19), (20), Scheideggar (51),

Dunlap (8), Kehle (23), and Fairhurst (9), (10).

The Model of Fairhurst

This model simulates the hydraulic fracturing technique used in the petroleum industry to stimulate production from a depleted oil well. It consists of a cyclindrical zone sealed off with packers. Fluid pressure is applied to the packed off interval and the pressure increased until a fracture develops at the wall and is then extended by the pressurized fluid flowing into it.

The mathematical analysis is made on the assumption that the material in which the fracturing is taking place is elastic such that a state of plane stress and strain is maintained. The stress variations are calculated by the principle of superposition by introducing a borehole into a biaxially loaded rock body. The stress variation is the difference between the stresses before and the stresses after introduction of the hole.

From this analysis, the maximum (least compressive) induced tangential stress at the wall of the hole is

$$(13) \quad (\Sigma\sigma_{\phi})_{max} = 3P - Q$$

and the maximum induced longitudal stress at the wall of the hole is

$$(14) \quad (\Sigma\sigma_{z})_{max} = R + 2\nu(P - Q)$$

where P, Q, and R are respectively the principal regional

stresses in the radial, tangential, and axial directions with respect to the bore hole and ν is Poisson's ratio.

From the results of this analysis, it is concluded that a hydraulic fracture may develop in one of three ways: (1) radial initiation and propagation, (2) normal initiation and propagation, and (3) normal initiation and radial propagation. The fracture being initiated at some point on the wall as soon as the fluid pressure reaches the critical value which creates a net tension K_p on the wall sufficient to cause failure under the loading conditions.

In the special case of a vertical drill hole where it is assumed that the principal stresses are vertical and horizontal with the vertical stress $R = \rho gd$, the determination of the state of stress may proceed as follows:

If the value of the pressure at the time of fracture initiation is less than the absolute value of R, then the fracture must have been vertical and will propagate as such. Knowing the value of K_p, P_i, and P_f where P_f is the so-called "instantaneous shut-in pressure", P_i is the pressure of the fluid which initiates the fracture, and K_p is the required tension on the bore hole wall to cause failure (20), the regional stresses may be calculated from the following equations:

$$(15) \quad \sigma_\phi = 3P - Q + P_i = K_p$$

$$(16) \quad \sigma_z = R + P_i < K_p$$

(17) $P = -P_f$

The orientation being determined by an inflatable packer (7), borehole camera, or some other method.

If the value of P_i is greater than R, then the fracture must have been initiated normal to the hole and propagation of the fracture could occur in one of two different ways.

(1) If the value of P_f is less than the value of R, then the fracture must have changed during propagation to a radial fracture. The state of stress cannot be determined in this case except that P and Q are less than R and bounds may be placed on the value of Q.

(2) If the value of P_f is greater than the value of R, then the fracture was both initiated and propagated horizontally and no new information is obtained.

When it is possible to drill into the region of interest with holes of different orientation more information may be obtained, such would be the case in underground mines. If the principal stress directions do not coincide with the hole direction this method cannot be used for stress determination.

In principle, once the fracture has been initiated, the fluid pressure necessary to expand and propagate these fractures is approximately equal to the total earth stress perpendicular to the direction of propagation plus the velocity losses necessary to continue the fracture. Once a fracture has been established and is then allowed to close by release

of the fluid pressure and then forced open a second time by increasing the fluid pressure at a slow rate the pressure recorded to do this should be approximately equal to the total stress perpendicular to the plane of the fracture, since the velocity of the fluid would be extremly low and there would be no energy used in creating any new surface area for the fracture.

In order that the technique of hydraulic fracturing be useful in the measurement of in-situ stress it is essential that control of the orientation of the fracture propagation be possible.

CHAPTER III

EXPERIMENTAL PROCEDURE

Sample Preparation

The models for this investigation were prepared from a mixture of hydrostone and water in the ratio of three parts hydrostone to one part water by weight. This combination was mixed thoroughly by hand to insure an even consistency by adding water to the hydrostone and mixing for about five minutes. The mixture was then poured immeadiately into a mold which consisted of three 6 inch cube compartments. The time required for the hydrostone mixture to start setting up after pouring was of the order of one minute and the models could be removed from their mold after a time lapse of approximately 45 minutes.

Basically, three different types of models were prepared: (1) models which contained either circular or elliptical prefractures, (2) models which had circular sand inclusions, (3) models with cyclindrical zones.

The circular prefractures consisted of two concentric five thousandths inch thick brass foil of 1 and 1/2 inch diameter glued onto a 1/8 inch outside diameter steel tube. This assembly was placed into the mold and held rigid so that the center of the circular foil was located at the center of the hollow cavity and the plane of the foil was placed parallel to one set of faces of the mold which was

later designated as the X-Z plane with the entry tube lying along the Z-axis as is shown in Figure 1. The elliptical prefractures were made of the same brass foil having a 1 and 3/4 inch major axis and a 1 inch minor axis similarly assembled as the circular discs and placed in the mold with the minor axis parallel to the direction of Z and the major axis parallel to the direction of X.

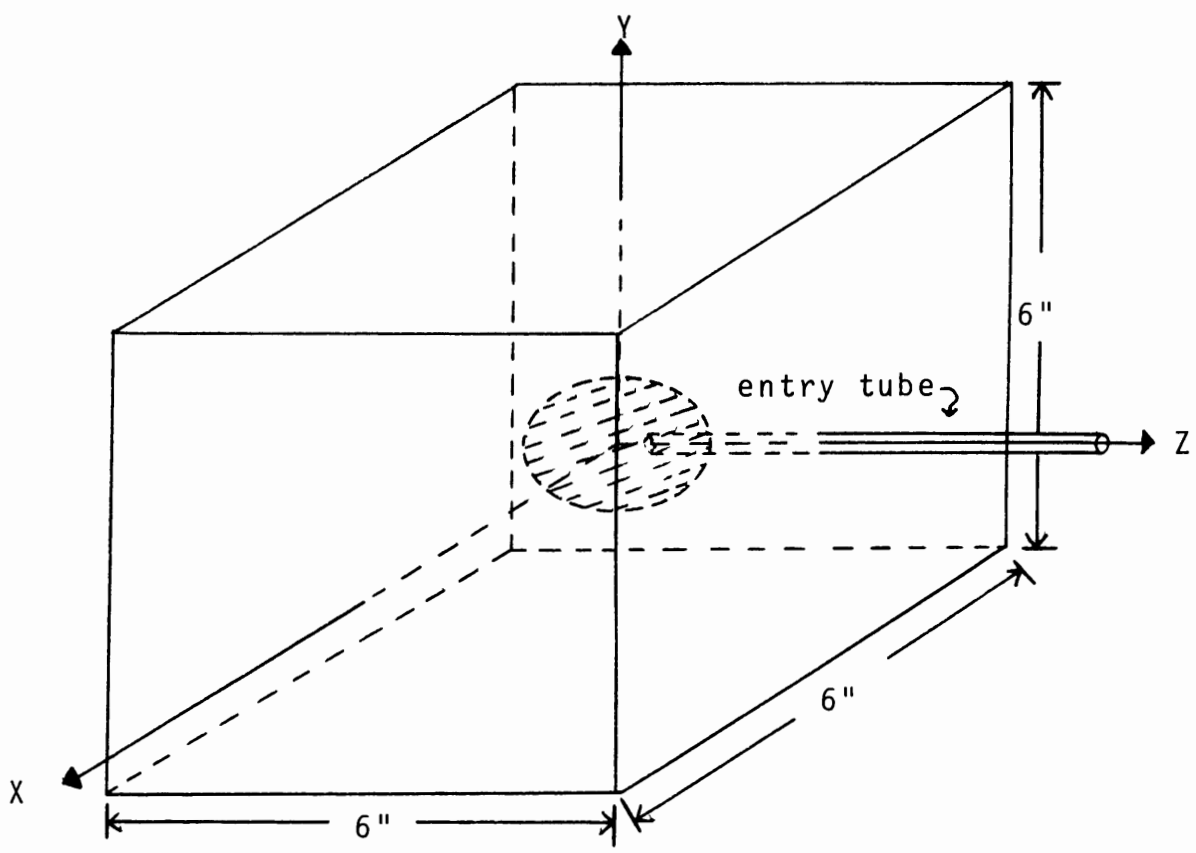

Figure 1. Sketch of the Model illustrating the position of the Circular Prefracture.

The steel entry tube was fitted with a wire which extended slightly out of the end so that it was positioned approximately at the geometrical center of the brass foil. This was introduced to keep the hydrostone slury from flow-

ing into the entry tube while curing and plugging it up.

The sand inclusions were made by preparing the hydrostone mixture in two separate batches. The mold for these models had the same geometry as that for the circular and elliptical models except that in this case the front face of the mold was divided into two equal parts. With the lower face intact, the first batch of the hydrostone mixture was poured in until it came to within approximately 1/8 inch of the top of the bottom half. As soon as this mixture was sufficiently set to support weight, 39 grams of a fine grain sand was introduced on this surface encompasing a circle of 1 and 1/2 inch radius into which the entry tube was placed. The top half of the front face was then fitted into place and the second batch of hydrostone mixture prepared and poured in.

The third type of model contained a two inch square metal plate of 3/32 inch thickness with a 5/32 inch hole drilled in its center. This plate was welded to a 1/4 inch nipple. The model was then prepared by using the mold of the first models and filling with the hydrostone mixture. When the mixture had set sufficiently so that it became like a thick jelly, the plate assembly was introduced by embedding it into the mixture until the top of the nipple was flush with the surface; this made the bottom of the plate a distance on one inch from the surface. A 1/4 inch bolt extending to the top of the submerged plate was screwed

into the nipple to restrict the mixture from flowing in.

The models prepared for this investigation are summurized in Table 1 where the following symbolization has been adopted: (1) PHC refers to the hydrostone blocks containing the circular prefractures, (2) PHE refers to the blocks containing elliptical prefractures, (3) PHS refers to the blocks containing the sand inclusions, and (4) HCZ refers to the blocks with cylindrical zones.

When the model specimens were removed from the mold, their weights were recorded and then placed on a rack to cure. Later, each specimen was assigned an identification number and a X-Y coordinate system was painted on the face containing the entry tube to identify the orientation of the enclosed prefracture.

Three samples from each batch of hydrostone mixture were taken by filling cylindrical plexiglas molds of 1 and 1/2 inch inside diameter and 2 inches in length. These synthetic cores were numbered to correspond with the identification number of the block specimens which were made from the same batch. Later, these cores were used to determine some of the physical and elastic properties of the hydrostone. The nature and results of these tests are given in Appendix A.

Periodically the hydrostone blocks were weighed and their weight recorded. From these observations, as is shown in Figure A-1 in Appendix A, it is seen that the weights of the

TABLE I

THE DATE, NATURE AND NUMBER OF HYDROSTONE MODELS PREPARED FOR THIS INVESTIGATION

Preparation Date	Type of model	Number made
May 20, 1965	PHC	5
May 20, 1965	PHE	7
May 26, 1965	PHC	5
May 26, 1965	PHE	7
June 20, 1965	PHC	6
June 20, 1965	PHE	6
June 21, 1965	PHC	6
June 21, 1965	PHE	6
July 19, 1965	PHC	2
July 19, 1965	PHE	1
July 19, 1965	PHS	9
July 20, 1965	PHS	15
July 23, 1965	HCZ	3
July 30, 1965	HCZ	9

blocks stablized after a curing period of from 25 to 35 days. The block specimens were considered to be properly cured when this weight stabilization had been reached.

As a final step in the model preparation, each specimen which was to be hydraulically fractured under a biaxial load was ground down on the four sides on which the biaxial load was to be applied by use of the Norton Grinding machine as depicted in Figure 2. The specimens which were fractured under an uniaxial load were sanded by hand until smooth on the two faces on which the load was applied. Table 2 gives the dimensions and the corresponding areas of each block used in the experimental biaxial phase.

Figure 2. A block being ground in the Norton Grinding Machine.

TABLE II

DIMENSIONS AND AREAS OF THE HYDROSTONE BLOCKS HYDRAUICALLY FRACTURED UNDER A BIAXIAL LOAD

Block Identification and Number	X-Length (inches)	Y-Length (inches)	Z-Length (inches)	Area-XZ (sq. in.)	Area-YZ (sq. in.)
PHC - 18	5.75	5.69	6.06	34.9	34.5
PHE - 19	5.81	5.75	5.94	34.5	34.1
PHE - 26	5.69	5.75	6.00	34.1	34.5
PHE - 27	5.69	5.75	6.06	34.5	34.9
PHE - 28	5.81	5.81	5.81	33.8	33.8
PHC - 29	5.81	5.81	5.88	34.2	34.2
PHC - 30	5.75	5.88	5.88	33.8	34.5
PHE - 31	5.91	5.75	5.88	34.2	33.8
PHC - 32	5.75	5.75	5.94	34.1	34.1
PHC - 33	5.75	5.75	6.00	35.3	35.3
PHC - 34	5.75	5.88	6.00	34.5	35.3
PHC - 35	5.75	5.81	5.94	34.1	34.5
PHE - 36	5.75	5.75	6.00	34.5	34.5
PHS - 46	5.75	5.75	6.13	35.2	35.2
PHS - 47	5.75	5.69	6.13	35.2	34.9
PHS - 48	5.75	5.75	6.06	34.9	34.9
PHS - 49	5.81	5.63	6.13	35.6	34.5
PHS - 50	5.75	5.75	6.06	34.9	34.9
PHS - 51	5.75	5.69	6.06	34.9	34.5
PHS - 52	5.75	5.56	6.13	35.2	34.1
PHS - 53	5.75	5.63	6.13	35.2	34.5
PHS - 54	5.75	5.69	6.06	34.9	34.5
PHS - 55	5.75	5.63	6.06	34.9	34.1
PHS - 56	5.75	5.75	6.06	34.9	34.9
PHS - 57	5.69	5.69	6.06	33.8	33.8
PHS - 58	5.81	5.63	5.94	34.5	33.4

Hydraulic Fracturing Procedure

The original hydraulic fracturing mechanism consisted of a machined, stainless steel hydraulic cell originally designed by Panek (36), a 10,000 psi bourdon type Blackhawk pressure gauge, and a hydraulic fluid reservoir assembled together and fitted with 1/8 inch stainless steel tubing and fittings. The stainless steel hydraulic cell was hand operated with the capability of effecting a 10,000 psi pressure and was volumetrically calibrated to have a volume displacement of 1/3 cubic centimeter per turn with an effective volume capacity of 6 cubic centimeters. The pressure gauge was calibrated by use of a Dead-Weight Tester procured from the Petroleum department.

This assemblage proved to be ineffective for this investigation on two accounts: (1) the volume capability of the hydraulic cell was too small requiring many refills to complete a fracture of the model specimens, (2) metal failure resulted in the hydraulic cell from the repeated turning of the piston under high pressures. If a suitable lubricant for stainless steel can be found and an accurate knowledge of the fracturing fluid volume be required, this system would be most desirable.

The stainless steel hydraulic cell was replaced by a Blackhawk hand pump with a 10,000 psi capability. This pump had an effective volume capacity of 1000 cubic centimeters and a stroke volume of approximately 1 cubic centi-

meter. The previously calibrated 10,000 psi pressure gauge was connected to the hand pump and a 1/8 inch stainless steel tube connected the pressure gauge to a high pressure valve and coupling mechanism. Figure 3. depicts the fracturing system.

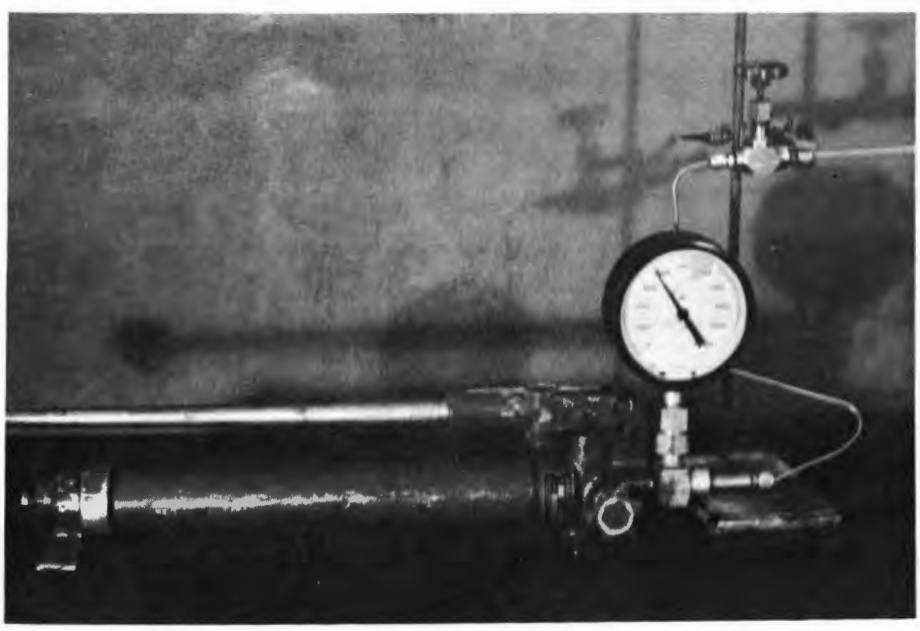

Figure 3. The Hydraulic Fracturing pressurizing system.

Uniaxial Testing. For uniaxial testing, the hydrostone specimens were placed into the Tinius Olsen Universal testing machine and connected to the hydraulic fracturing system. Figure 4. illustrates a hydrostone model under an uniaxial applied load being hydraulically fractured. The surface area of the specimens were determined in advance and the

required load calculated to correspond to the desired applied stress. The external load was applied and maintained constant while the fracturing process took place. A piece of blotter type material was inserted between the specimen and the two faces of the testing machine to insure a more even distribution of load. To minimize fluid loss due to porosity leak off during the fracturing procedure a high viscosity oil was used for the fracturing fluid. A red dye, Sudan III, was used in the fracturing fluid to give a permanent record of the actual surface which was hydrauically fractured. Table III summarizes the data obtained from the uniaxial testing.

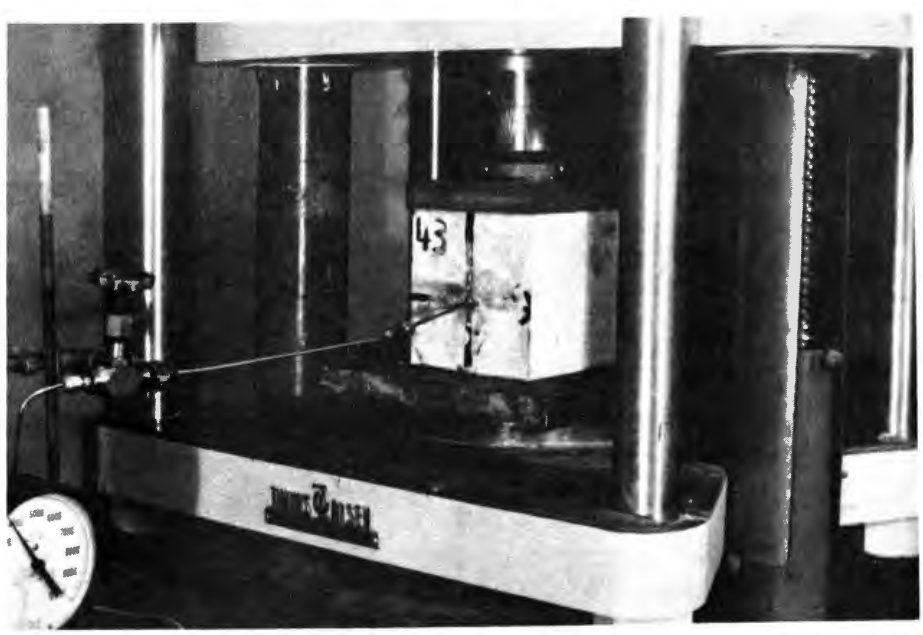

Figure 4. A test specimen under an uniaxial load being hydraulically fractured.

TABLE III

DATA OBTAINED FROM UNIAXIAL TESTING

Block	Cure Time (days)	Surface Area (sq. in.)	Load (pds.)	Stress (psi)	Breakdown Pressure (psi)	Pumping Pressure (psi)	Fluid Volume to Fracture (c.c.)
PHE-1	29	36.0	10,800	300	4200	1500	21
PHC-2	29	35.0	10,500	300	2550	1000	25
PHE-3	30	36.0	14,400	400	3200	1500	16
PHE-4	29	36.0	14,400	400	2650	1500	27
PHC-5	28	36.0	18,000	500	2750	1500	26
PHE-6	32	36.0	54,000	1500	1950	2500	67
PHE-7	28	36.8	18,400	500	2250	2000	33
PHC-8	26	36.0	36,000	1000	2100	2000	55
PHE-9	35	36.0	21,600	600	1900	1500	75
PHE-10	35	36.0	21,600	600	2250	2000	37
PHE-11	34	36.0	7,200	200	2450	1800	18
PHC-12	31	36.0	7,200	200	2300	1200	48
PHC-13	34	36.8	7,350	200	1850	1500	28
PHC-14	36	36.0	10,800	300	1700	1800	27
PHE-15	31	36.0	7,200	200	2300	1200	21
PHC-16	36	32.5	9,750	300	1750	1200	18
PHE-17	37	36.0	3,600	100	1450	1500	9
PHC-18	37	36.0	14,400	400	2150	1800	30
PHE-19	37	36.0	0	0	1950	2500	8

Biaxial Testing. To obtain biaxial loading capabilities a hydraulic loading unit was designed, as shown in Figure 5, to be used in conjunction with the Tinius Olsen testing machine.

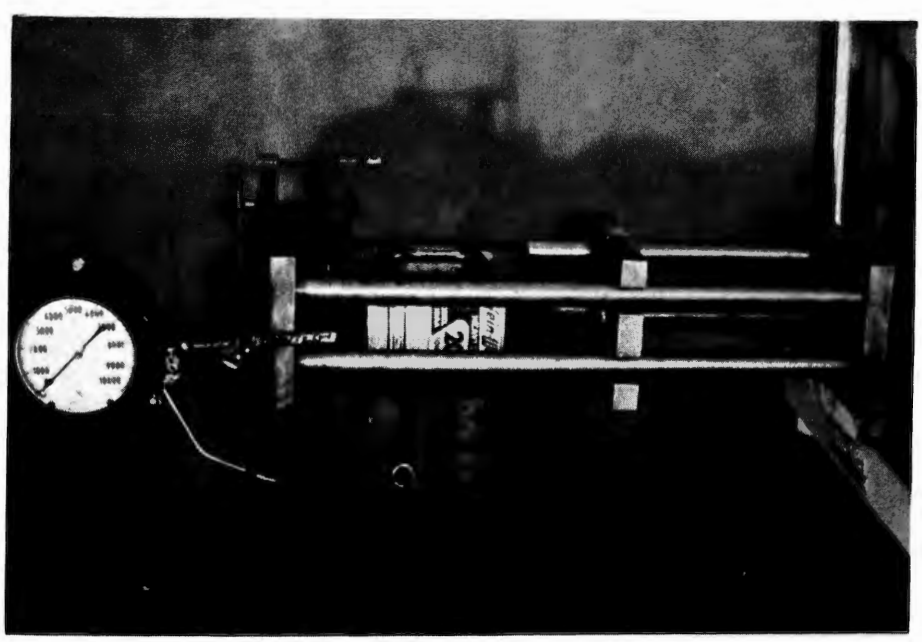

Figure 5. The Hydraulic Loading Unit used in conjunction with the Tinius Olsen Testing Machine to obtain a biaxial stress condition.

The hydraulic unit consisted of a 20 ton jack mounted on a steel frame with the loading head of the jack seated into a collar of a moveable 1 inch thick, slotted steel plate of 5 and 3/4 inch height. A 10,000 psi bourdon type pressure gauge was connected to the pressurized chamber of the 20 ton hydraulic jack and calibrated with the Tinius

Olsen to read the applied load directly. Figure 6 depicts the calibration curve of the 10,000 psi pressure gauge with respect to the applied load of the hydraulic jack.

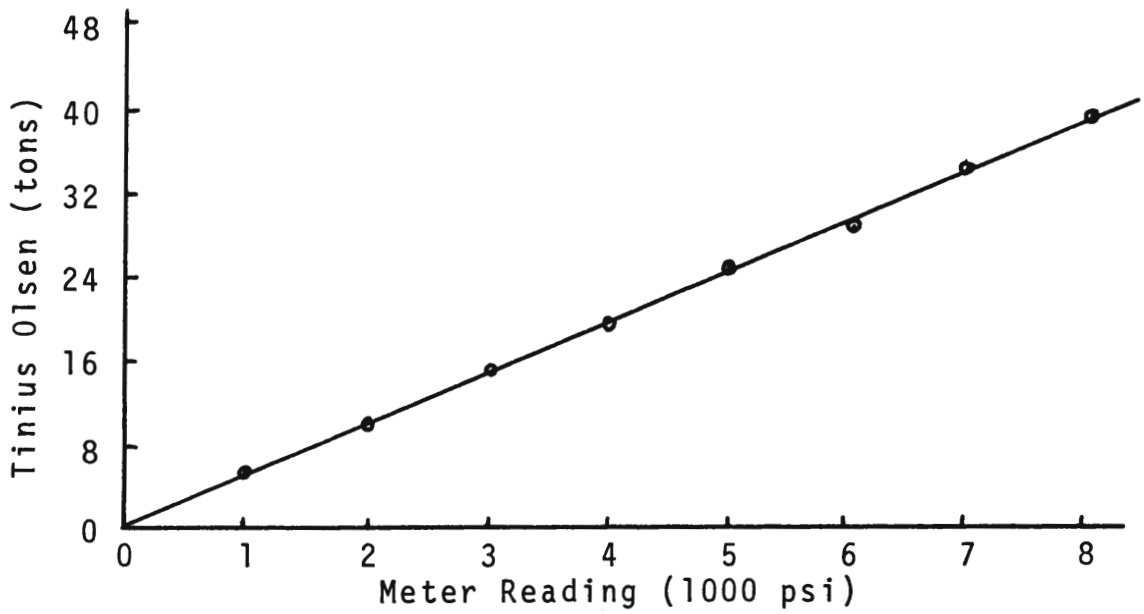

Figure 6. Calibration curve of the 10,000 psi gauge with the applied load of the Hydraulic Jack.

A number of 1/16 inch thick metal plates were made to place on the top of the test specimen to give approximately a 1/16 inch clearance between the moveable plate of the hydraulic jack mechanism acting in the X-direction and the Tinius Olsen acting in the Y-direction. Blotter material of the same areal dimensions as those of the test specimens were inserted between the test specimens and the loading plates. Figure 7 illustrates a test specimen being hydraulically fractured under a biaxially loaded condition and Table IV summarizes the data obtained from the biaxial testing.

TABLE IV

DATA OBTAINED FROM BIAXIAL TESTING

Block	σ_x (psi)	σ_y (psi)	$\Delta\sigma$ (psi)	Breakdown Pressure (psi)	Pumping Pressure (psi)	Fluid Volume to Fracture (cc)
PHE-26	1000	1800	800	5300	3000	25
PHE-27	1000	2000	1000	5500	3000	30
PHE-28	1200	1200	0	3300	2500	35
PHC-29	500	1000	500	2600	2000	21
PHC-30	1100	1400	300	2800	2000	60
PHE-31	600	800	200	4500	2500	25
PHC-32	200	400	200	5200	2000	20
PHC-33	1000	1600	600	3500	2500	18
PHC-34	800	1500	700	2100	3000	13
PHC-35	1200	1700	500	4100	3000	25
PHE-36	1200	2000	800	2800	3000	26
PHE-37	300	600	300	3600	2000	23
PHS-46	900	1200	300	600	3000	15
PHS-47	300	600	300	800	1500	15
PHS-48	500	1000	500	500	1500	20
PHS-49	0	800	800	400	1500	14
PHS-50	1000	1600	600	1100	1500	16
PHS-51	200	400	200	600	1500	15
PHS-52	1000	1000	0	1100	2000	18
PHS-53	400	800	400	400	1500	16
PHS-54	200	600	400	400	1500	13
PHS-55	1200	1700	500	700	1500	22
PHS-56	600	800	200	1300	2000	15
PHS-57	500	1000	500	No Data	2000	14
PHS-58	400	600	500	No Data	2000	12
HCP-70	1200	1200	0	No Data	2000	8
HCP-71	1200	2400	1200	1250	2500	10
HCZ-80	0	200	200	4300	1500	8
HCZ-81	600	800	200	800	3000	11

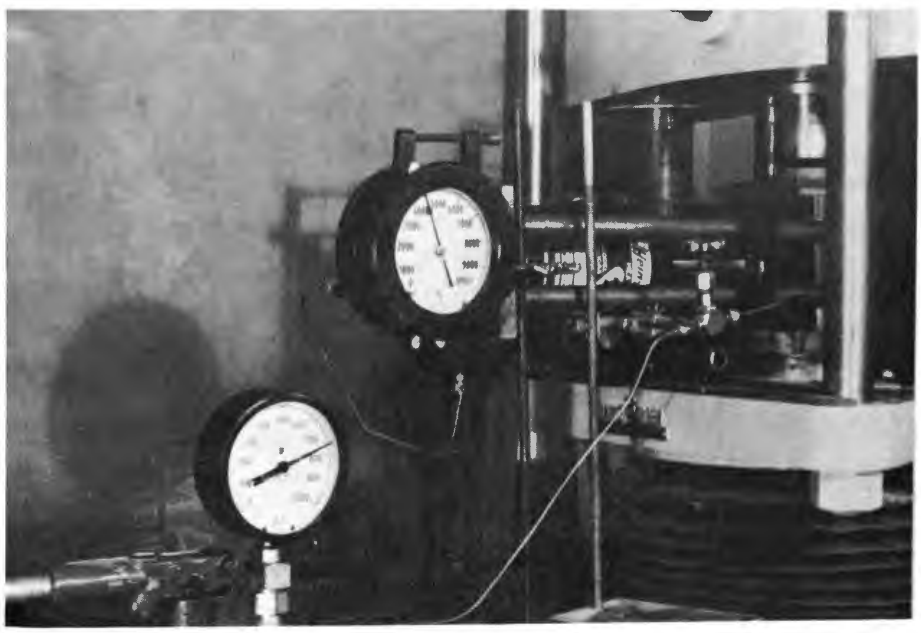

Figure 7. A Test Specimen under a biaxial load being Hydraulically Fractured.

Fracture Contour

For the experimental analysis and the correlation of the experimental results with that predicted by the mathematical model, a point by point contour of the fractured surface of a number of specimens was made.

A represenative number of fractured specimens was selected and a contour of their fractured surface made by measuring the spatial coordinates of 61 points lying within a four inch diameter circle. The center of the prefracture was chosen as the origin of coordinates and the remaining 60 points were selected in the following manner: circles of

1/2, 1, 3/2, and 2 inches radius were taken and these circles were divided respectively into 6, 12, 18, and 24 equal parts. This gave a polar grid of approximately 1/2 inch between points.

A mechanical apparatus was designed, Figure 8, which enabled the measurement of these grid points to within 1/16 of an inch in the vertical direction. Table V gives the Y-displacements for selected blocks in relation to the center of the prefractured plane. All displacements are expressed in units of 1/16 of an inch.

Figure 8. The Fractured Surface of a block being measured by use of the Contour Apparatus.

TABLE V

SURFACE CONTOUR DATA

Stress Pt.	R (in.)	θ (deg.)	HYDROSTONE SPECIMEN PHE 1	PHE 4	PHC 5	PHE 7	PHE 11	PHE 15	PHC 16	PHC 29	PHE 31	PHE 32	PHC 37
(0, 0)	0.0	00	0	0	0	0	0	0	0	0	0	0	0
(1, 1)	0.5	00	1	0	1	0	0	0	-1	0	-1	0	1
(1, 2)	0.5	60	0	0	0	-1	0	1	0	0	0	1	0
(1, 3)	0.5	120	1	0	-1	-1	0	0	2	3	2	0	-1
(1, 4)	0.5	180	1	1	-1	0	0	0	2	2	2	-1	-1
(1, 5)	0.5	240	1	1	0	0	-1	1	0	1	1	-1	0
(1, 6)	0.5	300	0	0	0	-1	0	0	-1	0	0	0	1
(2, 1)	1.0	00	1	0	3	0	0	0	-1	-3	-2	1	1
(2, 2)	1.0	30	2	-1	2	-1	0	1	1	-2	-3	2	2
(2, 3)	1.0	60	2	-2	0	-2	-1	1	1	1	0	2	2
(2, 4)	1.0	90	1	-2	-2	-3	-2	0	3	5	3	0	2
(2, 5)	1.0	120	1	0	-2	-1	-1	0	5	8	4	-1	1
(2, 6)	1.0	150	1	0	-3	-1	0	-1	7	9	4	-3	0
(2, 7)	1.0	180	2	1	-2	0	0	1	9	7	3	-3	-1
(2, 8)	1.0	210	2	1	-1	1	-1	0	5	5	2	-1	-2
(2, 9)	1.0	240	1	1	2	1	1	2	1	2	1	-1	-1
(2,10)	1.0	270	1	-1	4	1	1	2	-1	-3	-2	1	0
(2,11)	1.0	300	0	0	4	1	2	-1	-1	-3	-2	1	1
(2,12)	1.0	330	0	-1	4	1	1	-1	-1	-3	-2	1	1
(3, 1)	1.5	00	2	-1	4	0	-2	-1	1	-9	-3	4	1
(3, 2)	1.5	20	3	-1	3	-1	-2	0	3	-7	-3	4	1
(3, 3)	1.5	40	3	-2	1	-2	-2	1	4	-4	-2	4	2
(3, 4)	1.5	60	3	-2	0	-3	-3	1	4	0	0	3	3
(3, 5)	1.5	80	3	-2	-2	-4	-3	0	4	9	3	0	4
(3, 6)	1.5	100	2	-2	-4	-4	-3	0	6	18	5	-2	6
(3, 7)	1.5	120	2	-2	-4	-3	-2	0	7	27	8	-5	6

TABLE V (continued)

(3, 8)	1.5	140	2	-5	-1	-1	-1	-1	10	22	7	3	-7
(3, 9)	1.5	160	2	-4	0	1	0	-1	12	15	5	1	-7
(3,10)	1.5	180	3	-3	2	2	1	-1	14	11	4	0	-5
(3,11)	1.5	200	3	-3	2	2	2	0	13	8	2	1	-4
(3,12)	1.5	220	2	2	2	3	1	1	8	3	-1	-1	-3
(3,13)	1.5	240	1	4	3	3	2	2	3	-4	-5	-1	-1
(3,14)	1.5	260	1	6	3	3	2	3	1	-10	-7	0	0
(3,15)	1.5	280	0	7	0	3	1	1	0	-12	-8	0	2
(3,16)	1.5	300	0	7	-1	3	2	-1	-1	-11	-7	1	3
(3,17)	1.5	320	0	6	-2	3	1	-2	-1	-10	-5	0	3
(3,18)	1.5	340	1	5	-2	2	-1	-1	-1	-10	-3	0	3
(4, 1)	2.0	00	4	4	-3	2	-4	-1	3	-18	-5	0	6
(4, 2)	2.0	15	4	3	-2	0	-5	0	5	-11	-5	0	6
(4, 3)	2.0	30	4	1	-2	-2	-5	0	6	-5	-4	2	6
(4, 4)	2.0	45	4	-1	-2	-4	-5	1	6	2	-4	3	5
(4, 5)	2.0	60	4	-3	-2	-4	-6	1	6	23	2	4	4
(4, 6)	2.0	75	4	-5	-2	-6	-6	0	6	--	7	7	1
(4, 7)	2.0	90	4	-6	-2	-6	-6	0	6	--	11	10	-3
(4, 8)	2.0	105	3	-8	-2	-5	-5	-1	8	--	13	13	-7
(4, 9)	2.0	120	3	-8	-2	-4	-3	-1	9	--	15	13	-12
(4,10)	2.0	135	3	-8	-2	-4	-1	-1	11	32	13	11	-15
(4,11)	2.0	150	4	-7	0	0	0	-2	13	22	10	7	-15
(4,12)	2.0	165	4	-5	0	3	1	-1	15	17	8	4	-12
(4,13)	2.0	180	5	-3	2	5	2	-1	--	15	4	1	-10
(4,14)	2.0	195	4	2	4	5	4	0	--	6	2	0	-7
(4,15)	2.0	210	4	5	6	5	4	1	--	2	-1	0	-5
(4,16)	2.0	225	4	7	7	6	5	2	12	-3	-6	0	-4
(4,17)	2.0	240	2	10	7	7	5	3	7	-12	-11	2	-3
(4,18)	2.0	255	2	11	5	7	5	4	8	-20	-15	3	-2
(4,19)	2.0	270	1	11	3	7	4	3	-1	-26	-16	5	-1
(4,20)	2.0	285	0	11	1	8	4	1	0	-28	-15	4	1
(4,21)	2.0	300	1	10	-1	7	2	-1	-1	-24	-12	2	3
(4,22)	2.0	315	1	8	-2	6	0	-2	-1	-23	-8	1	4
(4,23)	2.0	330	2	7	-3	5	-1	-2	1	-20	-6	0	5
(4,24)	2.0	345	3	6	-3	3	-3	-1	2	-19	-5	0	6

CHAPTER IV

EXPERIMENTAL RESULTS

Experimentally, the hydraulic fracture was assumed completed when the fracturing fluid was visually seen flowing from the fractured block. The block was then removed from the fracturing apparatus and by means of hammer and chisel the block was completely separated by starting in the region where the hydraulic fluid was observed to be flowing out and wedging apart. A red dye was included in the fracturing fluid to give a permanent stain to the hydraulically fractured surface and aid in the resolving of that part of the surface which was hydraulically fractured to that which was mechanically separted.

Uniaxial Results

The results of the uniaxial testing indicate that for small confining loads, of the order of 400 psi and less, the orientation of the prefracture can control, at least within a restricted range, the orientation of the hydraulically fractured plane. For larger applied loads the orientation of the prefracture exhibits less control and with an uniaxial load in the neighborhood of 1000 psi essentially no control of the fracture orientation was possible.

The observed breakdown pressure varied from a maximum

of 4200 psi to a minimum of 1450 psi with the majority of the breakdown pressures lying between 2700 psi and 1700 psi. The average uniaxial breakdown pressure was computed to be 2290 psi. There does not appear to be any correlation between the magnitude of the applied stress and the breakdown pressure for the range of stress used in this investigation, this may indicate that the breakdown pressure is a function of the material itself along with the nature of the fracturing fluid.

Once the fracture was initiated, the propagation of the fracture was accomplished by maintaining a constant fluid pressure referred to as the "fracture extension pressure" in the subsequent discussion. There appeared to be no relation between the nature of the fractured surface and the magnitude of the fracture extension pressure for the range of pressures used. The only noticeable effect of varying the fracture extension pressure was in the time required to complete the fracture and the amount of fluid used: the lower the fracture extension pressure the greater the time and the more fluid necessary to complete the fracture.

The magnitude of the uniaxial stress influenced the amount of fluid used to complete the fracture; the greater the applied stress the more fluid was required. This indicates that for high stress concentrations the porosity of the material being fractured along with its pore fluid pressure becomes increasingly important in the fracturing

phenomena.

Figures 9 through 17 show pictorially the results of a selected representative number of blocks fractured under uniaxial conditions.

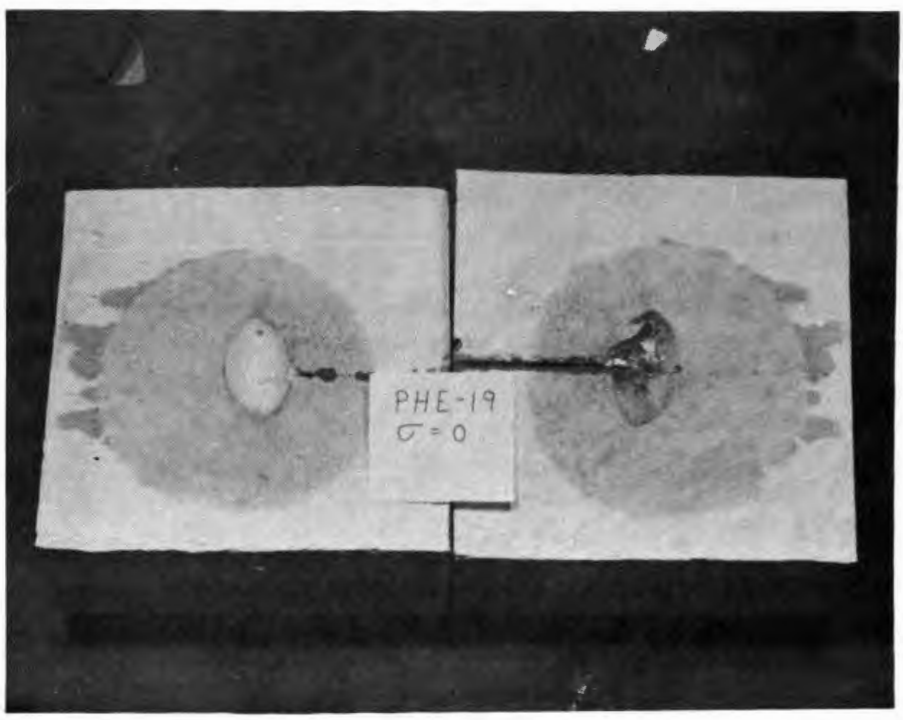

Figure 9. Fractured Block PHE-19.

This block was not subjected to any external load such that the stress within the block was due solely to that of the pressurized circular crack. The breakdown pressure was observed to be 1950 psi. The fracture extension pressure was kept at 2500 psi and 8 cubic centimeters of fluid was required to complete the fracture which broke through on three sides simultaneously with no indication of any fracturing fluid emanating from the sides. The fractured plane was exceptionally flat containing the elliptical prefracture and the fluid flow within the block was symmetrical. With no external load, the orientation of the prefracture completely controls the direction of the ensuing fracture.

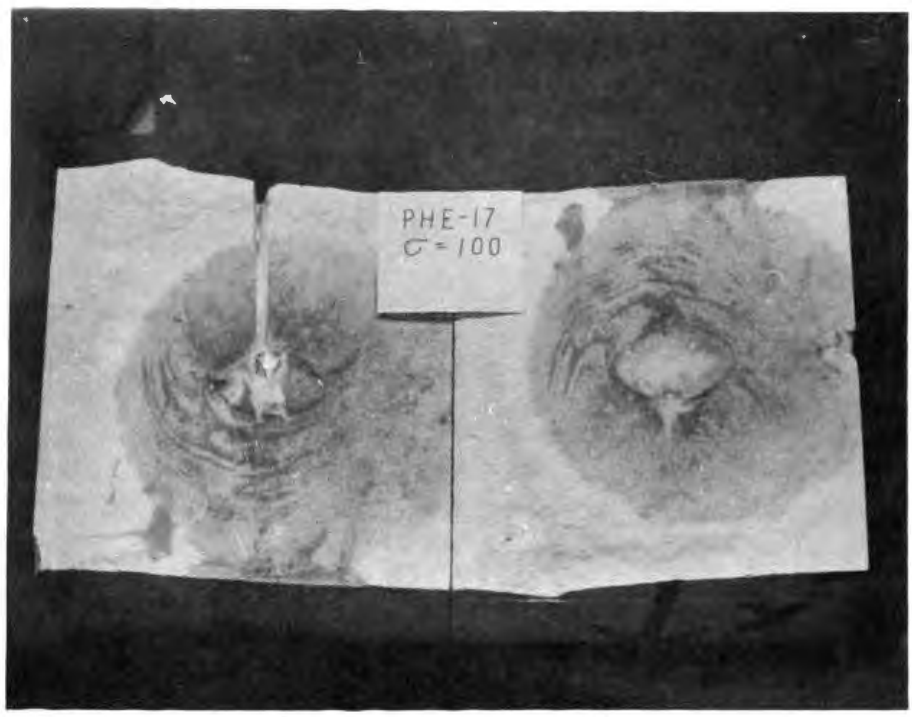

Figure 10. Fractured Block PHE-17.

The block was subjected to an uniaxial load of 100 psi and contained an elliptical prefracture. The breakdown pressure was observed to be 1450 psi. The fracture extension pressure was kept at 1500 psi. There was some difficulty experienced in keeping the uniaxial load constant due to the interaction of the pressurized crack; the influence became greater as the crack increased. The fractured surface followed the plane of the prefracture very closely which was inclined slightly to the X-Z plane. The fractured region was essentially that of a circle even though the prefracture was that of an ellipse which indicates that the geometrical nature of the prefracture has a negligeable effect on the geometrical shape of the ensuing fracture.

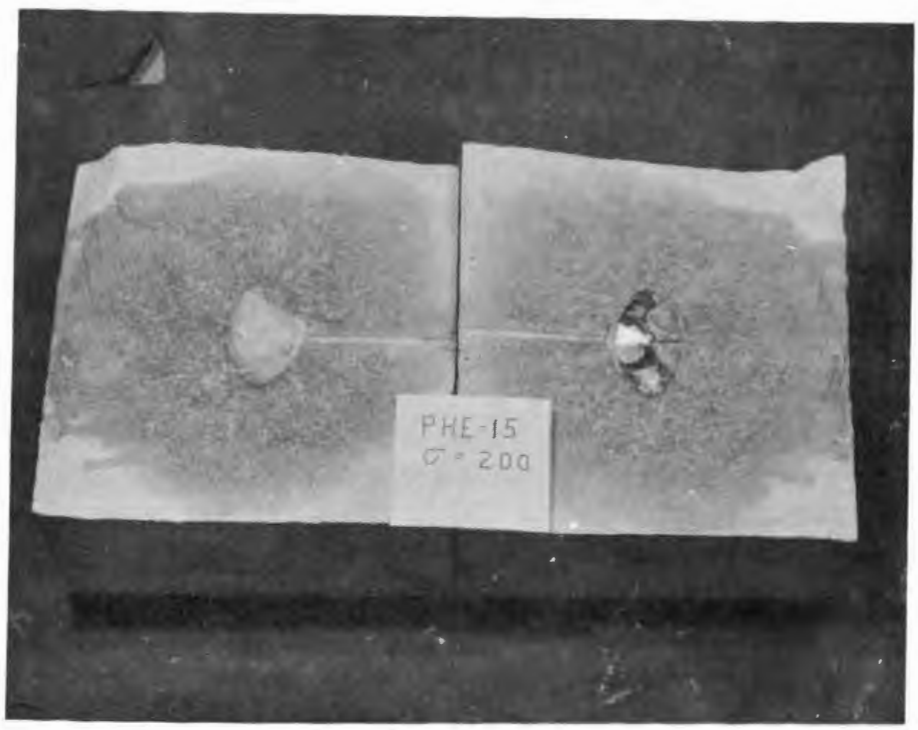

Figure 11. Fractured Block PHE-15.

The block was subjected to an uniaxial load of 200 psi and contained an elliptical prefracture. The breakdown pressure was observed to be 2300 psi. The fracture extension pressure was kept at 1500 psi with 21 cubic centimeters of fluid being required to complete the fracture which broke out on the two sides. The fractured surface was essentially horizontal following the plane of the prefracture. The fractured region was that of a circular zone exhibiting a smooth tensile break. During the fracturing process there was a noticeable interaction on the applied uniaxial load due to the pressurized crack although not as severe as was the case of Block PHE-17 with the 100 psi confining load.

Figure 12. Fractured Block PHC-13.

The block was subjected to an uniaxial load of 200 psi and contained a circular prefracture. Of the four hydrostone blocks fractured with an uniaxial load of 200 psi, this block was the only one exhibiting to any degree a curvature in the fractured surface. The fractured surface shows that the fracture was propagated more in the direction in which the fractured surface was essentially horizontal as compared to the region which exhibits a turning tendency. It may be theorized that this block was subjected to an asymmetrical load with the load concentration being predominate in the region which exhibits the greater curvature.

Figure 13. Fractured Block PHE-1.

The block was subjected to an uniaxial load of 300 psi and contained an elliptical prefracture. The breakdown pressure was observed to be 4200 psi which was exceptionally high. The epoxy used to secure the entry tube to the brass foil could have been an influencing factor in this high breakdown pressure. The fracture extension pressure was kept at 1500 psi with 21 cubic centimeters of fluid required to complete the fracture. The fracture broke through on the back side with the fractured surface being fairly horizontal in the plane containing the prefracture. The fractured zone was again approximately circular despite the elliptical prefracture.

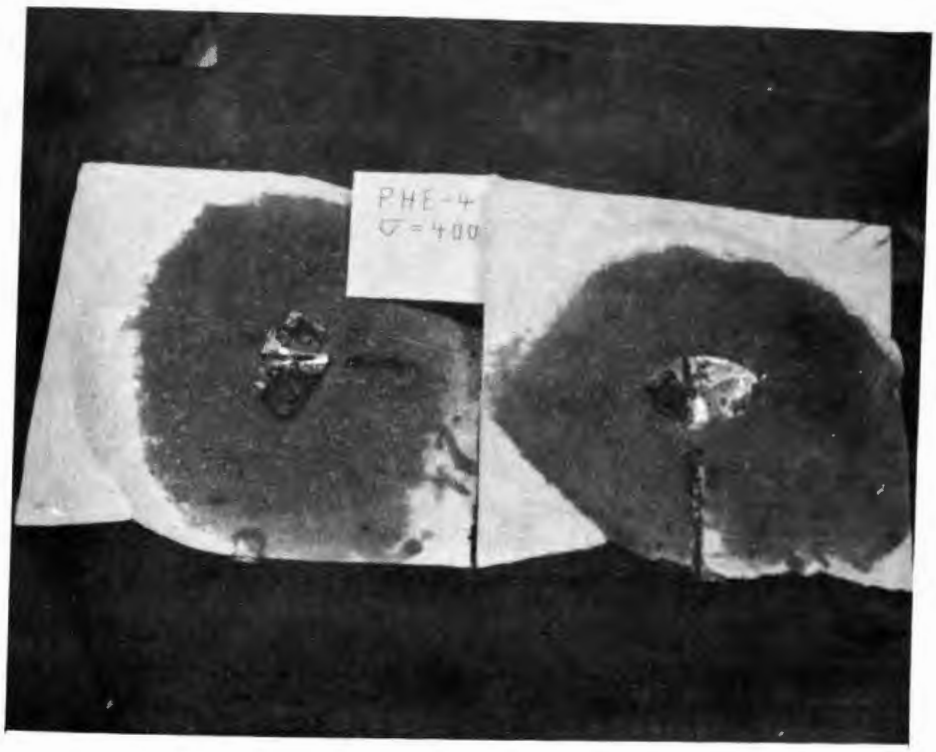

Figure 14. Fractured Block PHE-4.

The block was subjected to an uniaxial load of 400 psi and contained an elliptical prefracture. The breakdown pressure was observed to be 2650 psi. The fracture extension pressure was kept at 1500 psi with 27 cubic centimeters of fluid required to complete the fracture which broke through on the front side. The fracture zone was approximately elliptical resembling the shape of the prefracture. The fractured surface was horizontal in the plane containing the prefracture for a radius of approximately 3 inches and then started to turn such that the surface tended to orientate itself in a direction parallel to the applied load. The surface exhibited a smooth tensile break.

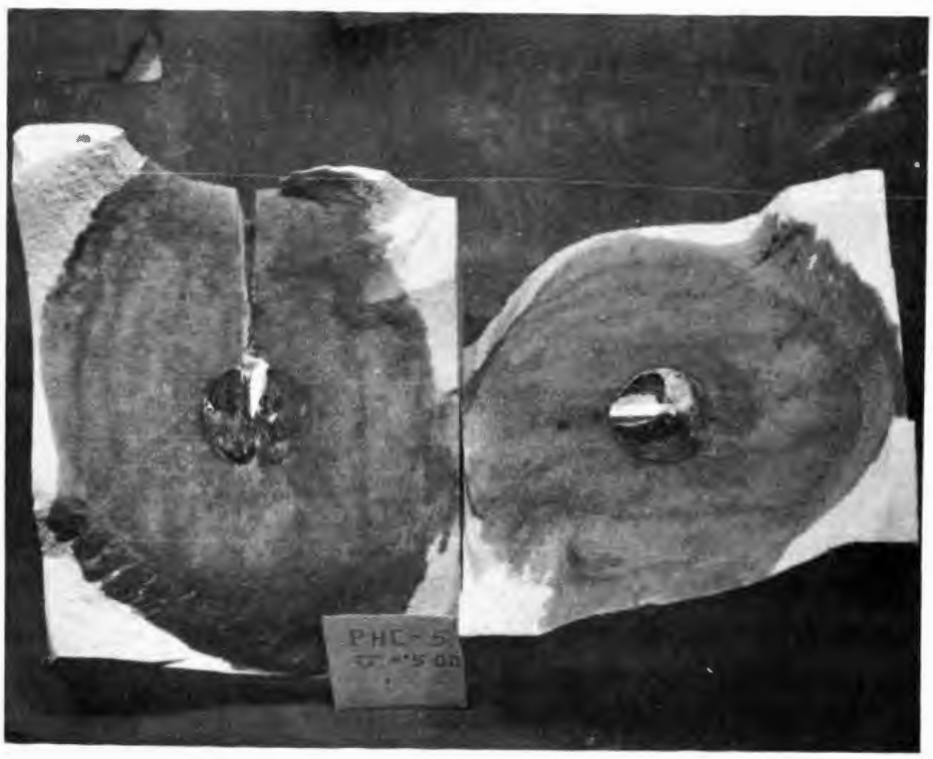

Figure 15. Fractured Block PHC-5.

The block was subjected to an uniaxial load of 500 psi and contained a circular prefracture. The breakdown pressure was observed to be 2750 psi. The fracture extension pressure was kept at 1500 psi with 28 cubic centimeters of fluid required to complete the fracture which broke through on the front side. The fracture zone was that of a circle being distorted because of the curving nature of the fractured surface. The fractured surface started turning immeadiately after leaving the prefracture in a direction parallel to the applied load. The turning rate was greatest in the forward and backward directions corresponding to the Z-axis with the curvature of the front being opposite in direction to that of the back.

Figure 16. Fractured Block PHE-9.

The block was subjected to an uniaxial load of 600 psi and contained an elliptical prefracture. The breakdown pressure was observed to be 1900 psi. The fracture extension pressure was kept at 1500 psi with 75 cubic centimeters of fluid required to complete the fracture which broke out on the top face in a direction parallel to the applied load. The fracture immeadiately turned after leaving the elliptical prefracture in a direction parallel to the applied load forming a continuous curved tensile fracture. The fractured surface approximated that of an elliptical paraboloid. The prefracture exhibited little control on the direction of the fracture propagation.

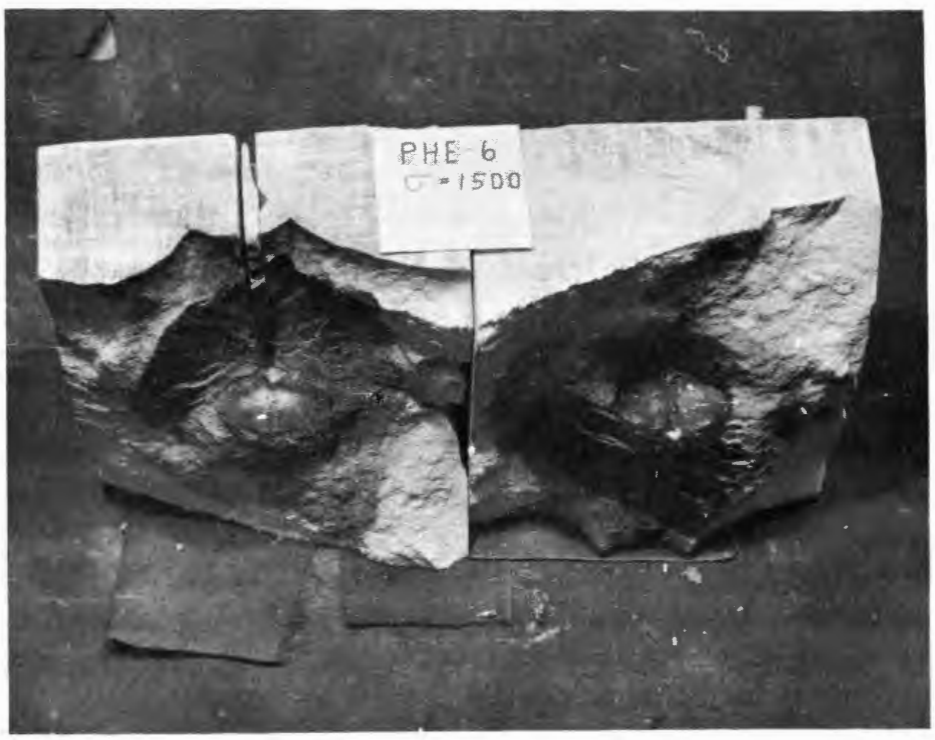

Figure 17. Fractured Block PHE-6

The block was subjected to an uniaxial load of 1500 psi and contained an elliptical prefracture. The breakdown pressure was observed to be 1950 psi. The fracture extension pressure was kept at 2500 psi and 67 cubic centimeters of fluid was required to complete the fracture which first broke out on the top face in a direction parallel to the X-axis. The fractured surface turned immeadiately upon leaving the prefracture in a direction parallel to the applied uniaxial load exhibiting a tensile break. The figure indicates that no control of the fracture orientation due to the presence of the prefracture existed, such that the state of stress of the block at the time of fracture is the governing factor for high stress concentrations.

Biaxial Results

The transition region, where control of the fracture orientation ceases and little or no control is possible, for blocks under biaxial loads was not as definite as was the case with uniaxial loading. Two new parameters enter in, the magnitude of the additional stress and the stress difference.

The lower of the two confining stresses does not appear to affect the orientation of the fracture directly, but plays a secondary role. If the stress difference lies in the neighborhood of 400 psi or less and the maximum stress is kept below 1000 psi, some control of fracture orientation is exhibited. For stress difference of 500 psi or greater, little or no control was possible; the fracture plane immeadiately turned so as to become parallel with the free faces. If the principal stress was much greater than 1000 psi, little or no control was possible irrespective of the magnitude of the secondary stress.

The breakdown pressure for the biaxial loading condition was much higher than that found for the uniaxial case. For the twelve blocks with circular and elliptical prefractures, the average breakdown pressure was 3770 psi with a maximum of 5500 psi and a minimum of 2100 psi.

Figures 18 through 23 show the results of a representative number of blocks containing circular and elliptical prefractures fractured under biaxial loads.

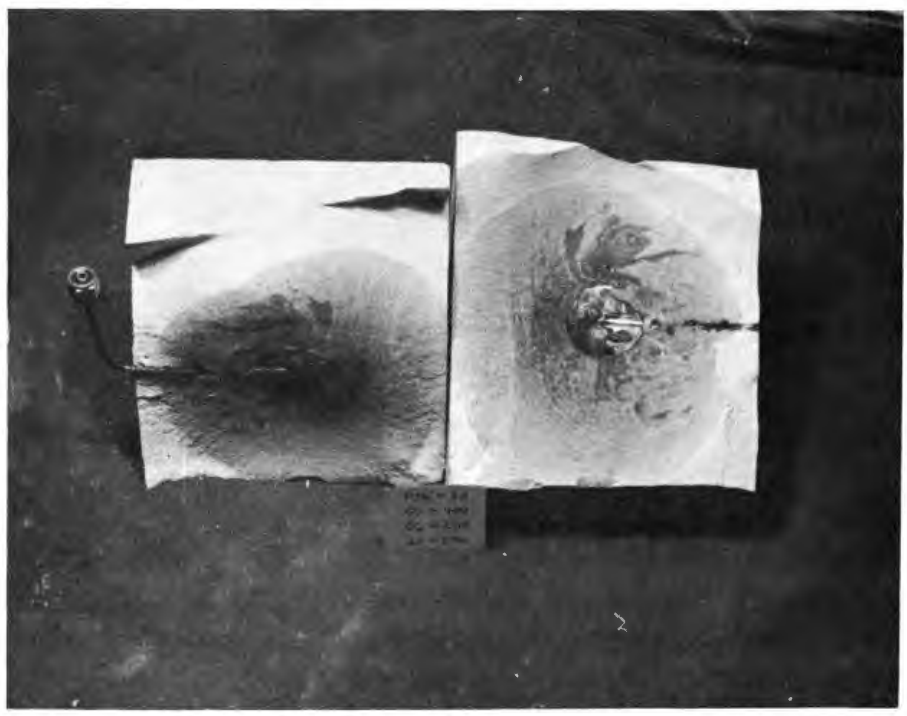

Figure 18. Fractured Block PHC-32.

The block was subjected to a biaxial load of 200 psi in the X-direction and 400 psi in the Y-direction giving a 200 psi stress differential and contained a circular prefracture. The breakdown pressure was observed to be 5200 psi. The fracture extension pressure was kept at 2000 psi requiring 20 cubic centimeters of fluid to complete the fracture which broke out on the back side. The fractured surface followed the plane of the circular prefracture until the edge of the block where it then started to curve so as to align itself parallel to the block's free surface. The fractured surface exhibited a tensile break with the prefracture controlling the orientation of the fracture.

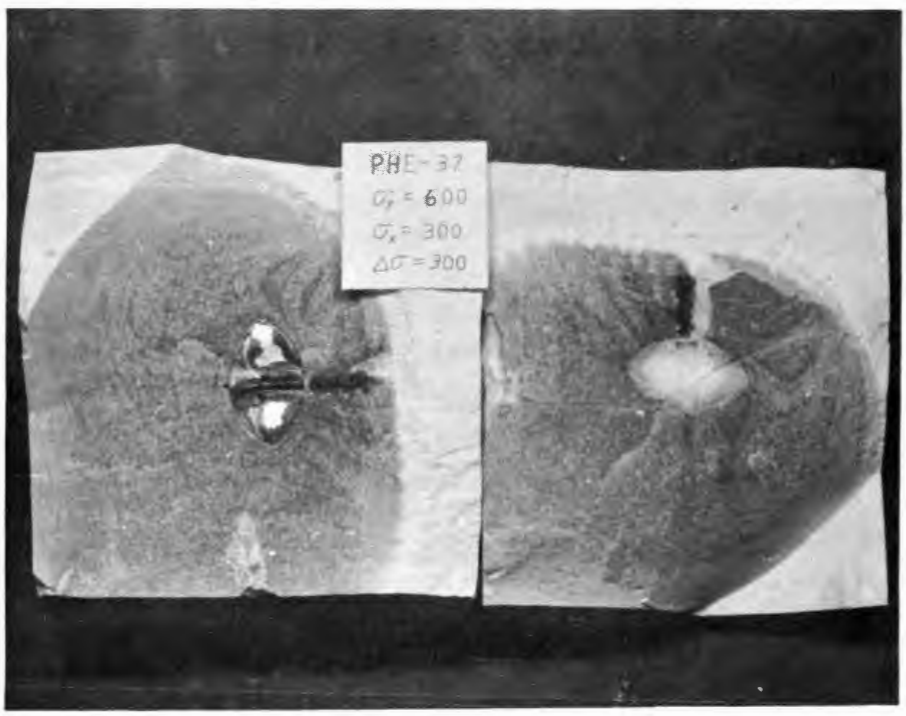

Figure 19. Fractured Block PHE-37.

The block was subjected to a biaxial load of 300 psi in the X-direction and 600 psi in the Y-direction giving a 300 psi stress differential and contained an elliptical prefracture. The breakdown pressure was observed to be 3600 psi. The fracture extension pressure was kept at 2000 psi requiring 23 cubic centimeters of fluid to complete the fracture which broke through on the back face and an adjacent side. The fractured surface exhibits a smooth tensile break, followed the plane of the elliptical prefracture for approximately an inch and a half, and then started turning slowly such as to align itself in a direction perpendicular to the direction of minimum stress.

Figure 20. Fractured Block PHE-31.

The block was subjected to a biaxial load of 600 psi in the X-direction and 800 psi in the Y-direction giving a 200 psi stress differential in the applied load and contained an elliptical prefracture. The breakdown pressure was observed to be 4500 psi. The fracture extension pressure was kept at 2500 psi requiring 25 cubic centimeters of fluid to complete the fracture which broke out on the back face. The fractured surface initiated at the edge of the elliptical prefracture and remained parallel to the surface of the prefracture along the X-direction, but curved in a direction parallel to the maximum stress as it propagated in the Z-direction exhibiting a smooth tensile break.

Figure 21. Fractured Block PHC-29.

The block was subjected to a biaxial load of 500 psi in the X-direction and 1000 psi in the Y-direction giving a differential of 500 psi in the applied stress and contained a circular prefracture. The breakdown pressure was observed to be 2600 psi. The fracture extension pressure was kept at 2000 psi requiring 21 cubic centimeters of fluid to complete the fracture which broke out on the bottom face. The fractured surface initiated from the edge of the circular disc and immeadiately started to curve such as to become parallel to the maximum applied stress as it propagated out. The fractured surface exhibited a continuous curved tensile break.

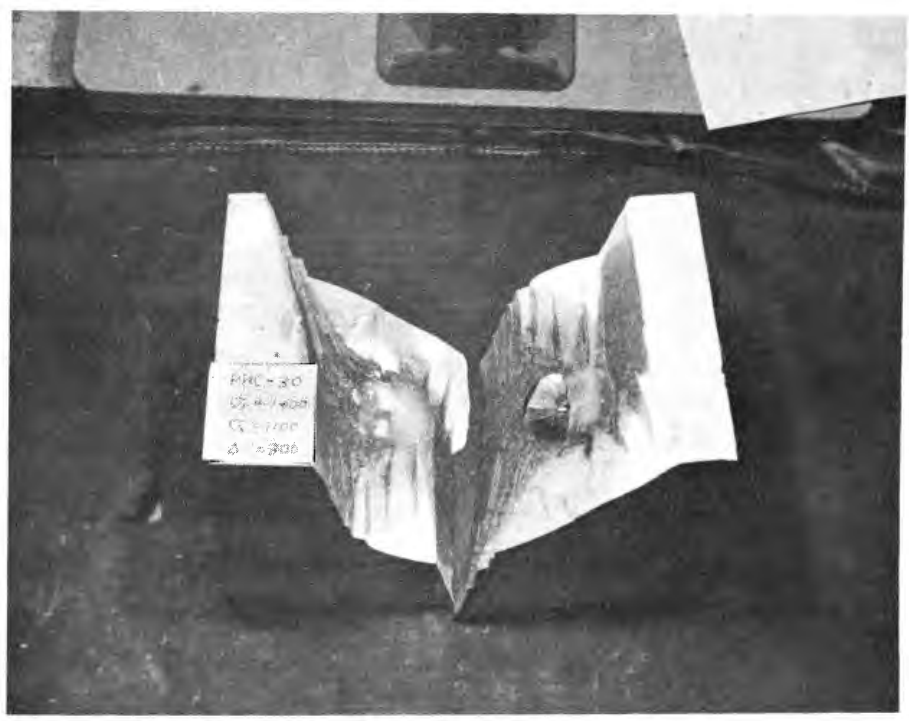

Figure 22. Fractured Block PHC-30.

The block was subjected to a biaxial load of 1100 psi in the X-direction and 1400 psi in the Y-direction giving a stress differential of 300 psi in the applied stress and contained a circular prefracture. The breakdown pressure was observed to be 2800 psi. The fracture extension pressure was kept at 2000 psi requiring 60 cubic centimeters of fluid to complete the fracture which broke out first on the bottom of the block and then on the top face. The fractured surface was irregular consisting of many planes orientated perpendicular to the minimum stress and indicating stepped tensile fractures. Little control of fracture orientation was indicated.

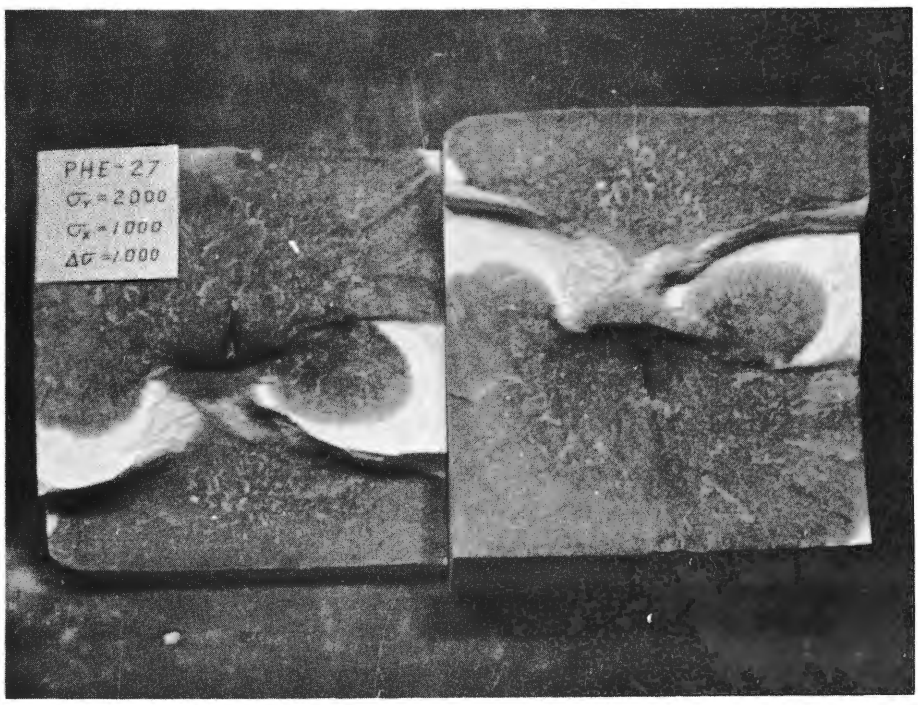

Figure 23. Fractured Block PHE-27.

The block was subjected to a biaxial load of 1000 psi in the X-direction and 2000 psi in the Y-direction giving a stress differential of 1000 psi and contained an elliptical prefracture. The breakdown pressure was observed to be about 5500 psi. The fracture extension pressure was kept at 3000 psi requiring 30 cubic centimeters of fluid to complete the fracture which broke out simulataneously on all four faces in planes perpendicular to the minimum stress. The fractured surfaces consisted of two planes perpendicular to the minimum stress and displaced by the width of the disc, indicating that the initiating points occured where the elliptical brass discs did not overlap.

Hydrostone blocks containing sand inclusions of circular geometry were hydraulically fractured under the same biaxial stress conditions as the blocks with the circular and elliptical brass foils. The experimental results obtained from these block models were not considered satisfactory because of the geometric size of the sand inclusions. During the model preparation the sand flowed such that the inclusions became of the order of three inches in diameter. Nevertheless, the fracture patterns exhibited the same general features as those of the blocks containg the brass foils and subjected to the same loading conditions.

The breakdown pressures of the blocks with sand inclusions were considerably less than those of the blocks with the brass foils. The average breakdown pressure for eleven of the blocks with sand inclusions was 720 psi as compared with 2290 psi for the prefractured blocks under uniaxial loads and 3770 psi for the ones under biaxial loads. This compares favorably to the tensile strength of 140 psi as determined by Haas and Rinehart (14) for hydrostone of the same mixture. Figures 24 and 25 show two blocks with sand inclusions hydraulically fractured under biaxial loads.

Several hydrostone blocks were sawed in half, ground smooth and then clamped together and drilled with a bit of 9/64 inch diameter to a depth of 3 and 1/4 inches. A 1/8 inch steel tube placed within a thin walled rubber insulator was inserted into this cylindrical cavity leaving

a 1/2 inch zone. The models were placed in the biaxial loading apparatus and fractured.

With a biaxial load of 1200 psi in both the X and Y-directions, the fractured surface followed the cut plane exactly giving a symmetrical circular pattern. With a biaxial load of 1200 psi in the X-direction and 2400 psi in the Y-direction, the fractured surface did not follow the cut planes to any extent but was perpendicular to them. Figures 26 and 27 show the results.

The model specimens cast with the two inch square plates proved to be experimental failures. Because of the significant difference in the compressibility of the metal plates as compared to that of the hydrostone, mechanical fractures developed in the neighborhood of the plates when the external load was applied resulting in loss of fluid.

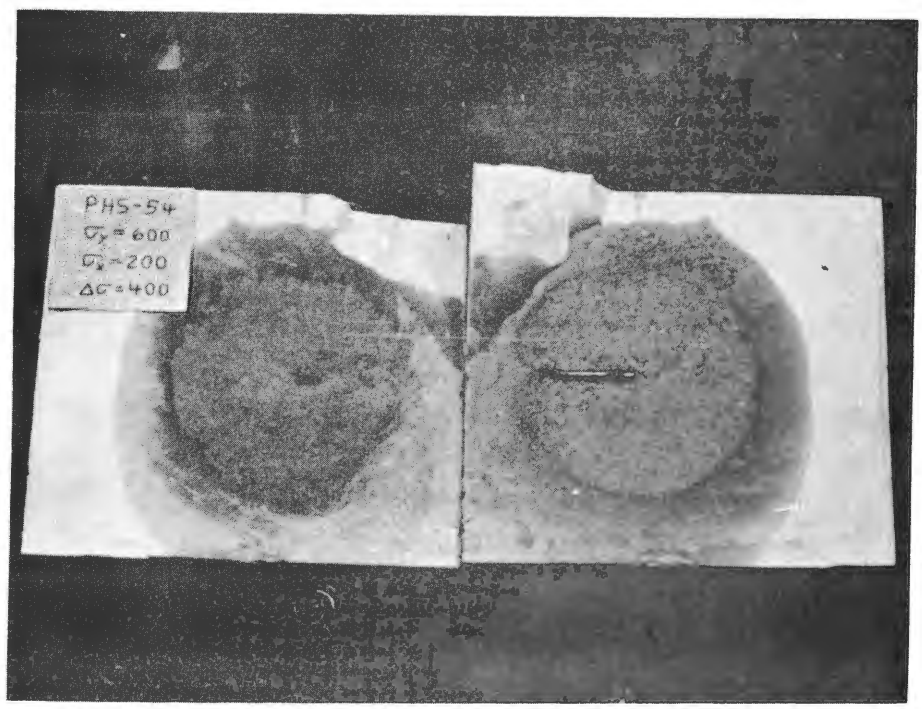

Figure 24. Fractured Block PHS-54.

The block was subjected to a biaxial load of 200 psi in the X-direction and 600 psi in the Y-direction giving a stress differential of 400 psi. The breakdown pressure was observed to be 400 psi. The fracture extension pressure was kept at 1500 psi requiring 13 cubic centimeters of fluid to complete the fracture which broke out on the corner of the front face in a horizontal direction. The fractured surface followed the plane of the sand inclusion, perpendicular to the maximum stress, except for the corner in the front face, opposite where the fracture initially broke out, where it started turning so as to become parallel to the maximum stress indicating asymmetrical loading.

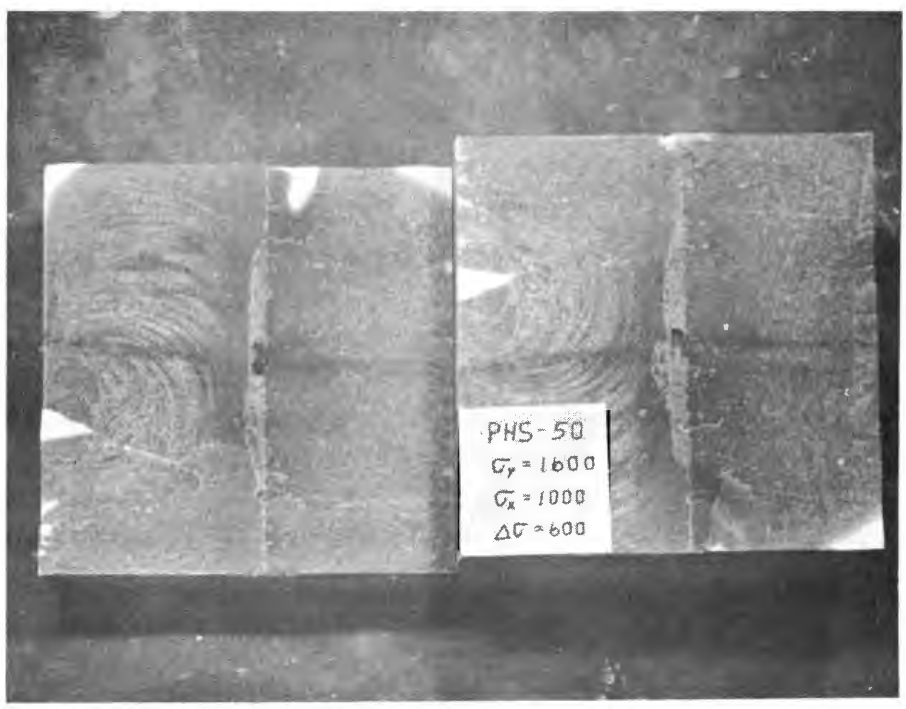

Figure 25. Fractured Block PHS-50.

The block was subjected to a biaxial load of 1000 psi in the X-direction and 1600 psi in the Y-direction giving a stress differential of 600 psi. The breakdown pressure was observed to be 1100 psi. The fracture extension pressure was held at 1500 psi requiring 16 cubic centimeters of fluid to complete the fracture which broke out simultaneously on all four sides parallel to the maximum stress. The fractured surface was perpendicular to the plane formed by the sand inclusion and parallel to the free surfaces of the block. No control of the fracture orientation was exhibited.

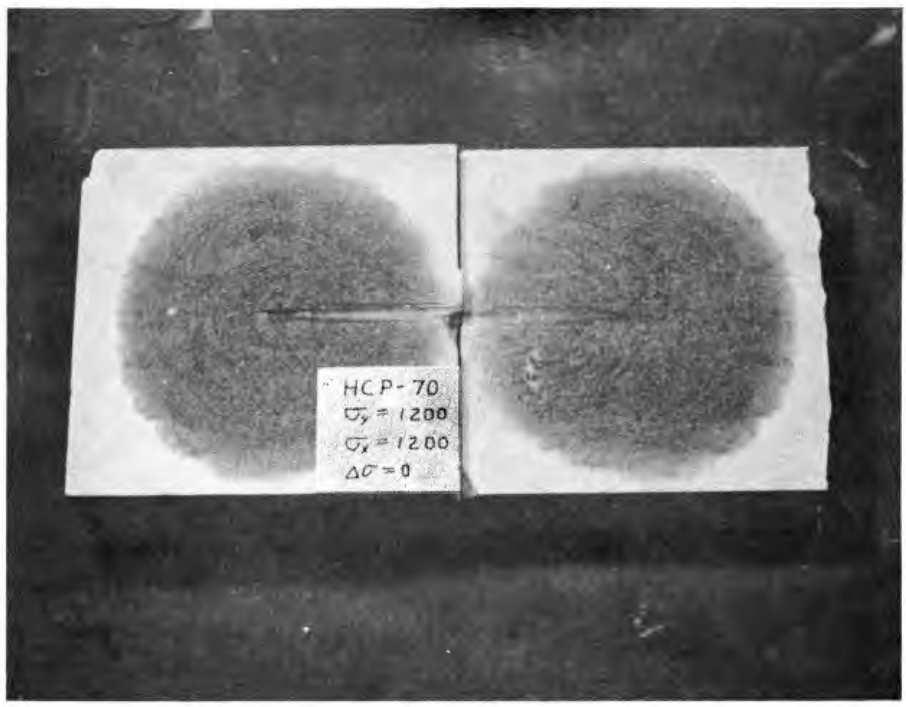

Figure 26. Fractured Block HCP-70.

This hydrostone model consisted of two half blocks ground smooth and then pressed together and drilled with a 9/64 inch bit to a depth of 3 and 1/4 inches. A 1/8 inch steel tube placed inside of a rubber insulator was inserted into the block leaving a cylindrical zone of 1/2 inch length. The block was subjected to a biaxial load of 1200 psi in both the X and Y-directions and hydraulically fractured. The fracture extension pressure was held at 2000 psi requiring 8 cubic centimeters of fluid to complete the fracture which broke out on the front face. The fracture followed the cut planes exactly giving a symmetrical circular pattern. No definite breakdown pressure was observed.

Figure 27. Fractured Block HCP-71.

This hydrostone block model was prepared in the identical manner as HCP-70. The block was subjected to a biaxial load of 1200 psi in the X-direction and 2400 psi in the Y-direction giving a stress differential of 1200 psi. The breakdown pressure was observed to be 1250 psi. The fracture extension pressure was kept at 2000 psi requiring 10 cubic centimeters of fluid to complete the fracture. The resulting fractured surface was two-fold, there was a small, secondary circular fracture lying in the precut planes with the primary fracture perpendicular to the cut planes and initially parallel to the axis of the cylindrical zone and then rotating parallel to the free faces.

CHAPTER V

MATHEMATICAL ANALYSIS

From the analysis of the experimental investigation given in Chapter IV, the controlability of fracture propagation is seen to be influenced by the state of stress of the body being fractured. There appears to be a region of transition, which is evidently a function of the magnitudes and orientations of the principal stresses among other things, where a fracture once initiated in a given direction can be extended in this direction, and in the other extreme, little or no control is possible such that the fracture immeadiately turns and propagates in the direction perpendicular to the least principal stress.

To investigate this transition region in greater detail a mathematical model is presented and calculations made for those stress conditions imposed on the experimental models which exhibited to some degree control of fracture propagation. An analysis is made in Chapter VI between these calculated stresses and the corresponding fractured surfaces of the hydrostone blocks.

The Mathematical Model

The mathematical model used for this development is assumed to be a perfectly elastic material subjected to two independent stress distributions. The first being that

stress associated with a biaxial or uniaxial stress field and the second resulting from the stress associated with an internal circular crack of negligible width under the action of a constant fluid pressure of magnitude P_o.

Consider a biaxial stress acting normally in the X and Y directions with magnitudes σ_x and σ_y respectively. This stress field can be transformed to cylindrical polar coordinates by the following set of equations:

$$(18) \quad \sigma'_r = (\sigma_x+\sigma_y)/2 + [(\sigma_x-\sigma_y)/2]\cos(2\phi)$$

$$(19) \quad \sigma'_\phi = (\sigma_x+\sigma_y)/2 - [(\sigma_x-\sigma_y)/2]\cos(2\phi)$$

$$(20) \quad \sigma'_z = -2\mu(\sigma_x-\sigma_y)\cos(2\phi)$$

$$(21) \quad \tau'_{r\phi} = [(\sigma_x-\sigma_y)/2]\sin(2\phi)$$

$$(22) \quad \tau'_{rz} = \tau'_{z\phi} = 0$$

where μ is Poisson's ratio and r, ϕ, and z are the cylindrical polar coordinates

The distribution of stress in the interior of an elastic solid produced under the action of pressure applied to an internal circular crack has been developed in cylindrical polar coordinates making use of Hankel transforms by Sneddon (46). The introduction of Hankel transforms reduces the problem to that of a pair of dual integral equations.

The development of this stress distribution associated with the pressure applied to an internal circular crack is

given in Appendix B. In this analysis the circular crack of radius c is assumed to lie in the X-Z plane such that there is symmetry about the Y-axis. The stress in the interior of the medium is then specified completely by the stress components σ''_r, σ''_θ, σ''_y and τ''_{ry}. Only the results of this development will be included here; the reader may refer to Appendix B for the detailed analysis.

The components of stress are analyzed by considering three regions of interest which may be expressed as follows:

1. In the plane Y = 0 and r < c.

(23) $\sigma''_r = -P_o(\mu+\frac{1}{2})$

(24) $\sigma''_\theta = -P_o(\mu+\frac{1}{2})$

(25) $\sigma''_y = -P_o$

(26) $\tau''_{ry} = 0$

2. In the plane Y = 0 and r > c.

(27) $\sigma''_r = (2P_o)/\pi[1/(\rho^2-1)^{\frac{1}{2}} - (\mu+\frac{1}{2})\mathrm{Sin}^{-1}(1/\rho)]$

(28) $\sigma''_\theta = (2P_o)/\pi[2\mu/(\rho^2-1)^{\frac{1}{2}} - (\mu+\frac{1}{2})\mathrm{Sin}^{-1}(1/\rho)]$

(29) $\sigma''_y = (2P_o)/\pi[1/(\rho^2-1)^{\frac{1}{2}} - \mathrm{Sin}^{-1}(1/\rho)]$

(30) $\tau''_{ry} = 0$

3. In the region Y ≠ 0.

(31) $\sigma''_y = (2P_o)/\pi[C_2^0 - S_1^2 + (C_3^0 - S_2^0)]$

$$(32)\quad \sigma''_r = P_o/\pi[(1+2\mu)(C_2^0-S_1^0) + \eta(C_3^2-C_3^0+S_2^0-S_2^2) + (S_1^2-C_2^2)(1-2\mu)]$$

$$(33)\quad \sigma''_\theta = P_o/\pi[(1+2\mu)(C_2^0-S_1^0) + \eta(S_2^2-C_3^2+S_2^0-C_3^0) + (C_2^2-S_1^2)(1-2\mu)]$$

$$(34)\quad \tau''_{ry} = [(2P_o)/\pi](C_3^1-S_2^1)$$

where P_o is the fracturing fluid pressure, c is the radius of the circular crack, η is the ratio of Y with c, ρ is the ratio of r with c, and the symbols C_α^β and S_α^β represent various Bessel combinations as defined in Appendix B.

By the method of superposition, these two stress distributions may be combined to give the effective state of stress of the elastic body. This may be accomplished by developing a transformation matrix to transform the biaxial or uniaxial stresses to the coordinate system of the circular crack. The resulting symmetric stress matrix will then be represented by a second order tensor having three components of stress and six components of shear.

Stress Transformation

The stress matrix will be represented in the cylindrical coordinates of the circular shaped crack and may be expressed by the following second order tensor

$$(35)\quad \sigma_{\alpha\beta} = \sigma'_{\alpha\beta} + \sigma''_{\alpha\beta}$$

where $\sigma'_{\alpha\beta}$ is the stress associated with the biaxial or uniaxial stress field and $\sigma''_{\alpha\beta}$ the stress due to the pressurized circular crack. These stresses are given by

$$(36)\quad \sigma''_{\alpha\beta} = \begin{bmatrix} \sigma''_r & 0 & \tau''_{ry} \\ 0 & \sigma''_\theta & 0 \\ \tau''_{ry} & 0 & \sigma''_y \end{bmatrix}$$

and

$$(37)\quad \sigma'_{\alpha\beta} = \begin{bmatrix} \sigma'_{11} & \sigma'_{12} & \sigma'_{13} \\ \sigma'_{21} & \sigma'_{22} & \sigma'_{23} \\ \sigma'_{31} & \sigma'_{32} & \sigma'_{33} \end{bmatrix}$$

The elements of $\sigma'_{\alpha\beta}$ can be found by transforming the components of stress of the biaxial or uniaxial field expressed in terms of the cylindrical polar coordinates (r',ϕ,z) to the cylindrical polar coordinates (r'',θ,y) of the circular crack.

Referring to Figure 28, the following vector relations are obtained:

$$(38)\quad \vec{e}'_1 = \vec{i}\cos\phi + \vec{j}\sin\phi$$

$$(39)\quad \vec{e}'_2 = -\vec{i}\sin\phi + \vec{j}\cos\phi$$

$$(40)\quad \vec{e}'_3 = \vec{k}$$

and

$$(41)\quad \vec{e}''_1 = \vec{i}\cos\theta + \vec{k}\sin\theta$$

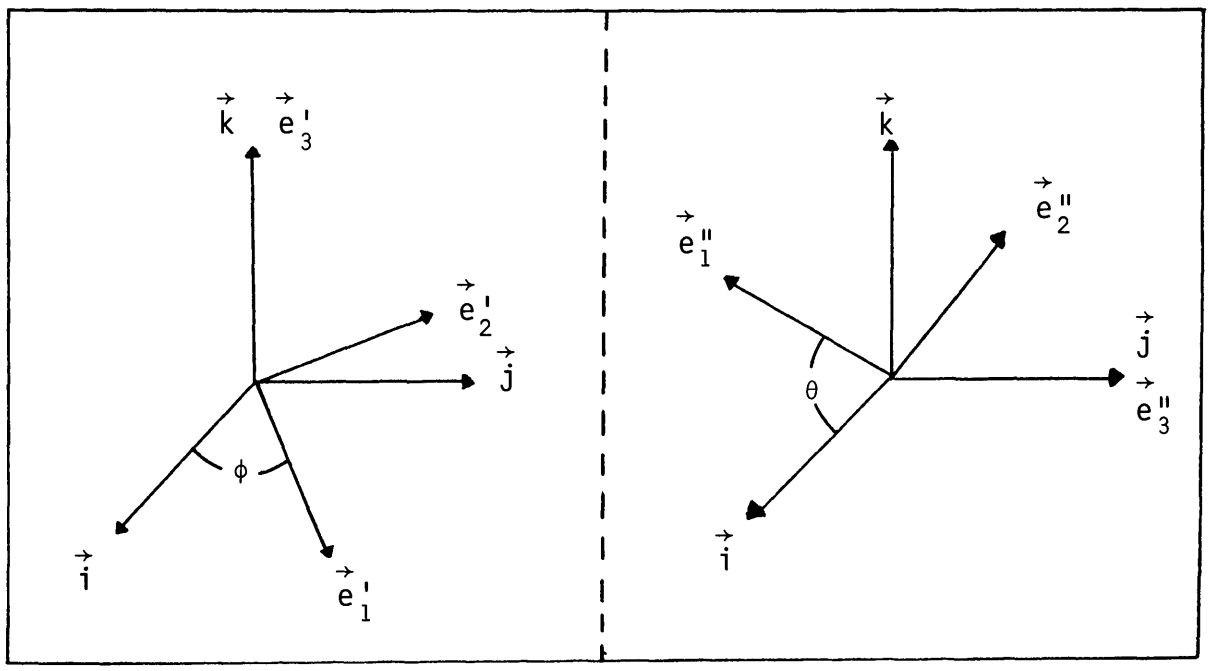

Figure 28. Vector diagrams relating the two cylindrical coordinate systems to the cartesian coordinate system.

$$(42)\quad \vec{e}''_2 = -\vec{i}\sin\theta + \vec{k}\cos\theta$$

$$(43)\quad \vec{e}''_3 = \vec{j}$$

To express the stress components of the cylindrical system (r',ϕ,z) to those of the cylindrical system (r'',θ,y) use is made of the transformation equation

$$(44)\quad \sigma'_{\alpha\beta} = a_{\alpha m}a_{\beta n}\sigma_{mn}$$

where $a_{\alpha m}a_{\beta n}$ are the direction cosines and σ_{mn} represents the components of stress resulting from the biaxial or uniaxial stress field and expressed by

$$(45)\quad \sigma_{mn} = \begin{bmatrix} \sigma'_r & \tau'_{r\phi} & 0 \\ \tau'_{\phi r} & \sigma'_\phi & 0 \\ 0 & 0 & \sigma'_z \end{bmatrix}$$

The direction cosines are found by the following vector multiplications:

$$(46)\quad a_{11} \equiv \vec{e}_1'' \cdot \vec{e}_1' = (\vec{i}\cos\theta + \vec{k}\sin\theta)\cdot(\vec{i}\cos\phi + \vec{j}\sin\phi)$$

$$= \cos\theta\cos\phi$$

$$(47)\quad a_{12} \equiv \vec{e}_1'' \cdot \vec{e}_2' = (\vec{i}\cos\theta + \vec{k}\sin\theta)\cdot(-\vec{i}\sin\phi + \vec{j}\cos\phi)$$

$$= -\cos\theta\sin\phi$$

$$(48)\quad a_{13} \equiv \vec{e}_1'' \cdot \vec{e}_3' = (\vec{i}\cos\theta + \vec{k}\sin\theta)\cdot(\vec{k})$$

$$= \sin\theta$$

$$(49)\quad a_{21} \equiv \vec{e}_2'' \cdot \vec{e}_1' = (-\vec{i}\sin\theta + \vec{k}\cos\theta)\cdot(\vec{i}\cos\phi + \vec{j}\sin\phi)$$

$$= -\sin\theta\cos\phi$$

$$(50)\quad a_{22} \equiv \vec{e}_2'' \cdot \vec{e}_2' = (-\vec{i}\sin\theta + \vec{k}\cos\theta)\cdot(\vec{i}\sin\phi + \vec{j}\sin\phi)$$

$$= \sin\theta\sin\phi$$

$$(51)\quad a_{23} \equiv \vec{e}_2'' \cdot \vec{e}_3' = (-\vec{i}\sin\theta + \vec{k}\cos\theta)\cdot(\vec{k})$$

$$= \cos\theta$$

$$(52)\quad a_{31} \equiv \vec{e}_3'' \cdot \vec{e}_1' = (\vec{j})\cdot(\vec{i}\cos\phi + \vec{j}\sin\phi)$$

$$= \sin\phi$$

$$(53)\quad a_{32} \equiv \vec{e}_3'' \cdot \vec{e}_2' = (\vec{j})\cdot(-\vec{i}\sin\phi + \vec{j}\cos\phi)$$

$$= \cos\phi$$

$$(54)\quad a_{33} \equiv \vec{e}''_3 \cdot \vec{e}'_3 = (\vec{j}) \cdot (\vec{k}) = 0$$

Making use of equations (46) through (54) and expanding equation (44) there is obtained

$$(55)\quad \sigma'_{11} = \cos^2\theta[\sigma'_r\cos^2\phi + \sigma_\phi\sin^2\phi - \tau_{r\phi}\sin(2\phi)] + \sigma_z\sin^2\theta$$

$$(56)\quad \sigma'_{22} = \sin^2\theta[\sigma'_r\cos^2\phi + \sigma_\phi\sin^2\phi] + \sin^2\theta[\sin^2\phi\sigma_z - \tau_{r\phi}\sin(2\phi)]$$

$$(57)\quad \sigma'_{33} = \sigma'_r\sin^2\phi + \sigma_\phi\cos^2\phi + \tau_{r\phi}\sin(2\phi)$$

$$(58)\quad \sigma'_{12} = \sigma'_{21} = (1/2)\sin(2\theta)[-\sigma'_r\cos^2\phi - \sigma_\phi\sin^2\phi + \sigma_z + \tau_{r\phi}\sin(2\phi)]$$

$$(59)\quad \sigma'_{13} = \sigma'_{31} = (1/2)[(\sigma'_r - \sigma_\phi)\sin(2\phi)\cos\theta - 2\tau_{r\phi}\cos(2\phi)\cos\theta]$$

$$(60)\quad \sigma'_{23} = \sigma'_{32} = (1/2)[(\sigma_\phi - \sigma'_r)\sin(2\phi)\sin\theta - 2\tau_{r\phi}\cos(2\phi)\sin\theta]$$

The stress at a point of the elastic solid resulting from the stress associated with the biaxial or uniaxial field and that of the pressurized circular crack is completely represented by the six equations

$$(61)\quad \sigma_r = \sigma_{11} = \sigma''_r + \sigma'_{11}$$

$$(62)\quad \sigma_\theta = \sigma_{22} = \sigma''_\theta + \sigma'_{22}$$

$$(63)\quad \sigma_y = \sigma_{33} = \sigma''_y + \sigma'_{33}$$

$$(64)\quad \tau_{r\theta} = \tau_{\theta r} = \sigma_{12} = \sigma''_{12}$$

$$(65)\quad \tau_{ry} = \tau_{yr} = \sigma_{13} = \sigma'_{13} + \tau''_{ry}$$

$$(66)\quad \tau_{\theta y} = \tau_{y\theta} = \sigma_{23} = \sigma'_{23}$$

or in matrix notation

$$(67)\quad \sigma_{\alpha\beta} = \begin{bmatrix} \sigma''_r + \sigma'_{11} & \sigma''_{12} & \sigma'_{13} + \tau''_{ry} \\ \sigma''_{12} & \sigma''_\theta + \sigma'_{22} & \sigma'_{23} \\ \sigma'_{13} + \tau''_{ry} & \sigma'_{23} & \sigma''_y + \sigma'_{33} \end{bmatrix}$$

The matrix given by equation (67) can be put into canonical form thus exhibiting the principal stresses and their associated directions by obtaining the characteristic numbers and vectors. This facilitates the determination of the maximum shear components at the various points of interest and serve as a means of comparing the actual fractured surface with the expected surface of fracture.

Numerical Calculations and Results

The numerical results from the various stress distributions of interest were obtained by use of the IBM 1620 computer. To obtain maximum diversity of stress distributions and econimization of computer time, the computer program was divided into three phases with the output of the first

two phases serving as input for the third phase. The three phases were: (1) stress around a circular crack on the plane Y = 0, (2) stress around a circular crack for Y ≠ 0, and (3) stress due to biaxial or uniaxial loading, transformation of coordinates and diagonalization to quadratic form. The format of these programs is given in Appendix C.

Tables VI through IX give the results of the calculations of the stress ratios with the internal pressure for a sequence of values of ρ and η taking Poisson's ratio as .18. These tables show that the stress associated with the pressurized internal circular crack decrease rapidly as one moves away from the crack such that the contribution falls to a fraction of a percent at a distance of approximately four times the crack radius. Figures 29 through 32 give a graphical representation of the variation of the stress ratios with P_o as a function of ρ for several values of η.

Tables X through XIX give the stress calculations for a number of represenative points corresponding to the experimental stress conditions of the fractured hydrostone specimens upon which contour data was taken and tabularized in Table V. The selected points were chosen from a cylindrical region extending a distance of three crack radii in the radial direction and a distance of two crack radii in the Y-direction.

The tables are interpreted as follows. The first column gives the geometrical location of the stress points under consideration with respect to the center of the pre-

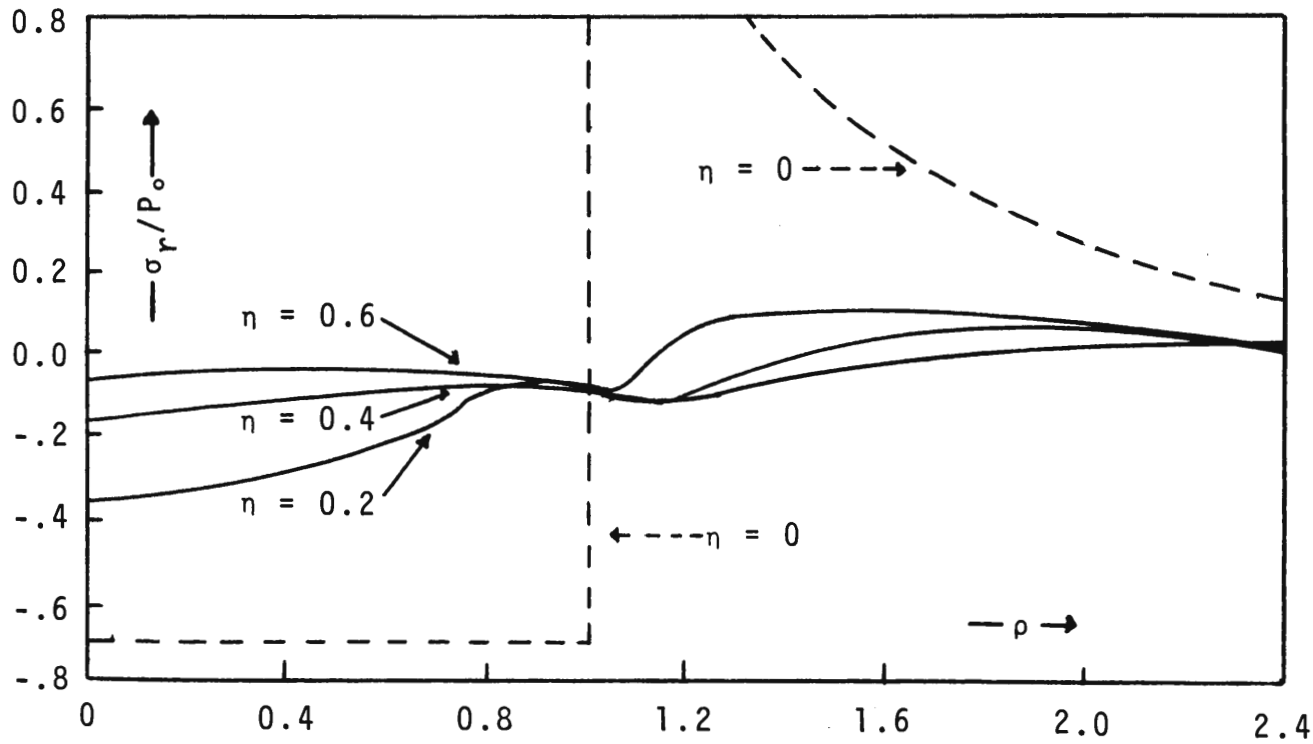

Figure 29. The variation of the radial component of stress, σ_r' with ρ and η.

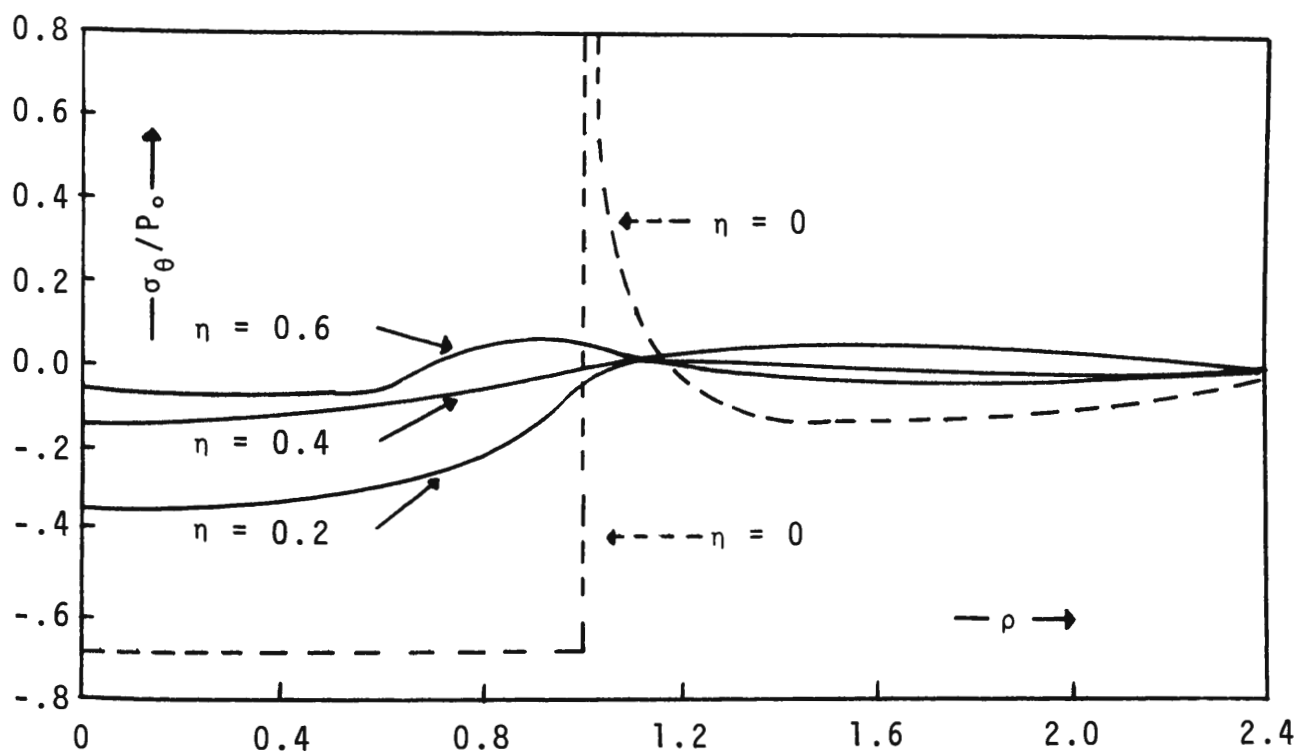

Figure 30. The variation of the hoop stress, σ_θ, with ρ and η.

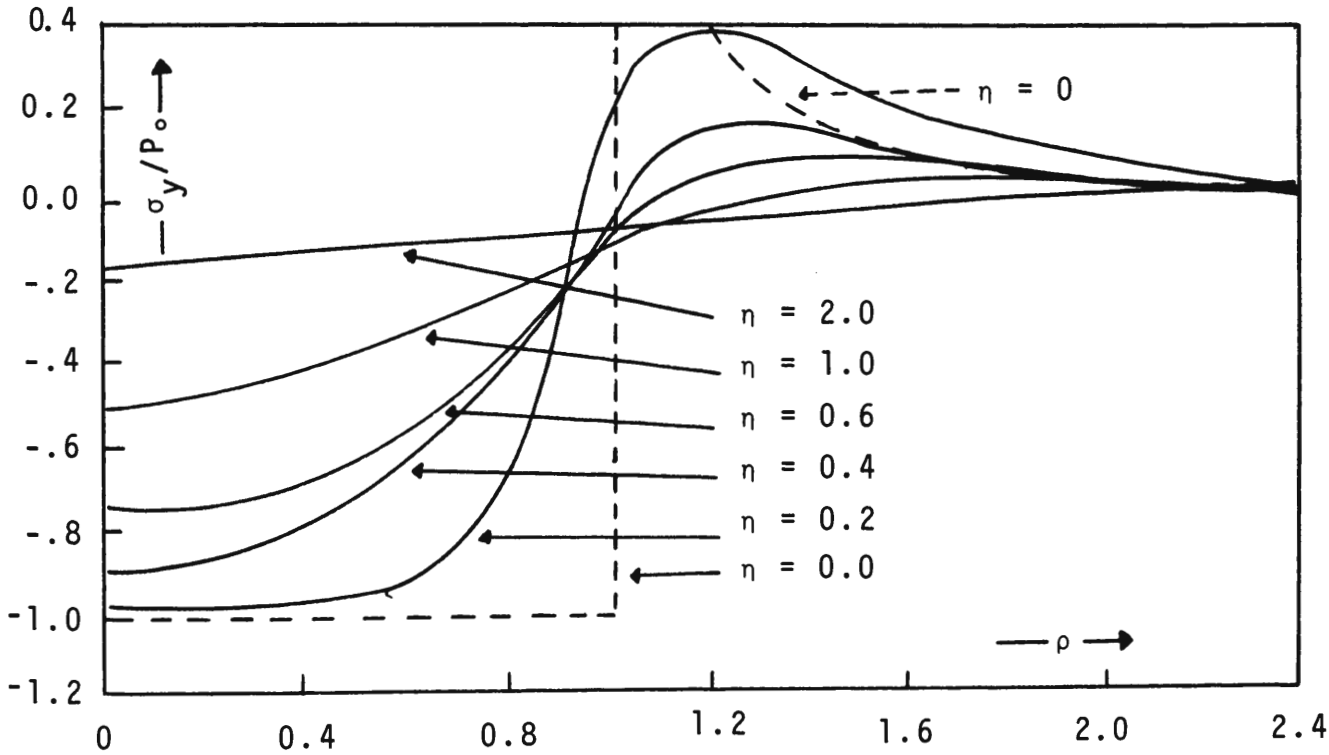

Figure 31. The variation of the normal component of stress, σ'_y, with ρ and η.

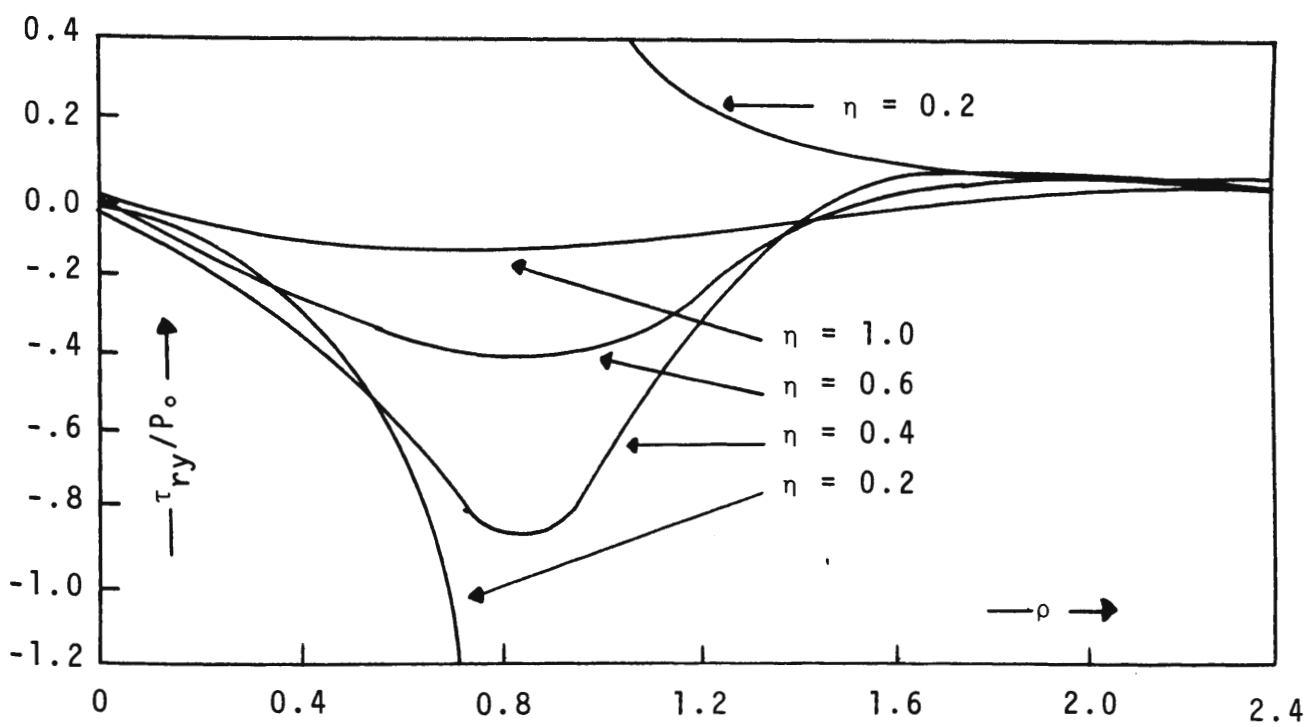

Figure 32. The variation of shearing stress, τ'_{ry}, with ρ and η.

TABLE VI

THE VARIATION OF σ_r WITH ρ AND η

η \ ρ	0.2	0.4	0.6	0.8	1.0	1.2	1.6	2.0	2.4	2.8	3.2	3.6	4.0
0.0	-.680	-.680	-.680	-.680	∞	1.154	.512	.271	.134	.044	-.020	-.069	-.107
0.2	-.380	-.334	-.233	-.062	-.142	.027	.080	.044	.026	.016	.010	.008	.006
0.4	-.164	-.127	-.080	-.076	-.148	-.114	.012	.024	.019	.013	.009	.007	.005
0.6	-.044	-.035	-.038	-.520	-.118	-.115	-.031	.003	.009	.009	.007	.005	.004
0.8	.011	.002	-.041	-.053	-.086	-.093	-.048	-.013	.000	.004	.004	.004	.003
1.0	.031	.018	-.006	-.035	-.059	-.070	-.050	-.022	-.007	-.001	.002	.002	.002
1.2	.036	.023	.003	-.020	-.040	-.050	-.044	-.025	-.011	-.004	-.001	.001	.001
1.4	.034	.023	.008	-.010	-.025	-.035	-.036	-.025	-.014	-.007	-.003	-.001	.000
1.6	.030	.022	.010	-.004	-.016	-.024	-.029	-.023	-.015	-.008	-.004	-.002	-.001
1.8	.026	.020	.011	.001	-.009	-.016	-.022	-.020	-.014	-.009	-.005	-.003	-.001
2.0	.022	.018	.011	.003	-.005	-.011	-.017	-.017	-.013	-.009	-.006	-.004	-.002
2.2	.018	.015	.010	.004	-.002	-.007	-.013	-.014	-.012	-.009	-.006	-.004	-.003
2.4	.015	.013	.009	.005	.000	-.004	-.009	-.011	-.010	-.008	-.006	-.004	-.003
2.6	.013	.011	.008	.005	.001	-.002	-.007	-.009	-.009	-.007	-.006	-.004	-.003
2.8	.011	.010	.007	.005	.002	-.001	-.005	-.007	-.007	-.007	-.005	-.004	-.003
3.0	.009	.008	.007	.005	.002	.000	-.003	-.006	-.006	-.006	-.006	-.005	-.003
3.2	.008	.007	.006	.004	.003	.001	-.002	-.004	-.005	-.005	-.004	-.004	-.003
3.4	.007	.006	.005	.004	.003	.001	-.002	-.003	-.004	-.004	-.004	-.004	-.003
3.6	.006	.005	.005	.004	.003	.001	-.001	-.003	-.004	-.004	-.004	-.003	-.003
3.8	.005	.005	.004	.003	.002	.001	.000	-.002	-.003	-.003	-.003	-.003	-.003
4.0	.004	.004	.004	.003	.003	.002	.001	.001	-.001	-.002	-.003	-.003	-.002

TABLE VII

THE VARIATION OF σ_θ WITH ρ AND η

η \ ρ	0.2	0.4	0.6	0.8	1.0	1.2	1.6	2.0	2.4	2.8	3.2	3.6	4.0
0.0	-.680	-.680	-.680	-.680	∞	-.081	-.112	-.096	-.082	-.071	-.062	-.055	-.050
0.2	-.387	-.364	-.315	-.207	-.033	.002	-.007	-.005	-.004	-.002	-.002	-.001	-.001
0.4	-.169	-.146	-.105	-.049	-.004	.005	-.003	-.004	-.003	-.002	-.001	-.001	-.001
0.6	-.044	-.031	-.012	.621	.015	.013	.002	-.001	-.002	-.002	-.001	-.001	-.001
0.8	.014	.019	.075	.026	.024	.018	.006	.001	-.001	-.001	-.001	-.001	-.001
1.0	.036	.036	.035	.032	.026	.020	.009	.003	.001	.000	.000	-.001	.000
1.2	.040	.039	.035	.031	.026	.020	.010	.004	.002	.000	.000	.000	.000
1.4	.037	.036	.032	.028	.024	.019	.011	.005	.002	.001	.000	.000	.000
1.6	.033	.031	.028	.025	.021	.017	.010	.006	.003	.001	.001	.000	.000
1.8	.028	.026	.024	.022	.019	.015	.010	.006	.003	.002	.001	.000	.000
2.0	.023	.022	.020	.018	.016	.014	.009	.006	.003	.002	.001	.001	.000
2.2	.019	.018	.017	.016	.014	.012	.008	.006	.003	.002	.001	.001	.000
2.4	.016	.015	.015	.013	.012	.011	.008	.005	.003	.002	.001	.001	.000
2.6	.013	.013	.012	.011	.010	.009	.007	.005	.003	.002	.001	.001	.001
2.8	.011	.011	.010	.010	.009	.008	.006	.005	.003	.002	.001	.001	.001
3.0	.010	.009	.009	.008	.008	.007	.006	.004	.003	.002	.002	.001	.001
3.2	.008	.008	.008	.007	.007	.006	.005	.004	.003	.002	.002	.001	.001
3.4	.007	.007	.007	.006	.006	.005	.004	.004	.003	.002	.001	.001	.001
3.6	.006	.006	.006	.005	.005	.005	.004	.003	.003	.002	.001	.001	.001
3.8	.005	.005	.005	.005	.005	.004	.004	.003	.002	.002	.001	.001	.001
4.0	.005	.005	.004	.004	.004	.004	.003	.003	.002	.002	.001	.001	.001

TABLE VIII

THE VARIATION OF σ_y WITH ρ AND η

η \ ρ	0.2	0.4	0.6	0.8	1.0	1.2	1.6	2.0	2.4	2.8	3.2	3.6	4.0
0.0	-1.00	-1.00	-1.00	-1.00	∞	.332	.074	.030	.016	.009	.006	.004	.003
0.2	-.985	-.975	-.937	-.729	.232	.358	.089	.036	.019	.011	.007	.005	.004
0.4	-.905	-.861	-.742	-.451	-.005	.189	.095	.040	.021	.012	.008	.005	.004
0.6	-.768	-.700	-.561	-.425	-.081	.068	.080	.041	.022	.013	.008	.005	.004
0.8	-.617	-.548	-.413	-.269	-.108	.002	.055	.038	.022	.013	.009	.006	.004
1.0	-.481	-.424	-.333	-.222	-.113	-.032	.032	.031	.021	.013	.009	.006	.004
1.2	-.371	-.328	-.263	-.185	-.109	-.049	.012	.022	.018	.013	.009	.006	.004
1.4	-.286	-.255	-.209	-.154	-.100	-.055	-.001	.014	.015	.011	.008	.006	.004
1.6	-.223	-.201	-.168	-.129	-.090	-.056	-.010	.007	.011	.010	.008	.006	.004
1.8	-.175	-.159	-.136	-.108	-.079	-.053	-.016	.002	.007	.008	.007	.005	.004
2.0	-.139	-.127	-.111	-.091	-.070	-.050	-.019	-.003	.004	.006	.006	.005	.004
2.2	-.111	-.103	-.091	-.076	-.061	-.046	-.021	-.006	.002	.004	.005	.004	.004
2.4	-.090	-.084	-.076	-.065	-.053	-.041	-.021	-.008	-.001	.003	.004	.004	.003
2.6	-.074	-.070	-.063	-.055	-.046	-.037	-.021	-.009	-.002	.001	.003	.003	.003
2.8	-.061	-.058	-.053	-.047	-.040	-.033	-.020	-.010	-.004	.000	.002	.002	.002
3.0	-.051	-.049	-.045	-.040	-.035	-.029	-.019	-.010	-.005	-.001	.001	.002	.002
3.2	-.043	-.041	-.039	-.035	-.031	-.026	-.018	-.010	-.005	-.002	.000	.001	.002
3.4	-.037	-.035	-.033	-.030	-.027	-.023	-.017	-.010	-.006	-.002	.000	.001	.001
3.6	-.031	-.030	-.029	-.026	-.024	-.021	-.015	-.010	-.006	-.003	-.001	.000	.001
3.8	-.027	-.026	-.025	-.023	-.021	-.019	-.014	-.009	-.006	-.003	-.001	.000	.000
4.0	-.024	-.023	-.022	-.020	-.019	-.017	-.013	-.009	-.006	-.003	-.002	-.001	.000

TABLE IX

THE VARIATION OF τ_{ry} WITH ρ AND η

η \ ρ	0.2	0.4	0.6	0.8	1.0	1.2	1.6	2.0	2.4	2.8	3.2	3.6	4.0
0.0	.000	.000	.000	.000	.000	.000	.000	.000	.000	.000	.000	.000	.000
0.2	-.098	-.252	-.604	-1.63	-2.09	.195	.149	.054	.024	.012	.007	.004	.003
0.4	-.137	-.316	-.583	-.885	-.772	-.243	.053	.035	.019	.010	.006	.004	.003
0.6	-.124	-.259	-.397	-.318	-.408	-.222	-.010	.016	.012	.008	.005	.003	.002
0.8	-.092	-.181	-.600	-.280	-.244	-.164	-.036	.001	.001	.001	.001	.003	.002
1.0	-.063	-.119	-.159	-.173	-.155	-.117	-.042	-.009	.001	.003	.003	.002	.002
1.2	-.041	-.077	-.101	-.110	-.103	-.083	-.039	-.013	-.003	.001	.001	.001	.001
1.4	-.027	-.050	-.066	-.072	-.070	-.060	-.034	-.014	-.005	-.001	.000	.001	.001
1.6	-.018	-.033	-.044	-.049	-.048	-.043	-.028	-.014	-.006	-.002	.000	.000	.000
1.8	-.012	-.022	-.029	-.033	-.034	-.032	-.022	-.013	-.006	-.003	-.001	.000	.000
2.0	-.008	-.015	-.020	-.023	-.024	-.023	-.018	-.011	-.006	-.003	-.001	-.001	.000
2.2	-.006	-.010	-.014	-.017	-.018	-.017	-.014	-.010	-.006	-.003	-.002	-.001	.000
2.4	-.004	-.007	-.010	-.012	-.013	-.013	-.011	-.008	-.005	-.003	-.002	-.001	.000
2.6	-.003	-.005	-.008	-.009	-.010	-.009	-.007	-.005	-.003	-.002	-.002	-.001	-.001
2.8	-.002	-.004	-.005	-.007	-.007	-.008	-.007	-.006	-.004	-.003	-.002	-.001	-.001
3.0	-.002	-.003	-.004	-.005	-.006	-.006	-.005	-.004	-.003	-.002	-.001	-.001	-.001
3.2	-.001	-.002	-.003	-.004	-.004	-.005	-.005	-.004	-.003	-.002	-.001	-.001	-.001
3.4	-.001	-.002	-.002	-.003	-.003	-.004	-.004	-.003	-.003	-.002	-.001	-.001	-.001
3.6	-.001	-.001	-.002	-.002	-.003	-.003	-.003	-.003	-.002	-.002	-.001	-.001	-.001
3.8	-.001	-.001	-.001	-.002	-.002	-.002	-.002	-.002	-.002	-.002	-.001	-.001	-.001
4.0	.000	-.001	-.001	-.001	-.002	-.002	-.002	-.002	-.002	-.001	-.001	-.001	-.001

fracture. R refers to the radial distance measured in increments of one-half inch such that R = 1 corresponds to a distance of one-half inch from the center of the prefracture. Y is the perpendicular distance from the plane of the block containing the prefracture measured in increments of one-half inch with Y = 1 representing the plane of zero displacement. Θ is the angle measured from the X-axis in the counter clockwise sense. The angular increment is a function of the radial displacement and is given by the relation

$$(68) \quad \Delta\Theta = 360°/6R$$

where, because of symmetry, only π radians have been included.

The columns headed by S_1, S_2, and S_3 give the principal stress components in units of psi. The columns headed "Vector" are the normalized unit vectors associated with these principal stresses where a factor of 10 has been introduced to eliminate the decimal and are expressed in the directions of R, Θ, and Y respectively.

TABLE X

MATHEMATICAL STRESS CALCULATIONS FOR BLOCK PHE-11 & PHC-12

Stress Pt. (R,Y,θ)	S_1	σ_x = 0 Vector	S_2	σ_y = -200 Vector	S_3	P_o = 1200 Vector
(1,1,1)	-816	(1, 0, 0)	-816	(0, 1, 0)	-1400	(0, 0, 1)
(1,1,2)	-824	(7,-7, 0)	-808	(7, 7, 0)	-1400	(0, 0, 1)
(1,1,3)	-808	(7,-7, 0)	-824	(7, 7, 0)	-1400	(0, 0, 1)
(2,1,1)	1001	(1, 0, 0)	-133	(0, 1, 0)	12	(0, 0, 1)
(2,1,2)	1001	(9, 0, 0)	-133	(0, 9, 0)	12	(0, 0, 1)
(2,1,3)	1001	(9, 0, 0)	-133	(0, 9, 0)	12	(0, 0, 1)
(2,1,4)	1001	(1, 0, 0)	-133	(0, 1, 0)	12	(0, 0, 1)
(2,1,5)	1001	(9, 0, 0)	-133	(0, 9, 0)	12	(0, 0, 1)
(2,1,6)	1001	(9, 0, 0)	-133	(0, 9, 0)	12	(0, 0, 1)
(3,1,1)	326	(1, 0, 0)	-116	(0, 1, 0)	-163	(0, 0, 1)
(3,1,2)	326	(9, 0, 0)	-116	(0, 9, 0)	-163	(0, 0, 1)
(3,1,3)	326	(9, 0, 0)	-116	(0, 9, 0)	-163	(0, 0, 1)
(3,1,4)	326	(9, 0, 0)	-116	(0, 9, 0)	-163	(0, 0, 1)
(3,1,5)	326	(9, 0, 0)	-116	(0, 9, 0)	-163	(0, 0, 1)
(3,1,6)	326	(9, 0, 0)	-116	(0, 9, 0)	-163	(0, 0, 1)
(3,1,7)	326	(9, 0, 0)	-116	(0, 9, 0)	-163	(0, 0, 1)
(3,1,8)	326	(9, 0, 0)	-116	(0, 9, 0)	-163	(0, 0, 1)
(3,1,9)	326	(9, 0, 0)	-116	(0, 9, 0)	-163	(0, 0, 1)
(1,2,1)	169	(8, 0,-4)	10	(0, 1, 0)	-958	(4, 0, 8)
(1,2,2)	170	(8, 0,-4)	9	(0, 9, 0)	-958	(4, 0, 8)
(1,2,3)	170	(8, 0,-4)	9	(0, 9, 0)	-958	(4, 0, 8)
(2,2,1)	33	(7, 0,-7)	13	(0, 1, 0)	-249	(7, 0, 7)
(2,2,2)	34	(6, 2,-6)	12	(-1, 9, 1)	-249	(7, 0, 7)
(2,2,3)	34	(6, 2,-6)	12	(-1, 9, 1)	-249	(7, 0, 7)
(2,2,4)	33	(7, 0,-7)	13	(0, 1, 0)	-249	(7, 0, 7)
(2,2,5)	34	(6,-2,-6)	12	(1, 9,-1)	-249	(7, 0, 7)
(2,2,6)	34	(6,-2,-6)	12	(1, 9,-1)	-249	(7, 0, 7)
(3,2,1)	-3	(9, 0, 0)	-1	(0, 1, 0)	-152	(0, 0, 9)
(3,2,2)	-7	(7,-6, 0)	4	(6, 7, 0)	-152	(0, 0, 9)
(3,2,3)	-10	(7,-6, 0)	7	(6, 7, 0)	-152	(0, 0, 9)
(3,2,4)	-9	(7,-6, 0)	6	(6, 7, 0)	-152	(0, 0, 9)
(3,2,5)	-5	(8,-5, 0)	2	(5, 8, 0)	-152	(0, 0, 9)
(3,2,6)	-5	(8, 5, 0)	2	(-5, 8, 0)	-152	(0, 0, 9)
(3,2,7)	-9	(7, 6, 0)	6	(-6, 7, 0)	-152	(0, 0, 9)
(3,2,8)	-10	(7, 6, 0)	7	(-6, 7, 0)	-152	(0, 0, 9)
(3,2,9)	-7	(7, 6, 0)	4	(-6, 7, 0)	-152	(0, 0, 9)
(3,3,1)	-28	(9, 0,-1)	6	(0, 1, 0)	-182	(1, 0, 9)
(3,3,2)	-29	(9,-1,-1)	7	(1, 9, 0)	-182	(1, 0, 9)
(3,3,3)	-31	(9,-2,-1)	8	(2, 9, 0)	-182	(1, 0, 9)
(3,3,4)	-30	(9,-2,-1)	8	(2, 9, 0)	-182	(1, 0, 9)
(3,3,5)	-29	(9, 0,-1)	6	(0, 9, 0)	-182	(1, 0, 9)
(3,3,6)	-29	(9, 0,-1)	6	(0, 9, 0)	-182	(1, 0, 9)
(3,3,7)	-30	(9, 2,-1)	8	(-2, 9, 0)	-182	(1, 0, 9)
(3,3,8)	-31	(9, 2,-1)	8	(-2, 9, 0)	-182	(1, 0, 9)
(3,3,9)	-29	(9, 1,-1)	7	(-1, 9, 0)	-182	(1, 0, 9)

TABLE XI

MATHEMATICAL STRESS CALCULATIONS FOR BLOCK PHE-1 & PHC-16

Stress Pt.		σ_x = 0		σ_y = -300		P_o = 1200
(R,Y,θ)	S_1	Vector	S_2	Vector	S_3	Vector
(1,1,1)	-816	(1, 0, 0)	-816	(0, 1, 0)	-1500	(0, 0, 1)
(1,1,2)	-828	(7,-7, 0)	-804	(7, 7, 0)	-1500	(0, 0, 1)
(1,1,3)	-804	(7,-7, 0)	-828	(7, 7, 0)	-1500	(0, 0, 1)
(2,1,1)	1001	(1, 0, 0)	-133	(0, 1, 0)	-88	(0, 0, 1)
(2,1,2)	1002	(9, 0, 0)	-133	(0, 9, 0)	-88	(0, 0, 1)
(2,1,3)	1002	(9, 0, 0)	-133	(0, 9, 0)	-88	(0, 0, 1)
(2,1,4)	1001	(1, 0, 0)	-133	(0, 1, 0)	-88	(0, 0, 1)
(2,1,5)	1001	(9, 0, 0)	-133	(0, 9, 0)	-88	(0, 0, 1)
(2,1,6)	1002	(9, 0, 0)	-133	(0, 9, 0)	-88	(0, 0, 1)
(3,1,1)	326	(1, 0, 0)	-116	(0, 1, 0)	-263	(0, 0, 1)
(3,1,2)	326	(9, 0, 0)	-116	(0, 9, 0)	-263	(0, 0, 1)
(3,1,3)	326	(9, 0, 0)	-116	(0, 9, 0)	-263	(0, 0, 1)
(3,1,4)	326	(9, 0, 0)	-116	(0, 9, 0)	-263	(0, 0, 1)
(3,1,5)	326	(9, 0, 0)	-116	(0, 9, 0)	-263	(0, 0, 1)
(3,1,6)	326	(9, 0, 0)	-116	(0, 9, 0)	-263	(0, 0, 1)
(3,1,7)	326	(9, 0, 0)	-116	(0, 9, 0)	-263	(0, 0, 1)
(3,1,8)	326	(9, 0, 0)	-116	(0, 9, 0)	-263	(0, 0, 1)
(3,1,9)	326	(9, 0, 0)	-116	(0, 9, 0)	-263	(0, 0, 1)
(1,2,1)	151	(9, 0,-4)	10	(0, 1, 0)	-1040	(4, 0, 9)
(1,2,2)	152	(9, 0,-4)	9	(0, 9, 0)	-1040	(4, 0, 9)
(1,2,3)	152	(9, 0,-4)	9	(0, 9, 0)	-1040	(4, 0, 9)
(2,2,1)	-8	(8, 0,-5)	13	(0, 1, 0)	-308	(5, 0, 8)
(2,2,2)	-11	(7,-3,-5)	17	(3, 9,-1)	-308	(5, 0, 8)
(2,2,3)	-11	(7,-3,-5)	17	(3, 9,-1)	-308	(5, 0, 8)
(2,2,4)	-8	(8, 0,-5)	13	(0, 1, 0)	-308	(5, 0, 8)
(2,2,5)	-11	(7, 3,-5)	17	(-3, 9,-1)	-308	(5, 0, 8)
(2,2,6)	-11	(7, 3,-5)	17	(-3, 9, 1)	-308	(5. 0, 8)
(3,2,1)	-3	(9, 0, 0)	-1	(0, 1, 0)	-252	(0, 0, 9)
(3,2,2)	-11	(7,-6, 0)	7	(6, 7, 0)	-252	(0, 0, 9)
(3,2,3)	-15	(7,-6, 0)	12	(6, 7, 0)	-252	(0, 0, 9)
(3,2,4)	-14	(7,-6, 0)	10	(6, 7, 0)	-252	(0, 0, 9)
(3,2,5)	-7	(7,-6, 0)	3	(6, 7, 0)	-252	(0, 0, 9)
(3,2,6)	-7	(7, 6, 0)	3	(-6, 7, 0)	-252	(0, 0, 9)
(3,2,7)	-14	(7, 6, 0)	10	(-6, 7, 0)	-252	(0, 0, 9)
(3,2,8)	-15	(7, 6, 0)	12	(-6, 7, 0)	-252	(0, 0, 9)
(3,2,9)	-11	(7, 6, 0)	7	(-6, 7, 0)	-252	(0, 0, 9)
(3,3,1)	-29	(9, 0, 0)	6	(0, 1, 0)	-281	(0, 0, 9)
(3,3,2)	-31	(9,-2, 0)	8	(2, 9, 0)	-281	(0, 0, 9)
(3,3,3)	-34	(9,-3, 0)	10	(3, 9, 0)	-281	(0, 0, 9)
(3,3,4)	-33	(9,-2, 0)	9	(2, 9, 0)	-281	(0, 0, 9)
(3,3,5)	-30	(9,-1, 0)	7	(1, 9, 0)	-281	(0, 0, 9)
(3,3,6)	-30	(9, 1, 0)	7	(-1, 9, 0)	-281	(0, 0, 9)
(3,3,7)	-33	(9, 2, 0)	9	(-2, 9, 0)	-281	(0, 0, 9)
(3,3,8)	-34	(9, 3, 0)	10	(-3, 9, 0)	-281	(0, 0, 9)
(3,3,9)	-31	(9, 2, 0)	8	(-2, 9, 0)	-281	(0, 0, 9)

TABLE XII

MATHEMATICAL STRESS CALCULATIONS FOR BLOCK PHE-4

Stress Pt. (R,Y,θ)	S_1	σ_x = 0 Vector	S_2	σ_y = -400 Vector	S_3	P_o = 1500 Vector
(1,1,1)	-1020	(1, 0, 0)	-1020	(0, 1, 0)	-1900	(0, 0, 1)
(1,1,2)	-1035	(7,-7, 0)	-1004	(7, 7, 0)	-1900	(0, 0, 1)
(1,1,3)	-1004	(7,-7, 0)	-1035	(7, 7, 0)	-1900	(0, 0, 1)
(2,1,1)	1252	(1, 0, 0)	-167	(0, 1, 0)	-136	(0, 0, 1)
(2,1,2)	1252	(9, 0, 0)	-167	(0, 9, 0)	-136	(0, 0, 1)
(2,1,3)	1252	(9, 0, 0)	-167	(0, 9, 0)	-136	(0, 0, 1)
(2,1,4)	1252	(1, 0, 0)	-167	(0, 1, 0)	-136	(0, 0, 1)
(2,1,5)	1252	(9, 0, 0)	-167	(0, 9, 0)	-136	(0, 0, 1)
(2,1,6)	1252	(9, 0, 0)	-167	(0, 9, 0)	-136	(0, 0, 1)
(3,1,1)	407	(1, 0, 0)	-145	(0, 1, 0)	-354	(0, 0, 1)
(3,1,2)	407	(9, 0, 0)	-145	(0, 9, 0)	-354	(0, 0, 1)
(3,1,3)	407	(9, 0, 0)	-145	(0, 9, 0)	-354	(0, 0, 1)
(3,1,4)	407	(9, 0, 0)	-145	(0, 9, 0)	-354	(0, 0, 1)
(3,1,5)	407	(9, 0, 0)	-145	(0, 9, 0)	-354	(0, 0, 1)
(3,1,6)	407	(9, 0, 0)	-145	(0, 9, 0)	-354	(0, 0, 1)
(3,1,7)	407	(9, 0, 0)	-145	(0, 9, 0)	-354	(0, 0, 1)
(3,1,8)	407	(9, 0, 0)	-145	(0, 9, 0)	-354	(0, 0, 1)
(3,1,9)	407	(1, 0, 0)	-145	(0, 1, 0)	-354	(0, 0, 1)
(1,2,1)	185	(9, 0,-4)	12	(0, 1, 0)	-1321	(4, 0, 9)
(1,2,2)	186	(9, 0,-4)	11	(0, 9, 0)	-1321	(4, 0, 9)
(1,2,3)	186	(9, 0,-4)	11	(0, 9, 0)	-1321	(4, 0, 9)
(2,2,1)	-17	(8, 0,-5)	16	(0, 1, 0)	-402	(5, 0, 8)
(2,2,2)	-22	(7,-3,-5)	21	(2, 9,-1)	-402	(5, 0, 8)
(2,2,3)	-22	(7,-3,-5)	21	(2, 9,-1)	-402	(5, 0, 8)
(2,2,4)	-17	(8, 0,-5)	16	(0, 1, 0)	-402	(5, 0, 8)
(2,2,5)	-22	(7, 3,-5)	21	(-2, 9, 1)	-402	(5, 0, 8)
(2,2,6)	-22	(7, 3,-5)	21	(-2, 9, 1)	-402	(5, 0, 8)
(3,2,1)	-4	(9, 0, 0)	-1	(0, 1, 0)	-400	(0, 0, 9)
(3,2,2)	-14	(7,-6, 0)	9	(6, 7, 0)	-400	(0, 0, 9)
(3,2,3)	-20	(7,-6, 0)	16	(6, 7, 0)	-400	(0, 0, 9)
(3,2,4)	-18	(7,-6, 0)	13	(6, 7, 0)	-400	(0, 0, 9)
(3,2,5)	-9	(7,-6, 0)	4	(6, 7, 0)	-400	(0, 0, 9)
(3,2,6)	-9	(7, 6, 0)	4	(-6, 7, 0)	-400	(0, 0, 9)
(3,2,7)	-18	(7, 6, 0)	13	(-6, 7, 0)	-400	(0, 0, 9)
(3,2,8)	-20	(7, 6, 0)	16	(-6, 7, 0)	-400	(0, 0, 9)
(3,2,9)	-14	(7, 6, 0)	9	(-6, 7, 0)	-400	(0, 0, 9)
(3,3,1)	-37	(9, 0, 0)	7	(0, 1, 0)	-376	(0, 0, 9)
(3,3,2)	-39	(9,-2, 0)	10	(2, 9, 0)	-376	(0, 0, 9)
(3,3,3)	-43	(9,-3, 0)	14	(3, 9, 0)	-376	(0, 0, 9)
(3,3,4)	-42	(9,-3, 0)	12	(3, 9, 0)	-376	(0, 0, 9)
(3,3,5)	-37	(9,-1, 0)	8	(1, 9, 0)	-376	(0, 0, 9)
(3,3,6)	-37	(9, 1, 0)	8	(-1, 9, 0)	-376	(0, 0, 9)
(3,3,7)	-42	(9, 3, 0)	12	(-3, 9, 0)	-376	(0, 0, 9)
(3,3,8)	-43	(9, 3, 0)	14	(-3, 9, 0)	-376	(0, 0, 9)
(3,3,9)	-39	(9, 2, 0)	10	(-2, 9, 0)	-376	(0, 0, 9)

TABLE XIII

MATHEMATICAL STRESS CALCULATIONS FOR BLOCKS PHC-5 & PHE-7

Stress Pt. (R,Y,θ)	S_1	σ_x = 0 Vector	S_2	σ_y = -500 Vector	S_3	P_o = 1500 Vector
(1,1,1)	-1020	(1, 0, 0)	-1020	(0, 1, 0)	-2000	(0, 0, 1)
(1,1,2)	-1039	(7,-7, 0)	-1000	(7, 7, 0)	-2000	(0, 0, 1)
(1,1,3)	-1000	(7,-7, 0)	-1039	(7, 7, 0)	-2000	(0, 0, 1)
(2,1,1)	1252	(1, 0, 0)	-167	(0, 1, 0)	-234	(0, 0, 1)
(2,1,2)	1252	(9, 0, 0)	-167	(0, 9, 0)	-234	(0, 0, 1)
(2,1,3)	1252	(9, 0, 0)	-167	(0, 9, 0)	-234	(0, 0, 1)
(2,1,4)	1252	(1, 0, 0)	-167	(0, 1, 0)	-234	(0, 0, 1)
(2,1,5)	1252	(9, 0, 0)	-167	(0, 9, 0)	-234	(0, 0, 1)
(2,1,6)	1252	(9, 0, 0)	-167	(0, 9, 0)	-234	(0, 0, 1)
(3,1,1)	407	(1, 0, 0)	-145	(0, 1, 0)	-454	(0, 0, 1)
(3,1,2)	407	(9, 0, 0)	-145	(0, 9, 0)	-454	(0, 0, 1)
(3,1,3)	408	(9, 0, 0)	-146	(0, 9, 0)	-454	(0, 0, 1)
(3,1,4)	408	(9, 0, 0)	-146	(0, 9, 0)	-454	(0, 0, 1)
(3,1,5)	407	(9, 0, 0)	-145	(0, 9, 0)	-454	(0, 0, 1)
(3,1,6)	407	(9, 0, 0)	-145	(0, 9, 0)	-454	(0, 0, 1)
(3,1,7)	408	(9, 0, 0)	-146	(0, 9, 0)	-454	(0, 0, 1)
(3,1,8)	408	(9, 0, 0)	-146	(0, 9, 0)	-454	(0, 0, 1)
(3,1,9)	407	(9, 0, 0)	-145	(0, 9, 0)	-454	(0, 0, 1)
(1,2,1)	170	(9, 0,-3)	12	(0, 1, 0)	-1405	(3, 0, 9)
(1,2,2)	172	(9, 1,-3)	10	(-1, 9, 0)	-1405	(3, 0, 9)
(1,2,3)	172	(9,-1,-3)	10	(1, 9, 0)	-1405	(3, 0, 9)
(2,2,1)	-42	(8, 0,-4)	16	(0, 1, 0)	-478	(4, 0, 8)
(2,2,2)	-47	(8,-2,-4)	21	(2, 9,-1)	-478	(4, 0, 8)
(2,2,3)	-47	(8,-2,-4)	21	(2, 9,-1)	-478	(4, 0, 8)
(2,2,4)	-42	(8, 0,-4)	16	(0, 1, 0)	-478	(4, 0, 8)
(2,2,5)	-47	(8, 2,-4)	21	(-2, 9, 1)	-478	(4, 0, 8)
(2,2,6)	-47	(8, 2,-4)	21	(-2, 9, 1)	-478	(4, 0, 8)
(3,2,1)	-4	(9, 0, 0)	-1	(0, 1, 0)	-440	(0, 0, 9)
(3,2,2)	-17	(7,-6, 0)	12	(6, 7, 0)	-440	(0, 0, 9)
(3,2,3)	-25	(7,-6, 0)	20	(6, 7, 0)	-440	(0, 0, 9)
(3,2,4)	-22	(7,-6, 0)	17	(6, 7, 0)	-440	(0, 0, 9)
(3,2,5)	-10	(7,-6, 0)	6	(6, 7, 0)	-440	(0, 0, 9)
(3,2,6)	-10	(7, 6, 0)	6	(-6, 7, 0)	-440	(0, 0, 9)
(3,2,7)	-22	(7, 6, 0)	17	(-6, 7, 0)	-440	(0, 0, 9)
(3,2,8)	-25	(7, 6, 0)	20	(-6, 7, 0)	-440	(0, 0, 9)
(3,2,9)	-17	(7, 6, 0)	12	(-6, 7, 0)	-440	(0, 0, 9)
(3,3,1)	-37	(9, 0, 0)	7	(0, 1, 0)	-476	(0, 0, 9)
(3,3,2)	-41	(9,-2, 0)	12	(2, 9, 0)	-476	(0, 0, 9)
(3,3,3)	-46	(9,-3, 0)	17	(3, 9, 0)	-476	(0, 0, 9)
(3,3,4)	-44	(9,-3, 0)	15	(3, 9, 0)	-476	(0, 0, 9)
(3,3,5)	-38	(9,-1, 0)	9	(1, 9, 0)	-476	(0, 0, 9)
(3,3,6)	-38	(9, 1, 0)	9	(-1, 9, 0)	-476	(0, 0, 9)
(3,3,7)	-44	(9, 3, 0)	15	(-3, 9, 0)	-476	(0, 0, 9)
(3,3,8)	-46	(9, 3, 0)	17	(-3, 9, 0)	-476	(0, 0, 9)
(3,3,9)	-41	(9, 2, 0)	12	(-2, 9, 0)	-476	(0, 0, 9)

TABLE XIV

MATHEMATICAL STRESS CALCULATIONS FOR BLOCK PHE-9

Stress Pt.		σ_x = 0		σ_y = -600		P_o = 1500
(R,Y,Θ)	S_1	Vector	S_2	Vector	S_3	Vector
(1,1,1)	-1020	(1, 0, 0)	-1020	(0, 1, 0)	-2100	(0, 0, 1)
(1,1,2)	-1043	(7,-7, 0)	-997	(7, 7, 0)	-2100	(0, 0, 1)
(1,1,3)	-997	(7,-7, 0)	-1043	(7, 7, 0)	-2100	(0, 0, 1)
(2,1,1)	1252	(1, 0, 0)	-167	(0, 1, 0)	-336	(0, 0, 1)
(2,1,2)	1252	(9, 0, 0)	-167	(0, 9, 0)	-336	(0, 0, 1)
(2,1,3)	1252	(9, 0, 0)	-167	(0, 9, 0)	-336	(0, 0, 1)
(2,1,4)	1252	(1, 0, 0)	-167	(0, 1, 0)	-336	(0, 0, 1)
(2,1,5)	1252	(9, 0, 0)	-167	(0, 9, 0)	-336	(0, 0, 1)
(2,1,6)	1252	(9, 0, 0)	-167	(0, 9, 0)	-336	(0, 0, 1)
(3,1,1)	407	(1, 0, 0)	-145	(0, 1, 0)	-554	(0, 0, 1)
(3,1,2)	407	(9, 0, 0)	-145	(0, 9, 0)	-554	(0, 0, 1)
(3,1,3)	408	(9, 0, 0)	-146	(0, 9, 0)	-554	(0, 0, 1)
(3,1,4)	408	(9, 0, 0)	-146	(0, 9, 0)	-554	(0, 0, 1)
(3,1,5)	407	(9, 0, 0)	-145	(0, 9, 0)	-554	(0, 0, 1)
(3,1,6)	407	(9, 0, 0)	-145	(0, 9, 0)	-554	(0, 0, 1)
(3,1,7)	408	(9, 0, 0)	-146	(0, 9, 0)	-554	(0, 0, 1)
(3,1,8)	408	(9, 0, 0)	-146	(0, 9, 0)	-554	(0, 0, 9)
(3,1,9)	407	(9, 0, 0)	-145	(0, 9, 0)	-554	(0, 0, 1)
(1,2,1)	156	(9, 0,-3)	12	(0, 1, 0)	-1491	(3, 0, 9)
(1,2,2)	159	(9, 1,-3)	9	(-1, 9, 0)	-1491	(3, 0, 9)
(1,2,3)	159	(9,-1,-3)	9	(1, 9, 0)	-1491	(3, 0, 9)
(2,2,1)	-59	(9, 0,-3)	16	(0, 1, 0)	-561	(3, 0, 9)
(2,2,2)	-65	(8,-2,-3)	22	(2, 9, 0)	-561	(3, 0, 9)
(2,2,3)	-65	(8,-2,-3)	22	(2, 9, 0)	-561	(3, 0, 9)
(2,2,4)	-59	(9, 0,-3)	16	(0, 1, 0)	-561	(3, 0, 9)
(2,2,5)	-65	(8, 2,-3)	22	(-2, 9, 0)	-561	(3, 0, 9)
(2,2,6)	-65	(8, 2,-3)	22	(-2, 9, 0)	-561	(3, 0, 9)
(3,2,1)	-4	(9, 0, 0)	-1	(0, 1, 0)	-540	(0, 0, 9)
(3,2,2)	-20	(7,-6, 0)	15	(6, 7, 0)	-540	(0, 0, 9)
(3,2,3)	-29	(7,-6, 0)	24	(6, 7, 0)	-540	(0, 0, 9)
(3,2,4)	-26	(7,-6, 0)	21	(6, 7, 0)	-540	(0, 0, 9)
(3,2,5)	-12	(7,-6, 0)	7	(6, 7, 0)	-540	(0, 0, 9)
(3,2,6)	-12	(7, 6, 0)	7	(-6, 7, 0)	-540	(0, 0, 9)
(3,2,7)	-26	(7, 6, 0)	21	(-6, 7, 0)	-540	(0, 0, 9)
(3,2,8)	-29	(7, 6, 0)	24	(-6, 7, 0)	-540	(0, 0, 9)
(3,2,9)	-20	(7, 6, 0)	15	(-6, 7, 0)	-540	(0, 0, 9)
(3,3,1)	-37	(9, 0, 0)	7	(0, 1, 0)	-575	(0, 0, 9)
(3,3,2)	-43	(9,-3, 0)	13	(3, 9, 0)	-575	(0, 0, 9)
(3,3,3)	-49	(9,-4, 0)	20	(4, 9, 0)	-575	(0, 0, 9)
(3,3,4)	-47	(9,-3, 0)	17	(3, 9, 0)	-575	(0, 0, 9)
(3,3,5)	-39	(9,-1, 0)	9	(1, 9, 0)	-575	(0, 0, 9)
(3,3,6)	-39	(9, 1, 0)	9	(-1, 9, 0)	-575	(0, 0, 9)
(3,3,7)	-47	(9, 3, 0)	17	(-3, 9, 0)	-575	(0, 0, 9)
(3,3,8)	-49	(9, 4, 0)	20	(-4, 9, 0)	-575	(0, 0, 9)
(3,3,9)	-43	(9, 3, 0)	13	(-3, 9, 0)	-575	(0, 0, 9)

TABLE XV

MATHEMATICAL STRESS CALCULATIONS FOR BLOCK PHC-32

Stress Pt.		σ_x = -200		σ_y = -400		P_o = 2000
(R,Y,Θ)	S_1	Vector	S_2	Vector	S_3	Vector
(1,1,1)	-1560	(1, 0, 0)	-1360	(0, 1, 0)	-2400	(0, 0, 1)
(1,1,2)	-1353	(8, 5, 0)	-1567	(-5, 8, 0)	-2400	(0, 0, 1)
(1,1,3)	-1353	(8,-5, 0)	-1567	(5, 8, 0)	-2400	(0, 0, 1)
(2,1,1)	1469	(1, 0, 0)	-222	(0, 1, 0)	-47	(0, 0, 1)
(2,1,2)	1524	(9, 0, 0)	-277	(0, 9, 0)	-47	(0, 0, 1)
(2,1,3)	1623	(9, 0, 0)	-377	(0, 9, 0)	-47	(0, 0, 1)
(2,1,4)	1669	(1, 0, 0)	-422	(0, 1, 0)	-47	(0, 0, 1)
(2,1,5)	1623	(9, 0, 0)	-377	(0, 9, 0)	-47	(0, 0, 1)
(2,1,6)	1524	(9, 0, 0)	-277	(0, 9, 0)	-47	(0, 0, 1)
(3,1,1)	343	(1, 0, 0)	-193	(0, 1, 0)	-338	(0, 0, 1)
(3,1,2)	374	(9, 1, 0)	-225	(-1, 9, 0)	-338	(0, 0, 1)
(3,1,3)	441	(9, 1, 0)	-292	(-1, 9, 0)	-338	(0, 0, 1)
(3,1,4)	503	(9, 1, 0)	-354	(-1, 9, 0)	-338	(0, 0, 1)
(3,1,5)	538	(9, 0, 0)	-389	(0, 9, 0)	-338	(0, 0, 1)
(3,1,6)	538	(9, 0, 0)	-389	(0, 9, 0)	-338	(0, 0, 1)
(3,1,7)	503	(9,-1, 0)	-354	(1, 9, 0)	-338	(0, 0, 1)
(3,1,8)	441	(9,-1, 0)	-292	(1, 9, 0)	-338	(0, 0, 1)
(3,1,9)	374	(9,-1, 0)	-225	(1, 9, 0)	-338	(0, 0, 1)
(1,2,1)	110	(8, 0,-4)	16	(0, 1, 0)	-1690	(4, 0, 8)
(1,2,2)	248	(8, 2,-4)	-152	(-1, 9, 0)	-1661	(4, 0, 8)
(1,2,3)	248	(8,-2,-4)	-152	(1, 9,-1)	-1661	(4, 0, 8)
(2,2,1)	-556	(7, 0, 6)	22	(0, 1, 0)	-70	(-6, 0, 7)
(2,2,2)	-536	(7,-1, 6)	29	(-4, 7,-3)	-97	(-4, 6, 6)
(2,2,3)	29	(6, 4,-5)	-148	(-1, 8, 4)	-486	(6,-1, 6)
(2,2,4)	25	(7, 0,-6)	-178	(0, 1, 0)	-451	(6, 0, 7)
(2,2,5)	29	(6,-4,-5)	-148	(1, 8,-4)	-486	(6, 1, 6)
(2,2,6)	-536	(7, 1, 6)	29	(-4, 7, 3)	-97	(-4,-6, 6)
(3,2,1)	-203	(9, 0, 1)	-1	(0, 1, 0)	-322	(-1, 0, 9)
(3,2,2)	-206	(9,-3, 1)	2	(3, 9, 0)	-322	(-1, 0, 9)
(3,2,3)	-210	(7,-6, 1)	6	(6, 7, 0)	-322	(-1, 0, 9)
(3,2,4)	3	(8, 5, 0)	-208	(-5, 8, 0)	-321	(0, 0, 9)
(3,2,5)	-4	(9, 1, 0)	-202	(-1, 9, 0)	-320	(0, 0, 9)
(3,2,6)	-4	(9,-1, 0)	-202	(1, 9, 0)	-320	(0, 0, 9)
(3,2,7)	3	(8,-5, 0)	-208	(5, 8, 0)	-321	(0, 0, 9)
(3,2,8)	-210	(7, 6, 1)	6	(-6, 7, 0)	-322	(-1, 0, 9)
(3,2,9)	-206	(9, 3, 1)	2	(-3, 9, 0)	-322	(-1, 0, 9)
(3,3,1)	-244	(9, 0,-2)	10	(0, 1, 0)	-373	(2, 0, 9)
(3,3,2)	-242	(9,-2,-2)	8	(2, 9, 0)	-372	(2, 0, 9)
(3,3,3)	-234	(8,-5,-1)	-2	(5, 8, 0)	-371	(1, 0, 9)
(3,3,4)	-22	(7, 6, 0)	-215	(-6, 7, 1)	-370	(1, 0, 9)
(3,3,5)	-44	(9, 2, 0)	-194	(-2, 9, 0)	-369	(0, 0, 9)
(3,3,6)	-44	(9,-2, 0)	-194	(2, 9, 0)	-369	(0, 0, 9)
(3,3,7)	-22	(7,-6, 0)	-215	(6, 7,-1)	-370	(1, 0, 9)
(3,3,8)	-234	(8, 5,-1)	-2	(-5, 8, 0)	-371	(1, 0, 9)
(3,3,9)	-242	(9, 2,-2)	8	(-2, 9, 0)	-372	(2, 0, 9)

TABLE XVI

MATHEMATICAL STRESS CALCULATIONS FOR BLOCK PHE-37

Stress Pt. (R,Y,)	S_1	x = -300 Vector	S_2	y = -600 Vector	S_3	P_o = 2000 Vector
(1,1,1)	-1660	(1, 0, 0)	-1360	(0, 1, 0)	-2600	(0, 0, 1)
(1,1,2)	-1350	(8, 5, 0)	-1670	(-5, 8, 0)	-2600	(0, 0, 1)
(1,1,3)	-1350	(8,-5, 0)	-1670	(5, 8, 0)	-2600	(0, 0, 1)
(2,1,1)	1369	(1, 0, 0)	-222	(0, 1, 0)	-247	(0, 0, 1)
(2,1,2)	1455	(9, 0, 0)	-309	(0, 9, 0)	-247	(0, 0, 1)
(2,1,3)	1604	(9, 0, 0)	-457	(0, 9, 0)	-247	(0, 0, 1)
(2,1,4)	1669	(1, 0, 0)	-522	(0, 1, 0)	-247	(0, 0, 1)
(2,1,5)	1604	(9, 0, 0)	-457	(0, 9, 0)	-247	(0, 0, 1)
(2,1,6)	1455	(9, 0, 0)	-309	(0, 9, 0)	-247	(0, 0, 1)
(3,1,1)	243	(1, 0, 0)	-193	(0, 1, 0)	-538	(0, 0, 1)
(3,1,2)	299	(9, 1, 0)	-249	(-1, 9, 0)	-538	(0, 0, 1)
(3,1,3)	403	(9, 2, 0)	-353	(-2, 9, 0)	-538	(0, 0, 1)
(3,1,4)	490	(9, 1, 0)	-440	(-1, 9, 0)	-538	(0, 0, 1)
(3,1,5)	537	(9, 0, 0)	-487	(0, 9, 0)	-538	(0, 0, 1)
(3,1,6)	537	(9, 0, 0)	-487	(0, 9, 0)	-538	(0, 0, 1)
(3,1,7)	490	(9,-1, 0)	-440	(1, 9, 0)	-538	(0, 0, 1)
(3,1,8)	403	(9,-2, 0)	-353	(2, 9, 0)	-538	(0, 0, 1)
(3,1,9)	299	(9,-1, 0)	-249	(1, 9, 0)	-538	(0, 0, 1)
(1,2,1)	-11	(8, 0,-4)	16	(0, 1, 0)	-1869	(4, 0, 8)
(1,2,2)	213	(8, 2,-3)	-247	(-2, 9, 1)	-1831	(4, 0, 9)
(1,2,3)	213	(8,-2,-3)	-247	(2, 9,-1)	-1831	(4, 0, 9)
(2,2,1)	-698	(7, 0, 6)	22	(0, 1, 0)	-228	(-6, 0, 7)
(2,2,2)	-677	(6,-1, 7)	14	(4, 8,-2)	-242	(-5, 4, 6)
(2,2,3)	-267	(3,-8,-4)	-16	(7, 5,-3)	-622	(5,-1, 7)
(2,2,4)	-41	(8, 0,-4)	-278	(0, 1, 0)	-585	(4, 0, 8)
(2,2,5)	-267	(3, 8,-4)	-16	(-7, 5, 3)	-622	(5, 1, 7)
(2,2,6)	-677	(6, 1, 7)	14	(-4, 8, 2)	-242	(-5,-4, 6)
(3,2,1)	-304	(9, 0, 0)	-1	(0, 1, 0)	-521	(0, 0, 9)
(3,2,2)	-309	(9,-3, 0)	4	(3, 9, 0)	-521	(0, 0, 9)
(3,2,3)	-316	(7,-6, 0)	10	(6, 7, 0)	-520	(0, 0, 9)
(3,2,4)	6	(8, 5, 0)	-312	(-5, 8, 0)	-520	(0, 0, 9)
(3,2,5)	-4	(9, 1, 0)	-303	(-1, 9, 0)	-520	(0, 0, 9)
(3,2,6)	-4	(9,-1, 0)	-303	(1, 9, 0)	-520	(0, 0, 9)
(3,2,7)	6	(8,-5, 0)	-312	(5, 8, 0)	-520	(0, 0, 9)
(3,2,8)	-316	(7, 6, 0)	10	(-6, 7, 0)	-520	(0, 0, 9)
(3,2,9)	-309	(9, 3, 0)	4	(-3, 9, 0)	-521	(0, 0, 9)
(3,3,1)	-347	(9, 0,-1)	10	(0, 1, 0)	-570	(1, 0, 9)
(3,3,2)	-346	(9,-3,-1)	9	(3, 9, 0)	-570	(1, 0, 9)
(3,3,3)	-339	(8,-5,-1)	1	(5, 8, 0)	-569	(0, 0, 9)
(3,3,4)	-21	(8, 5, 0)	-318	(-5, 8, 0)	-568	(0, 0, 9)
(3,3,5)	-45	(9, 2, 0)	-294	(-2, 9, 0)	-568	(0, 0, 9)
(3,3,6)	-45	(9,-2, 0)	-294	(2, 9, 0)	-568	(0, 0, 9)
(3,3,7)	-21	(8,-5, 0)	-318	(5, 8, 0)	-568	(0, 0, 9)
(3,3,8)	-339	(8, 5,-1)	1	(-5, 8, 0)	-569	(0, 0, 9)
(3,3,9)	-346	(9, 3,-1)	9	(-3, 9, 0)	-570	(1, 0, 9)

TABLE XVII

MATHEMATICAL STRESS CALCULATIONS FOR BLOCK PHE-31

Stress Pt.		σ_x = -600		σ_y = -800		P_o = 2000
(R,Y,Θ)	S_1	Vector	S_2	Vector	S_3	Vector
(1,1,1)	-1960	(1, 0, 0)	-1360	(0, 1, 0)	-2800	(0, 0, 1)
(1,1,2)	-1335	(8, 5, 0)	-1967	(-5, 8, 0)	-2800	(0, 0, 1)
(1,1,3)	-1335	(8,-5, 0)	-1967	(5, 8, 0)	-2800	(0, 0, 1)
(2,1,1)	1069	(1, 0, 0)	-222	(0, 1, 0)	-447	(0, 0, 1)
(2,1,2)	1263	(9, 1, 0)	-416	(-1, 9, 0)	-447	(0, 0, 1)
(2,1,3)	1551	(9, 1, 0)	-704	(-1, 9, 0)	-447	(0, 0, 1)
(2,1,4)	1669	(1, 0, 0)	-822	(0, 1, 0)	-447	(0, 0, 1)
(2,1,5)	1551	(9,-1, 0)	-704	(1, 9, 0)	-447	(0, 0, 1)
(2,1,6)	1263	(9,-1, 0)	-416	(1, 9, 0)	-447	(0, 0, 1)
(3,1,1)	-57	(1, 0, 0)	-193	(0, 1, 0)	-738	(0, 0, 1)
(3,1,2)	116	(8, 4, 0)	-367	(-4, 8, 0)	-738	(0, 0, 1)
(3,1,3)	313	(9, 3, 0)	-564	(-3, 9, 0)	-738	(0, 0, 1)
(3,1,4)	457	(9, 2, 0)	-708	(-2, 9, 0)	-738	(0, 0, 1)
(3,1,5)	533	(9, 0, 0)	-784	(0, 9, 0)	-738	(0, 0, 1)
(3,1,6)	533	(9, 0, 0)	-784	(0, 9, 0)	-738	(0, 0, 1)
(3,1,7)	457	(9,-2, 0)	-708	(2, 9, 0)	-738	(0, 0, 1)
(3,1,8)	313	(9,-3, 0)	-564	(3, 9, 0)	-738	(0, 0, 1)
(3,1,9)	116	(8,-4, 0)	-367	(4, 8, 0)	-738	(0, 0, 1)
(1,2,1)	-290	(8, 0,-4)	16	(0, 1, 0)	-2090	(4, 0, 8)
(1,2,2)	179	(8, 3,-3)	-527	(-3, 9, 2)	-2016	(3, 0, 9)
(1,2,3)	179	(8,-3,-3)	-527	(3, 9,-2)	-2016	(3, 0, 9)
(2,2,1)	-956	(7, 0, 6)	22	(0, 1, 0)	-470	(-6, 0, 7)
(2,2,2)	-920	(7,-2, 6)	3	(4, 8,-1)	-488	(-5, 3, 7)
(2,2,3)	-47	(7, 5,-3)	-533	(-2, 7, 5)	-824	(5,-3, 7)
(2,2,4)	-79	(9, 0,-3)	-578	(0, 1, 0)	-747	(3, 0, 9)
(2,2,5)	-47	(7,-5,-3)	-533	(2, 7,-5)	-824	(5, 3, 7)
(2,2,6)	-920	(7, 2, 6)	3	(-4, 8, 1)	-488	(-5,-3, 7)
(3,2,1)	-603	(9, 0, 1)	-1	(0, 1, 0)	-722	(-1, 0, 9)
(3,2,2)	-606	(9,-3, 0)	2	(3, 9, 0)	-722	(-1, 0, 9)
(3,2,3)	-610	(7,-6, 1)	6	(6, 7, 0)	-721	(-1, 0, 9)
(3,2,4)	2	(8, 5, 0)	-608	(-5, 8, 0)	-720	(0, 0, 9)
(3,2,5)	-4	(9,-1, 0)	-602	(-1, 9, 0)	-719	(0, 0, 9)
(3,2,6)	-4	(9,-1, 0)	-602	(1, 9, 0)	-719	(0, 0, 9)
(3,2,7)	2	(8,-5, 0)	-608	(5, 8, 0)	-720	(0, 0, 9)
(3,2,8)	-610	(7, 6, 1)	6	(-6, 7, 0)	-721	(-1, 0, 9)
(3,2,9)	-606	(9, 3, 1)	2	(-3, 9, 0)	-722	(-1, 0, 9)
(3,3,1)	-644	(9, 0,-2)	10	(0, 1, 0)	-773	(2, 0, 9)
(3,3,2)	-642	(9,-3,-2)	7	(3, 9, 0)	-772	(2, 0, 9)
(3,3,3)	-632	(7,-6,-1)	-5	(6, 7, 0)	-770	(1, 0, 9)
(3,3,4)	-26	(8, 5, 3)	-612	(-5, 8, 0)	-768	(0, 0, 9)
(3,3,5)	-46	(9, 1, 0)	-593	(-1, 9, 0)	-767	(0, 0, 9)
(3,3,6)	-46	(9,-1, 0)	-593	(1, 9, 0)	-767	(0, 0, 9)
(3,3,7)	-26	(8,-5, 0)	-612	(5, 8, 0)	-768	(0, 0, 9)
(3,3,8)	-631	(7, 6,-1)	-5	(-6, 7, 0)	-770	(1, 0, 9)
(3,3,9)	-642	(9, 3,-2)	7	(-3, 9, 0)	-772	(2, 0, 9)

TABLE XVIII

MATHEMATICAL STRESS CALCULATIONS FOR BLOCK PHC-29

Stress Pt.		σ_x = -500		σ_y = -1000		P_o = 2500
(R,Y,θ)	S_1	Vector	S_2	Vector	S_3	Vector
(1,1,1)	-2200	(1, 0, 0)	-1700	(0, 1, 0)	-3500	(0, 0, 1)
(1,1,2)	-1683	(8, 5, 0)	-2217	(-5, 8, 0)	-3500	(0, 0, 1)
(1,1,3)	-1683	(8,-5, 0)	-2217	(5, 8, 0)	-3500	(0, 0, 1)
(2,1,1)	1586	(1, 0, 0)	-278	(0, 1, 0)	-559	(0, 0, 1)
(2,1,2)	1737	(9, 1, 0)	-429	(-1, 9, 0)	-559	(0, 0, 1)
(2,1,3)	1982	(9, 0, 0)	-674	(0, 9, 0)	-559	(0, 0, 1)
(2,1,4)	2086	(1, 0, 0)	-778	(0, 1, 0)	-559	(0, 0, 1)
(2,1,5)	1982	(9, 0, 0)	-674	(0, 9, 0)	-559	(0, 0, 1)
(2,1,6)	1737	(9,-1, 0)	-429	(1, 9, 0)	-559	(0, 0, 1)
(3,1,1)	178	(1, 0, 0)	-241	(0, 1, 0)	-923	(0, 0, 1)
(3,1,2)	289	(9, 2, 0)	-352	(-2, 9, 0)	-923	(0, 0, 1)
(3,1,3)	464	(9, 2, 0)	-527	(-2, 9, 0)	-923	(0, 0, 1)
(3,1,4)	599	(9, 1, 0)	-662	(-1, 9, 0)	-923	(0, 0, 1)
(3,1,5)	669	(9, 0, 0)	-733	(0, 9, 0)	-923	(0, 0, 1)
(3,1,6)	669	(9, 0, 0)	-733	(0, 9, 0)	-923	(0, 0, 1)
(3,1,7)	599	(9,-1, 0)	-662	(1, 9, 0)	-923	(0, 0, 1)
(3,1,8)	464	(9,-2, 0)	-527	(2, 9, 0)	-923	(0, 0, 1)
(3,1,9)	289	(9,-2, 0)	-352	(2, 9, 0)	-923	(0, 0, 1)
(1,2,1)	-163	(9, 0,-4)	20	(0, 1, 0)	-2563	(4, 0, 9)
(1,2,2)	234	(8, 3,-3)	-433	(-3, 9, 1)	-2506	(3, 0, 9)
(1,2,3)	234	(8,-3,-3)	-433	(3, 9,-1)	-2506	(3, 0, 9)
(2,2,1)	-469	(7, 0,-6)	27	(0, 1, 0)	-1064	(6, 0, 7)
(2,2,2)	-481	(6,-4,-6)	13	(4, 8,-1)	-1038	(6,-1, 7)
(2,2,3)	-47	(7, 5,-2)	-486	(-4, 7, 4)	-973	(4,-1, 8)
(2,2,4)	-99	(9, 0,-3)	-473	(0, 1, 0)	-934	(3, 0, 9)
(2,2,5)	-47	(7,-5,-2)	-486	(4, 7,-4)	-973	(4, 1, 8)
(2,2,6)	-481	(6, 4,-6)	13	(-4, 8, 1)	-1038	(6, 1, 7)
(3,2,1)	-506	(9, 0, 0)	-1	(0, 1, 0)	-900	(0, 0, 9)
(3,2,2)	-515	(9,-3, 0)	8	(3, 9, 0)	-900	(0, 0, 9)
(3,2,3)	-526	(7,-6, 0)	18	(6, 7, 0)	-900	(0, 0, 9)
(3,2,4)	12	(8, 5, 0)	-519	(-5, 8, 0)	-900	(0, 0, 9)
(3,2,5)	-4	(9, 1, 0)	-504	(-1, 9, 0)	-899	(0, 0, 9)
(3,2,6)	-4	(9,-1, 0)	-504	(1, 9, 0)	-899	(0, 0, 9)
(3,2,7)	12	(8,-5, 0)	-519	(5, 8, 0)	-900	(0, 0, 9)
(3,2,8)	-526	(7, 6, 0)	18	(-6, 7, 0)	-900	(0, 0, 9)
(3,2,9)	-515	(9, 3, 0)	8	(-3, 9, 0)	-900	(0, 0, 9)
(3,3,1)	-560	(9, 0, 0)	12	(0, 1, 0)	-961	(0, 0, 9)
(3,3,2)	-561	(9,-3, 0)	13	(3, 9, 0)	-961	(0, 0, 9)
(3,3,3)	-554	(7,-5, 0)	5	(5, 8, 0)	-960	(0, 0, 9)
(3,3,4)	-23	(8, 5, 0)	-526	(-5, 8, 0)	-959	(0, 0, 9)
(3,3,5)	-56	(9, 2, 0)	-493	(-2, 9, 0)	-959	(0, 0, 9)
(3,3,6)	-56	(9,-2, 0)	-493	(2, 9, 0)	-959	(0, 0, 9)
(3,3,7)	-23	(8,-5, 0)	-526	(5, 8, 0)	-959	(0, 0, 9)
(3,3,8)	-554	(7, 5, 0)	5	(-5, 8, 0)	-960	(0, 0, 9)
(3,3,9)	-561	(9, 3, 0)	13	(-3, 9, 0)	-961	(0, 0, 9)

TABLE XIX

MATHEMATICAL STRESS CALCULATIONS FOR BLOCK PHC-35

Stress Pt.		σ_x = -1200		σ_y = -1700		P_o = 2000
(R,Y,θ)	S_1	Vector	S_2	Vector	S_3	Vector
(1,1,1)	-2560	(1, 0, 0)	-1360	(0, 1, 0)	-3700	(0, 0, 1)
(1,1,2)	-1343	(8, 5, 0)	-2577	(-5, 8, 0)	-3700	(0, 0, 1)
(1,1,3)	-1343	(8,-5, 0)	-2577	(5, 8, 0)	-3700	(0, 0, 1)
(2,1,1)	469	(1, 0, 0)	-222	(0, 1, 0)	-1347	(0, 0, 1)
(2,1,2)	964	(9, 3, 0)	-717	(-3, 9, 0)	-1347	(0, 0, 1)
(2,1,3)	1481	(9, 2, 0)	-1234	(-2, 9, 0)	-1347	(0, 0, 1)
(2,1,4)	1669	(1, 0, 0)	-1422	(0, 1, 0)	-1347	(0, 0, 1)
(2,1,5)	1481	(9,-2, 0)	-1234	(2, 9, 0)	-1347	(0, 0, 1)
(2,1,6)	964	(9,-3, 0)	-718	(3, 9, 0)	-1347	(0, 0, 1)
(3,1,1)	-657	(1, 0, 0)	-193	(0, 1, 0)	-1638	(0, 0, 1)
(3,1,2)	-836	(7,-6, 0)	-15	(6, 7, 0)	-1638	(0, 0, 1)
(3,1,3)	242	(8, 5, 0)	-1093	(-5, 8, 0)	-1638	(0, 0, 1)
(3,1,4)	433	(9, 3, 0)	-1284	(-3, 9, 0)	-1638	(0, 0, 1)
(3,1,5)	530	(9, 1, 0)	-1381	(-1, 9, 0)	-1638	(0, 0, 1)
(3,1,6)	530	(9,-1, 0)	-1381	(1, 9, 0)	-1638	(0, 0, 1)
(3,1,7)	433	(9,-3, 0)	-1284	(3, 9, 0)	-1638	(0, 0, 1)
(3,1,8)	242	(8,-5, 0)	-1093	(5, 8, 0)	-1638	(0, 0, 1)
(3,1,9)	-836	(7, 6, 0)	-15	(-6, 7, 0)	-1638	(0, 0, 1)
(1,2,1)	-948	(9, 0,-4)	16	(0, 1, 0)	-2933	(4, 0, 9)
(1,2,2)	114	(8, 4,-2)	-1140	(-4, 8, 2)	-2839	(3, 0, 9)
(1,2,3)	114	(8,-4,-2)	-1140	(4, 8,-2)	-2839	(3, 0, 9)
(2,2,1)	-1213	(8, 0,-5)	22	(0, 1, 0)	-1714	(5, 0, 8)
(2,2,2)	-1219	(7,-4,-5)	1	(4, 8, 0)	-1687	(4,-1, 8)
(2,2,3)	-76	(8, 5,-1)	-1205	(-4, 8, 3)	-1624	(2,-2, 9)
(2,2,4)	-137	(9, 0,-1)	-1178	(0, 1, 0)	-1590	(1, 0, 9)
(2,2,5)	-76	(8,-5,-1)	-1205	(4, 8,-3)	-1624	(2, 2, 9)
(2,2,6)	-1219	(7, 4,-5)	1	(-4, 8, 0)	-1687	(4, 1, 8)
(3,2,1)	-1205	(9, 0, 0)	-1	(0, 1, 0)	-1620	(0, 0, 9)
(3,2,2)	-1214	(9,-3, 0)	8	(3, 9, 0)	-1620	(0, 0, 9)
(3,2,3)	-1225	(7,-6, 0)	19	(6, 7, 0)	-1620	(0, 0, 9)
(3,2,4)	12	(8, 5, 0)	-1219	(-5, 8, 0)	-1619	(0, 0, 9)
(3,2,5)	13	(9, 1, 0)	-1204	(-1, 9, 0)	-1619	(0, 0, 9)
(3,2,6)	13	(9,-1, 0)	-1204	(1, 9, 0)	-1619	(0, 0, 9)
(3,2,7)	12	(8,-5, 0)	-1219	(5, 8, 0)	-1619	(0, 0, 9)
(3,2,8)	-1225	(7, 6, 0)	19	(-6, 7, 0)	-1620	(0, 0, 9)
(3,2,9)	-1214	(9, 3, 0)	8	(-3, 9, 0)	-1620	(0, 0, 9)
(3,3,1)	-1249	(9, 0, 0)	10	(0, 1, 0)	-1668	(0, 0, 9)
(3,3,2)	-1251	(9,-3, 0)	12	(3, 9, 0)	-1668	(0, 0, 9)
(3,3,3)	-1247	(7,-6, 0)	7	(6, 7, 0)	-1667	(0, 0, 9)
(3,3,4)	-17	(8, 5, 0)	-1223	(-5, 8, 0)	-1667	(0, 0, 9)
(3,3,5)	-45	(9, 1, 0)	-1195	(-1, 9, 0)	-1667	(0, 0, 9)
(3,3,6)	-45	(9,-1, 0)	-1195	(1, 9, 0)	-1667	(0, 0, 9)
(3,3,7)	-17	(8,-5, 0)	-1227	(5, 8, 0)	-1667	(0, 0, 9)
(3,3,8)	-1247	(7, 6, 0)	7	(-6, 7, 0)	-1667	(0, 0, 9)
(3,3,9)	-1251	(9, 3, 0)	12	(-3, 9, 0)	-1668	(0, 0, 9)

CHAPTER VI

MATHEMATICAL INTERPRETATION, CORRELATION, AND APPLICATION OF EXPERIMENTAL RESULTS

In attempting to obtain any correlation between the fracture pattern predicted by the mathematical model and the actual fracture surfaces obtained experimentally, several points should be kept in mind. (1) The stress distribution predicted by the mathematical model blows up at the tip of the crack which is the primary region of interest. (2) The circular crack is assumed to lie in the X-Z plane, which is initially correct; however, as the crack propagates and tends to turn or rotate, the stress distribution associated with the pressurized crack will be affected accordingly. (3) The fluid pressure used in the mathematical model for a given block was that indicated by the pressure gauge during the experimental phase and assumed constant within the crack. Because of the high viscosity of the fracturing fluid and frictional losses, there must be a pressure gradient within the crack and the actual fracturing pressure would be somewhat less than the pressure indicated and not constant within the crack interval. (4) The impressed uniaxial or biaxial load was probably not uniformly distributed over the block resulting in a non-symmetrical load distribution. (5) For lower impressed confining loads, there was some difficulty experienced in the keeping of the load constant

during the fracturing procedure because of the influencing nature of the pressurized crack.

From the mathematical analysis which is tabularized in Tables X through XIX for the various stress distributions, the following observations can be made.

For all stress distributions considered, the principal stresses in the plane Y = 0, corresponding to $\eta = 0$, are seen to lie in the Y-direction and the X-Z or R-θ plane. For the case of the uniaxial load, the principal stresses lie essentially in the R, θ, and Y directions; whereas, for the biaxial loading condition, the principal stress in the Y-direction remains, but a rotation occurs in the R-θ plane. As one moves away from the plane Y = 0, the principal stresses no longer remain in the R-θ plane or Y-direction but are seen to have in general, components in all three directions. This is undoubtly due to the influencing nature of the shear component τ_{ry} which is no longer zero as was the case in the plane Y = 0. However, the orientation of the principal stress S_3 tends to return to the Y-direction at distances removed from the circular crack.

The magnitude of the principal stress S_3 is essentially constant for a given ρ and η for both uniaxial and biaxial stress conditions and approaches the magnitude of σ_y as one moves away from the pressurized center. The sum of the principal stresses S_1 and S_2 remains constant for a given ρ and η and approaches 0 for uniaxial loading and σ_x for biaxial

loading as one moves away from the pressurized center. In the case of uniaxial loading, the components of S_1 and S_2 remain constant in the plane Y = 0.

In the plane Y = 0, under uniaxial loading, the components of principal shear remain, to within a close approximation, constant for a given ρ and their associated directions keep their same relative orientation. For the biaxial condition where the stresses S_1 and S_2 no longer remain constant for a given ρ, although the sum of S_1 and S_2 does remain constant, there results a θ dependence for the principal stress $\tau_{r\theta}$. Also, as a consequence of the variation of the principal stresses S_1 and S_2, the principal shear components fluctuate both in magnitude and direction for a given ρ. In the region $Y \neq 0$, the octahedral stresses are in general functions of the coordinates R,θ, and Y for both magnitudes and directions.

Restricting one's attention to the plane Y = 0, which is of particular interest in the development of fracture extension, the results of the mathematical model predict a region of transition in which the maximum principal shearing stress passes from the R-θ plane to the R-Y plane for the case of uniaxial loading and from the R-θ plane to a $f(R,\theta)$-Y plane for biaxial loading.

For uniaxial loading, this transition region is seen to be a function of the loading stress σ_y, the internal pressure P_o, the distance from the pressurized crack, and

Poisson's ratio. For a given homogeneous, isotropic media, Poisson's ratio is a constant and will be discounted as a variable in the subsequent discussion. In the actual fracturing mechanism, the region of interest is that in the immediate vicinity of the crack periphery. In this analysis, the region corresponding to $\rho = 4/3$ will be considered. As was indicated earlier, the stress distribution associated with a pressurized circular crack blows up at the crack periphery demanding an analysis at some region r which is greater than c.

Table XX shows the principal shear components for the various mathematical models analyzed under uniaxial loading. The region corresponds to $\eta = 0$ and $\rho = 1.33$ with the quantities being expressed in psi.

Table XX illustrates several interesting features associated with uniaxial fracturing. First, the shear component $\tau_{r\theta}$ is seen to be a function of the internal fracturing pressure "P_o" alone and is independent of the applied load. Secondly, the shear component "τ_{ry}" is a function of both the internal fracturing pressure and the uniaxial applied load. Thirdly, Table XX shows that the principle shearing stress changes from the direction of $\tau_{r\theta}$ to the direction of τ_{ry} and that this transition region is a function of both the uniaxial loading and the internal fracturing pressure.

To illustrate the dependence of this transition region

TABLE XX

VARIATION OF PRINCIPAL SHEAR AS A FUNCTION OF UNIAXIAL LOADING

σ_y	P_o	$\tau_{r\theta}$	τ_{ry}	$\tau_{\theta y}$
-100	1500	710	574	165
-200	1200	567	494	73
-300	1200	567	545	23
-400	1200	567	595	28
-400	1500	710	694	15
-500	1500	710	743	34
-600	1500	710	794	85
-1000	2000	946	1159	212

on the two variables, the uniaxial load "σ_y" and the internal fracturing pressure "P_o", the components of shear were determined for uniaxial loads of -100 psi to -700 psi in 100 psi intervals as a function of the internal fracturing fluid pressure. Table XXI tabularizes the information obtained from this analysis and Figure 33 gives a graphical representation of the transition region by plotting the uniaxial load as a function of the internal fracturing fluid pressure for the case where the two maximum, principal shearing components, $\tau_{\theta r}$ and τ_{ry}, are equal.

The transition region can be defined as that state of stress which makes the two principal maximum shear components equal in magnitude. Figure 33 is a graphical representation of this state and illustrates a linear relationship between the uniaxial load and the fracturing fluid pressure given by the following equation:

$$(69) \quad \sigma_y = -0.292P_o$$

This equation suggests that in order to maintain the maximum principal shear in the R-θ plane and thus extend the fracture in this preferred plane, the internal fracturing fluid pressure must be kept greater than approximately 3.4 times the uniaxial load. For small uniaxial loads, control of fracture orientation is possible; however, because of the low tensile strength of rock, control under large axial stress conditions would be difficult to achieve, if

TABLE XXI

COMPONENTS OF PRINCIPAL SHEAR ILLUSTRATING THE REGION OF TRANSITION

σ_y	P_o	$\tau_{r\theta}$	τ_{ry}
-100	300	145	152
-100	400	189	180
-200	600	283	297
-200	700	331	330
-300	1000	472	478
-300	1100	520	512
-400	1300	614	627
-400	1400	661	660
-500	1700	803	809
-500	1800	850	842
-600	2000	946	958
-600	2100	993	991
-700	2400	1134	1139
-700	2500	1182	1172

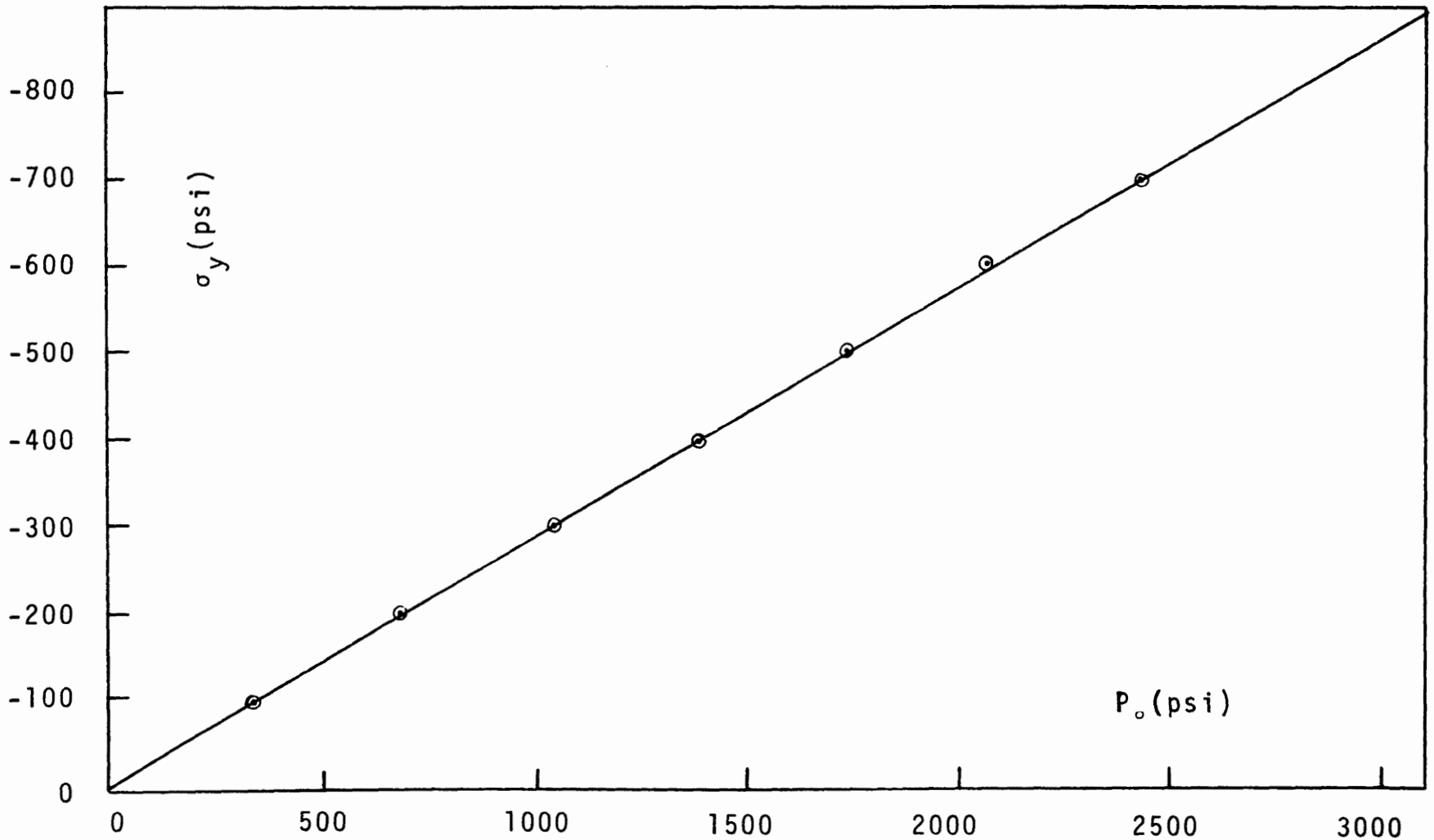

Figure 33. The Relationship between the Uniaxial Load, σ_y, and the Internal Fracturing Fluid Pressure, P_o, resulting in equal maximum shear components $\tau_{r\theta}$ and τ_{ry}.

not impossible.

Table XXII shows the principal shear components for the various mathematical models analyzed under biaxial loading conditions. The region again corresponds to $\eta = 0$ and $\rho = 1.33$ with all quantities being expressed in psi.

The most significant difference between the biaxial and uniaxial loading conditions is that the magnitudes of the principal shears are now functions of the polar angle θ for the biaxial condition whereas they are independent of θ for the case of uniaxial loading. Further, Table XXII shows that the principal shear component $\tau_{r\theta}$ is influenced to a greater extent by an angular change in θ than is the principal shear component τ_{ry}.

Both principal shear components assume a minimum value for the polar angle $\theta = 0°$ and $\theta = 180°$ corresponding to the X-axis and assume maximum values for the polar angle $\theta = 90°$ and $\theta = 270°$ corresponding to the Z-axis. If the magnitude of $\tau_{r\theta}$ is greater than the magnitude of τ_{ry} at $\theta = 0°$, then $\tau_{r\theta}$ will always be greater than τ_{ry} for all θ because of the greater dependence of $\tau_{r\theta}$ with respect to θ than is the dependence of τ_{ry}. However, if $\tau_{r\theta}$ is less than τ_{ry} at $\theta = 0°$, it may happen that $\tau_{r\theta}$ will become larger than τ_{ry} for some angular region $\theta = \pi/2 \pm \alpha$ and $\theta = 3\pi/2 \pm \alpha$ where α is a function of σ_x, σ_y, and P_o. The former is illustrated by the first set of data in Table XXII and the latter is illustrated by the following five sets of data in

TABLE XXII

VARIATION OF PRINCIPAL SHEAR AS A FUNCTION OF BIAXIAL LOADING

θ-(deg)	$\tau_{r\theta}$-(psi)	τ_{ry}-(psi)	$\tau_{\theta y}$-(psi)
	σ_x = - 200 psi	σ_y = - 400 psi	P_o = 2000 psi
0	845	758	88
30	900	785	115
60	1000	835	165
90	1045	858	188
	σ_x = - 300 psi	σ_y = - 600 psi	P_o = 2000 psi
0	795	808	7
30	882	852	31
60	1030	926	104
90	1115	959	137
	σ_x = - 600 psi	σ_y = - 800 psi	P_o = 2000 psi
0	646	758	113
30	840	855	15
60	1127	999	129
90	1246	1058	188
	σ_x = - 500 psi	σ_y = - 1000 psi	P_o = 2500 psi
0	932	1072	140
30	1083	1148	65
60	1328	1270	58
90	1432	1322	110
	σ_x = - 600 psi	σ_y = - 1000 psi	P_o = 1800 psi
0	551	792	241
30	753	893	140
60	1038	1006	2
90	1151	1092	59
	σ_x = - 1200 psi	σ_y = - 1700 psi	P_o = 2000 psi
0	345	908	563
30	840	1155	315
60	1357	1414	57
90	1546	1508	58
	σ_x = - 1000 psi	σ_y = - 1800 psi	P_o = 1800 psi
0	351	992	641
30	759	1196	436
60	1195	1415	120
90	1351	1493	141

Table XXII. A condition may be reached where the maximum principal shear always lies in the τ_{ry} direction, one such set of conditions is illustrated by the last set of data in Table XXII.

Table XXII also suggests that for higher stress concentrations and the appropiate fracturing fluid pressure, the component of shear "$\tau_{\theta y}$" may become the maximum principal shear component; indeed, the last two sets of data included in Table XXII show that for $\theta = 0$, $\tau_{\theta y}$ has replaced $\tau_{r\theta}$ as the second maximum principal shear.

The results of the experimental investigation indicate that the hydraulic fracture phenomena can be divided into three regions of interest: (1) a region where control of fracture propagation is possible, (2) a region of transition where an initial control of fracture propagation is demonstrated and then a rotation occurs such that the fracture aligns itself normal to the direction of the least compressive stress, and (3) a region in which no control of fracture propagation is possible.

The correlation of the mathematical model with the results of the experimental investigation indicates that the three regions of hydraulic fracturing can be defined in terms of the tensile strength and the shearing strength of the material being fractured, the maximum shearing stress acting, and the hydraulic fluid pressure of the internal crack.

In region 1, where control of fracture propagation has been demonstrated, the tensile strength of the material appears to be the controlling factor. The tensile strength of hydrostone has been determined to be of the order of 140 psi (14). For uniaxial loads of 300 psi and less, control of fracture propagation has been established experimentally. The mathematical model substantiates these findings. As long as the greatest compressive stress is less than the tensile strength of the material, the fracture propagation can be controlled irrespective of the direction of the least compressive stress. The magnitude of the internal fracturing fluid pressure acting within a circular prefracture has been shown, mathematically, to introduce a tensile stress in the neighborhood of the crack in a direction perpendicular to the plane of the crack and thus becomes an influencing factor in fracture control. The greater the internal fluid pressure, the better the control of fracture orientation.

In the transition region, the components of principal shear appear to control the rate at which the propagating fracture turns so as to become normal to the least compressive stress. In correlating the analysis of the mathematical model to the experimental findings, it appears that the shearing stress τ_{ry} can be directly related to the rate of curvature. The higher the value of τ_{ry}, the greater the rate of curvature. If τ_{ry} becomes greater than $\tau_{r\theta}$, the rate of curvature increases and the fracture turns

rapidly. The same could be said of $\tau_{\theta y}$; however, for all cases analyzed, $\tau_{\theta y}$ was always less than τ_{ry}.

The region of transition may thus be defined as that state of stress of a body where the maximum principal compressive stress is greater than the tensile strength of the material and the maximum principal shear is less than the shearing strength of the material.

The region in which no control of fracture propagation was exhibited appears to be where the principal shearing stress τ_{ry} approaches the shearing strength of the material being fractured.

The contour surfaces of the fractured blocks agree quite well with that predicted by the mathematical model. The curving nature of the fractured surfaces are seen to have an angular dependence, for the biaxial loading, and correspond, to the first approximation, with the angular dependence of the two shear components $\tau_{r\theta}$ and τ_{ry}. The larger the magnitude of τ_{ry} the greater the rate of curvature. Under uniaxial loading, the general fracture surfaces, was that of an ellipsoid indicating a θ independence in which case the shear components were constant for a given r. For the biaxial case, the fractured surfaces, in general, show a θ dependence in the curvature with the greatest curvature being in the Z-direction which corresponds to the maximum value of τ_{ry}.

Some Practical Applications

The following four examples illustrates descriptively how a knowledge of the stress conditions might be used in the planning of a water flood program in a secondary oil recovery operation.

Example 1. With reference to Figure 34, let it be assumed that $S_3 > S_2 > S_1$ where in this and the following examples a tensile stress is considered positive. Here S_3 lies in the Z-direction and is the least compressive stress. The resulting hydraulic fracture will be horizontal lying in a plane parallel to the XY-plane such that the fracture will intercept the producing well irrespective of the position of the fracturing well.

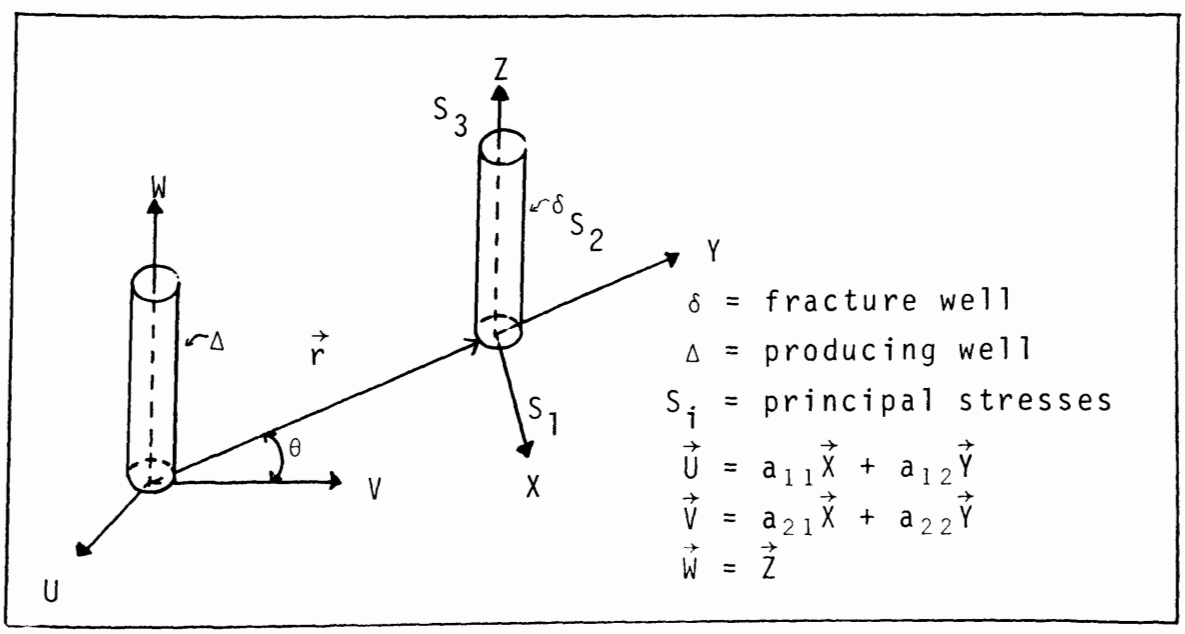

Figure 34. Schematic representation of a Hydraulic Fracturing Field Operation where the Principal Horizontal Stresses do not Correspond to the Horizontal Axis of the Production Well.

Example 2. With reference to Figure 34, let it be assumed that $S_1 > S_2 > S_3$. The least principal compressive stress is horizontal, lying in the X-direction so that the hydraulic fracture will be vertical and will propagate in the YZ-plane. In order that the hydraulic fracture will intercept the production well, the fracture well must be located at an angle θ to the V-axis where θ is given by the equation

$$(70) \quad \theta = \tan^{-1}(a_{21}/a_{22})$$

Example 3. With reference to Figure 35, let it be assumed that $S_3 > S_2 > S_1$. In this example the least principal stress lies in the Z-direction which makes an angle of inclination ϕ with the UV-plane. In order to intercept the

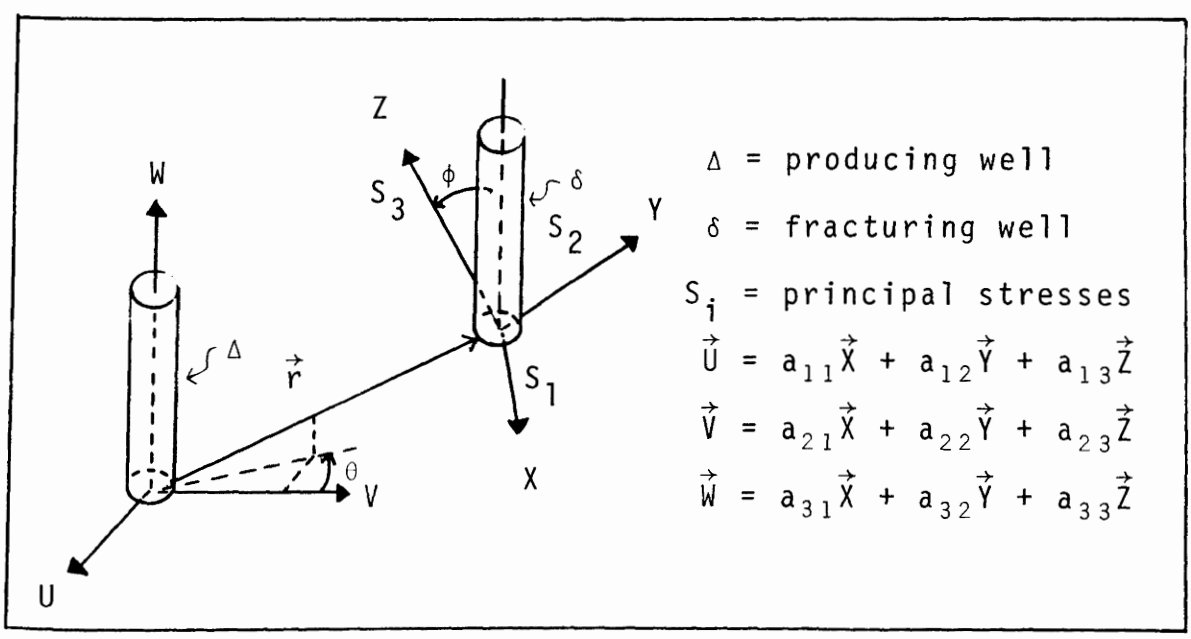

Figure 35. Schematic representation of a Hydraulic Fracturing Field Operation where the Principal Stresses do not correspond to the Axes of the Production Well.

production well at some depth "h", the radial distance "r" must be considered along with the depth of the initiating fracture "H". The angle of dip or inclination is given by

$$(71) \quad \phi = \cos^{-1}[a_{33}/(a_{31}^2 + a_{32}^2 + a_{33}^2)^{\frac{1}{2}}]$$

Example 4. With reference to Figure 35, let it be assumed that $S_1 > S_2 > S_3$ such that the least compressive stress lies in the X-direction. The fracture plane will be parallel to the XY-plane which will intersect the W-axis in an oblique manner. In order to intercept the production well at some depth "h" it will be necessary to know both the polar angle "θ" and the dip angle "ϕ" along with the radial separation "r" of the two wells and the depth "H" of the point of fracture initiation. For this example, the angle of dip will be given by

$$(72) \quad \phi = \cos^{-1}[a_{33}/(a_{31}^2 + a_{32}^2 + a_{33}^2)^{\frac{1}{2}}]$$

and the polar angle by

$$(73) \quad \theta = \cos^{-1}[a_{22}/(a_{21}^2 + a_{22}^2 + a_{23}^2)^{\frac{1}{2}}]$$

CHAPTER VII

SUMMARY, CONCLUSIONS, AND RECOMMENDATIONS

The objectives of this investigation were to determine experimentally if control of orientation of fracture propagation is possible by the introduction of prefractures orientated in a prescribed manner under uniaxial and biaxial loading conditions and to present a mathematical model which would represent the experimental findings.

Summary

The experimental results indicate that under proper stress conditions control of fracture orientation is possible; however, under general stress conditions, little control can be achieved such that the orientation of the developing fracture plane will seek that direction which is perpendicular to the least compressive stress.

Fracture control, or better, lack of control can be explained by the mathematical model presented. If the maximum principal stress at the tip of the crack is less than the tensile strength of the rock material being fractured, then control of fracture orientation can be achieved. If the maximum principal stress is greater than the tensile strength of the material being fractured while at the same time the principal shear components are less than the shear strength of the fracturing material, then the fracture will

initially propagate in the direction of the prefracture and immeadiately start turning at a rate which appears related to the principal shear stress so as to become perpendicular to the least compressive stress. No fracture control is exhibited when the maximum principal shear stress approaches or becomes greater than the shear strength of the rock material.

The fractured surfaces all exhibited tensile type failures. For the lower confining stress condition, the surfaces showed, in general, smooth plane or curved type breaks. For the larger confining stress conditions, the surfaces exhibited rougher, step-like tensile breaks. There appeared to be no shear failures; the shearing stresses present acted only as a secondary mechanism in the failure phenomena, controlling the rate at which the fracture turns so as to align itself up in a direction perpendicular to the least compressive stress.

The solution obtained for the mathematical model indicates that control of fracture orientation could be enhanced for larger stress concentrations by maintaining a higher internal fluid pressure. To accomplish this, it seems adviseable to use a less viscous type fracturing fluid in order to decrease the pressure gradient within the established fracture. Also, a pulsating fluid pressure appears to posses interesting possibilities in the building up of large pressures at the crack periphery while having

lower pressures within the interior of the crack.

From the experimental evidence obtained from this investigation and supported by the solution of the mathematical model, the nature and orientation of a hydraulic fracture can be predicted with reasonable certainty if the state of stress of the region being fractured is known along with the tensile and shearing strengths of the material. For industrial applications, in particular, secondary oil recovery by use of hydraulic fracturing techniques, the tectonic stress conditions, where fracturing is applicable, is such that the tensile and shearing strengths of the rock matrix is of little consequence in the fracturing operation and only the state of stress need be known to determine the nature and orientation of the fracture and thus plan the fracturing operation more intelligently.

Conclusions

Conclusions which appear to be warranted from this investigation are:

1. If the resulting principal stresses at the crack tip or periphery are less than the tensile strength of the material being fractured, fracture orientation can be controlled.

2. If the resulting principal stresses at the crack periphery are greater than the tensile strength of the material being fractured but the principal shear stresses are less than the shear strength, the fracture will ini-

tially propagate in the preferred direction while at the same time turning takes place at a rate proportional to the magnitude of the shear stress in a direction so as to align itself perpendicular to the least compressive stress.

3. If the resulting principal stresses at the crack periphery are greater than the tensile strength of the material being fractured and the shear stresses are equal to or greater than the shear strength, no control of fracture orientation is possible such that the fracture will immeadiately propagate in a direction perpendicular to the least compressive stress.

4. The mathematical model presented appears to represent accurately the hydraulic fracturing phenomena for prefractures of circular and elliptical nature.

5. The presence of a prefracture in a material produces a localized stress condition around the prefracture.

6. If the stress condition of a region is known along with the tensile and shearing strengths of the material, the orientation of a hydraulic fracture can be predicted with reasonable certainty.

7. The presence of a prefracture does influence the initiation of a hydraulic fracture.

8. In the transition region, the principal shear stresses influence the rate at which a fracture will turn so as to become perpendicular to the least principal compressive stress.

9. A hydraulic fracture can be extended across a plane of weakness, such as a joint or another fracture, in a rock substance.

10. The hydraulic fractures all exhibited tensile-type failures for the hydrostone specimens tested.

11. The magnitude of the internal fracturing pressure appears to affect favorably the localized stress condition at the crack periphery to control fracture orientation.

12. The geometrical shape of the prefracture, circular or elliptical, has little influence on the nature of the ensuing fracture.

13. The state of stress influences the breakdown pressure. The breakdown pressure for the blocks fractured under a biaxial load was noticeably higher than those fractured under an uniaxial load.

Recommendations

Areas of further investigation which seem warranted at this time are:

1. Investigations of the hydraulic fracturing problem similar to those of this investigation under triaxial loading conditions.

2. A study of the control of fracture orientation by employing a system of hydraulically pressurized prefractures or zones.

3. Investigations employing pressurizing fluids of a high, pulsating nature.

4. Model studies using plexiglas or other suitable transparent material to visually observe the fracture propagation. In the case of plexiglas, which has essentially no pore volume, the hydraulic fluid must be incompressible and the pressurizing system machined to a very close tolerance in order to control the fracture propagation.

5. An investigation into the possibilities of using the techniques of hydraulic fracturing under known stress conditions to determine directional tensile strengths.

BIBLIOGRAPHY

1. Brace, W. F., and Bombolakis, E. G. (1963): A note on Brittle Crack Growth in Compression. Jour. Geoph. Res. Vol. 68, No. 12, pp. 3709-3713.

2. Burton, P. (1961): A modification of the Coulomb-Mohr theory of fracture. Trans ASME, Jour. Appl. Mech. Vol. 28, No. 2, pp. 259-268.

3. Clark, J. B. (1949): Hydrafrac Process. Oil and Gas Jour. Vol. 13, No.3, pp. 75-85.

4. Clausing, D. P. (1959): Comparison of Griffith's Theory with Mohr's Failure Criteria. Col. Sch. Mines Quart. Vol. 54, No. 3, pp. 285-296.

5. Cleary, J. M. (1958): Hydraulic Fracture Theory Part I - Mechanics of Materials. Ill. Geological Survey, Circular 251.

6. _____ (1958): Hydraulic Fracture Theory Part II - Fracture Orientation and Possibility of Fracture Control. Ill. Geological Survey, Circular 252.

7. _____ (1959): Hydraulic Fracture Theory Part III - Elastic Properties of Sandstone. Ill. Geological Survey, Circular 281.

8. Dunlap, J. R. (1963): Factors Controlling the Orientation and Direction of Hydraulic Fracturing. Jour. of the Inst. of Pet. Vol. 49, pp. 282-288.

9. Fairhurst, C. (1964): Measurement of In-Situ Rock Stresses with Particular Reference to Hydraulic Fracturing. Jour. Int. Soc. Rock Mech. Vol. 2, No. 3-4, pp. 129-147.

10. _____ (1965): On the Determination of the State of Stress in Rock Masses. AIME Preprint, No. SPE-1062.

11. Fraser, C. D, and Pettitt, B. E. (1962): Results of a Field Test to Determine the Type and Orientation of a Hydraulically Induced Formation Fracture. Jour. Pet. Tech., Vol. 14, No. 5, pp. 463-499.

12. Geertsma, J. (1957): Effect of Fluid Pressure Decline on Volume Changes in Porous Rocks. Jour. Pet. Tech., Vol. 9, No. 12, pp. 33;-340.

13. Gupta, K. P. (1958): How to Measure Rock Pressures. Engrg. and Mining Jour., Vol. 159, No. 10, pp. 95-100.

14. Haas, C. J., and Rinehart, J. S. (1962): Measurement of Coupling Between Columns of Explosives and Artificial Rocks. Tech. Report, Colo. Sch. of Mines Res. Foundation Inc., Golden Colo., pp. 13-15.

15. Handin, J., (1957): Experimental Deformation of Rocks and Minerals. Second Symp. Rock Mech., Colo. Sch. Mines Quarterly, Vol. 52, No. 4, pp. 77-98.

16. Harrison, E., Kieschnick, J. W. Jr., and McGuire, W. J. (1954): The Mechanics of Fracture Induction and Extension. Petr. Trans., Vol. 201, pp. 252-263.

17. Hast, N. (1958): The Measurement of Rock Pressure in Mines. Svertiges Geologiska Undersokning, Arshok 52, 3, Stockholm.

18. Howard, G. C. and Fast, C. R. (1957): Optimum Fluid Characteristics for Fracture Extension. Drill. and Prod. Prac., Vol. 261.

19. Hubbert, M. K. (1951): Mechanical Basis for Certain Familiar Geological Structures. Bull. GSA, Vol. 63, pp. 355-371.

20. Hubbert, M. K., and Willis, P. G. (1957): Mechanics of Hydraulic Fracturing. Petr. Trans., Vol. 20, pp. 153-156.

21. Huitt, J. R. (1960): Hydraulic Fracturing with a Single Point Entry Technique. Jour. Petr. Tech., March, pp. 11-13.

22. Jaeger, J. C., and Cook, N. G. W. (1963): Theory and Application of Curved Jacks for Measurement of Stresses. Proc. Intern. Conf. on the State of Stress in the Earth's Crust. Santa Monica, Calif.

23. Kehle, R. O. (1964): The Determination of Tectonic Stresses Through Analysis of Hydraulic Well Fracturing. Jour. Geoph. Res., Vol. 69, No. 2, pp. 259-209.

24. Lamont, N., and Jensen, F. W. (1963): The Effects of Existing Fractures in Rocks on the Extension of Hydraulic Fractures. AIME Trans., Vol. 228, pp. 259-273.

25. Leeman, E. R. (1964): The Measurement of Stress in Rock, Part I - The Principles of Rock Stress Measurements. South African Inst. Mining and Met., Vol. 65, No. 2, pp. 45-81.

26. Leeman, E. R. (1964): The Measurement of Stress in Rock, Part II - Borehole Rock Stress Measuring Instruments. South African Inst. Mining and Met., Vol. 65, No. 2, pp. 82-114.

27. Lekhnitskii, S. G. (1963): Theory of Elasticity of an Anisotropic Elastic Body. San Francisco: Holden-Day Inc.

28. Love, A. E. H. (1944): The Mathematical Theory of Elasticity. New York: Dover Publications, Inc.

29. Lubinski, A. (1954): The Theory of Elasticity for Porous Bodies Displaying a Strong Pore Structure. Prock. Scnd. U.S. Nat. Cong. App. Mech., pp. 247-256.

30. Martin, C. W. (1952): Fracture of Plaster by Explosion. (Unpublished Doctorate Dissertation, U. of Iowa, Ames Iowa.) pp. 8-9.

31. Merrill, R. H. (1963): In-Situ Determination of Stress by Relief Techniques. Proc. Intern. Conf. on the State of Stress in the Earth's Crust. Santa Monica, Calif., Rand Corp.

32. Obert, L. (1940): Measurement of Pressures on Rock Pillars in Underground Mines. U.S. Bureau Mines, R. I. 3521.

33. Ode, H. (1956): A Note Concerning the Mechanism of Artificial and Natural Hydraulic Fracture Systems. Colo. Sch. of Mines Quart., Vol. 51, No. 3, pp. 19-29.

34. Olsen, O. J. (1957): Measurement of Residual Stress by the Strain Relief Method. Colo. Sch. of Mines Quart., Vol. 52, No. 3, pp. 183-204.

35. Orowan, E., (1948): Fracture and Strength of Solids. Reports on Progress in Physics, V. 12, pp. 185-232.

36. Panek, L. A. (1961): Measurement of Rock Pressure with a Hydraulic Cell. Mining Engrg., Vol. 220, pp. 282-285.

37. Perkins, T. K., and Kern, L. R. (1961): Widths of Hydraulic Fractures. Jour. Petr. Tech., pp. 937-949.

38. Poollen, van, H. K. (1957): Theories of Hydraulic Fracturing. Colo. Sch. of Mines Quart., Vol. 52, No. 3, pp. 113-128.

39. Potts, E. L. J. (1963): The In Situ Measurement of Rock Stress Based on Deformation Measurements. Proc. Intern. Conf. on the State of Stress in the Earth's Crust. Santa Monica, Calif., Rand Corp.

40. Potts, E. L. J. (1957): Underground Instrumentation. Colo. Sch. of Mines Quart., Vol. 52, No. 3, pp. 135-182.

41. Reynolds, J. J., and Popham, J. L. (1961): Hydraulic Fracture Field Test to Determine Areal Extent and Orientation. Jour. Petr. Tech., Vol. 13, pp. 371-377.

42. Reynolds, J. L., Bocquet, P. E., and Clark, C. Jr. (1954): A Method of Creating Vertical Hydraulic Fractures. Drill. and Prod. Pract., Vol. 136, pp. 206-211.

43. Roberts, A., Emery, C. L., Chakravarty, P. K., and Williams, F. T. (1961-1962): Photoelastic Coating Technique Applied to Research in Rock Mechanics. Trans. Inst. Mining and Met., Vol. 71, Part 10, pp. 581-617.

44. Scott, P. P. Jr., Bearden, W. J., and Howard, G. C. (1953): Rock Rupture as Affected by Fluid Properties. Trans. AIME, Vol. 198, pp. 111-124.

45. Silverman, I. K. (1957): Behavior of Materials and Theories of Failure. Second Sympt. Rock Mechanics, Colo. Sch. of Mines Quart., Vol. 52, pp. 3-17.

46. Sneddon, I. N., (1951): Fourier Transforms, McGraw-Hill Book Co., Inc., 542 p.

47. Sneddon, I. N., and Elliott, H. A. (1946): The Opening of a Griffith Crack Under Internal Pressure. Quart. of Appl. Math., Vol. 4, pp. 262-267.

48. Sokolnikoff, I. S. (1956): Mathematical Theory of Elasticity. McGraw Hill Book Co., New York.

49. Starr, A. T. (1928): Slip in a Crystal and Rupture in a Solid due to Shear. Cambridge Phil. Soc. Proc., Vol. 24, pp. 489-500.

50. Stefanko, R. (1960): Underground Stress Instrumentation. AIME Preprint 60A051.

51. Scheidegger, A. E. (1960): On the Connection between Tectonic Stresses and Well Fracturing Data. Geofis. Pura Appl., Vol. 46, pp. 66-76.

52. Timoshenko, S. P., and Goodier, J. N. (1951): Theory of Elasticity. McGraw Hill Book Co., New York.

53. Watson, G. N. (1922): The Theory of Bessel Functions. Cambridge, London, p. 405.

54. Willmore, T. J. (1949): The Distribution of Stress in the Neighborhood of a Crack. Quart. Jour. Mech. and Appl. Math., Vol. 2, pp. 53-63.

APPENDIX A

PROPERTIES OF HYDROSTONE

Figure A-1 graphically represents the average mass of the hydrostone blocks cast for this investigation as a function of the curing time in days. After preparation, the blocks were placed on an open shelf with no attempt to control the temperature or humidity during this curing time. The mass stablization starts leveling off after a time lapse of about 20 days and reaches a stable state in approximately 36 days.

Table A-1 lists some of the physical properties for hydrostone of the same general mixture as used in this investigation. The values represented are averages with a minimum of five determinations for any one given property.

The properties determined by the author were all done with synethic core samples of two inches in length and an inch and a half in diameter prepared from the same mixtures as that of the fracturing specimens. Each core sample had reached its stablization weight before testing.

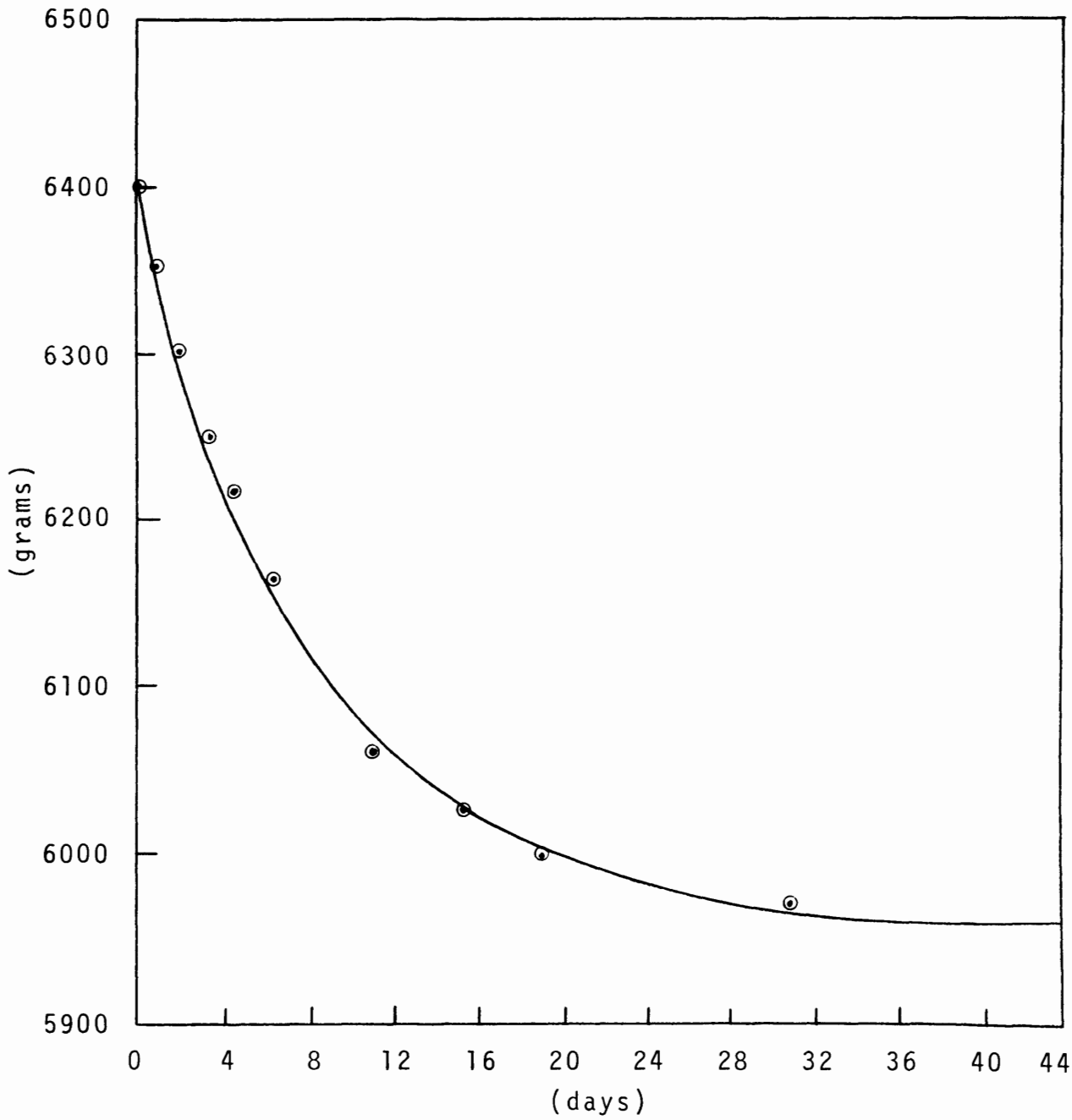

Figure A-1. Mass of Hydrostone Blocks as a Function of Time.

TABLE A-1

PHYSICAL PROPERTIES OF HYDROSTONE

Property	Haas & Rinehart (14)	Martin (30)	Author
Density[1]	----	106	104
Apparant Porosity[2]	----	17	19
Compressive Strength[3]	6640	4150	7230
Tensile Strength[3]	140[5]	385[6]	410[6]
Shearing Strength[3]	1780	----	----
Poisson's Ratio[4]	0.18	0.24	----
Young's Modulus[3]	1.94×10^6	2.18×10^6	2.75×10^6
Shear Modulus[3]	0.82×10^6	0.87×10^6	----

[1]Pounds/(cubic foot)

[2]The ratio of the volume of open pore space in the specimen to the exterior volume expressed in percent

[3]Pounds/(square inch)

[4]Dimensionless

[5]Direct test

[6]Brazilian test

APPENDIX B

AXIALLY SYMMETRICAL STRESS DISTRIBUTIONS IN CYLINDRICAL COORDINATES AND ITS APPLICATION TO A CIRCULAR CRACK

Let it be assumed, that the deformation is symmetrical with an axis of revolution having cylindrical coordinates r, θ, and y where the Y-axis is the axis of symmetry. Then, the components of displacement and the stress tensor will all be independent of the angle θ. Consider an element of volume in a solid of revolution, as shown in Figure B-1, where the state of stress at any point of the solid will be specified by the four components σ_r, σ_θ, σ_y, and τ_{ry}. Also,

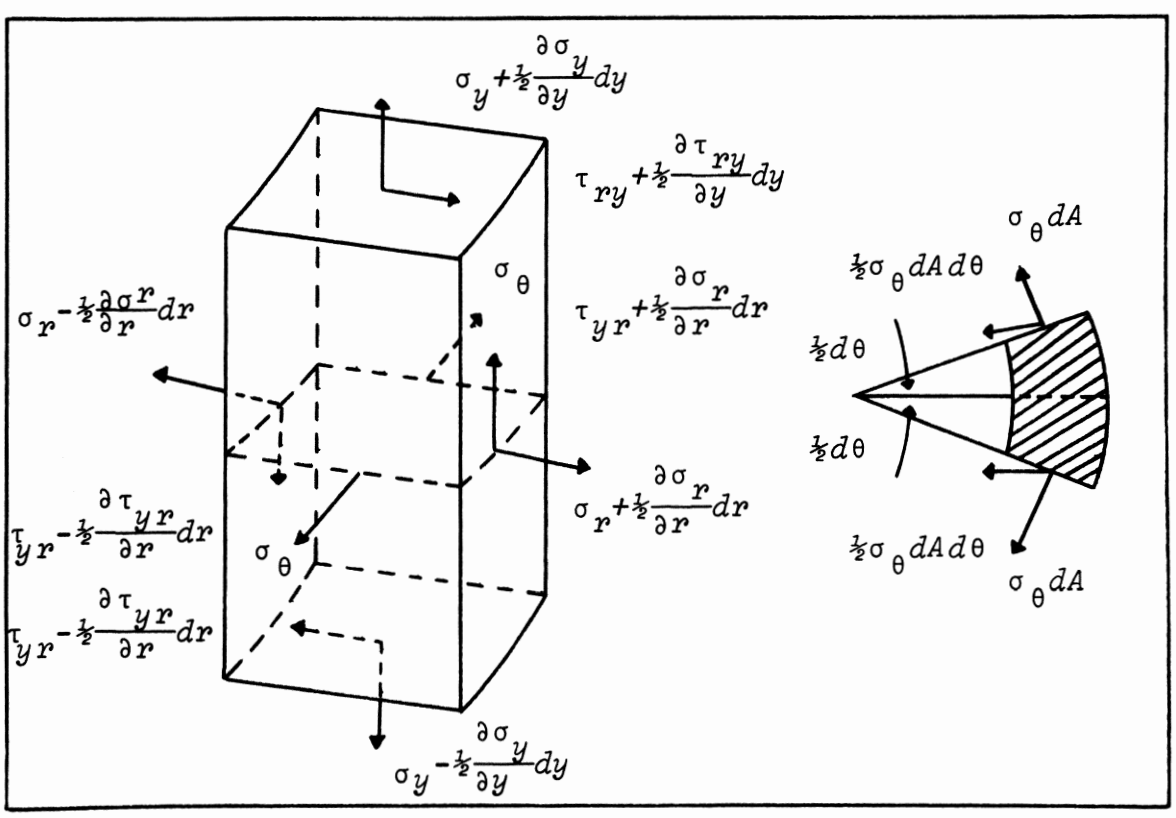

Figure B-1. Stresses acting on an element of a solid of revolution.

the displacement vector will be given by u_r in the radial direction and u_y in the axial direction with u_θ vanishing at each point because of symmetry.

If it is assumed that there are no body forces acting and that the element centered at the point (r,θ,y) has sides $(dr,d\theta,dy)$, then the equilibrium condition in the radial direction becomes

$$(B\text{-}1)\quad (\sigma_r+\frac{1}{2}\frac{\partial\sigma_r}{\partial r}dr)(r+\tfrac{1}{2}dr)d\theta dy - (\sigma_r-\frac{1}{2}\frac{\partial\sigma_r}{\partial r}dr)(r-\tfrac{1}{2}dr)d\theta dy$$
$$- \sigma_\theta d\theta dy dr + (\tau_{ry}+\frac{1}{2}\frac{\partial\tau_{ry}}{\partial y}dy)r dr d\theta$$
$$- (\tau_{ry}-\frac{1}{2}\frac{\partial\tau_{ry}}{\partial y}dy)r dr d\theta = 0$$

where the fact has been taken into account that the stress components σ_θ on each face of the element give rise to a force $-\sigma_\theta d\theta dr dy$ in the radial direction. Similarily, in the Y-direction there is

$$(B\text{-}2)\quad (\sigma_r+\frac{1}{2}\frac{\partial\sigma_y}{\partial y}dy)(y+\tfrac{1}{2}dy)d\theta dr + (\sigma_y-\frac{1}{2}\frac{\partial\sigma_y}{\partial y}dy)(y-\tfrac{1}{2}dy)d\theta dr$$
$$+ (\tau_{yr}-\frac{1}{2}\frac{\partial\tau_{yr}}{\partial r}dr)(r-\tfrac{1}{2}dr)d\theta dy$$
$$+ (\tau_{yr}+\frac{1}{2}\frac{\partial\tau_{yr}}{\partial r}dr)(r+\tfrac{1}{2}dr)d\theta dy = 0$$

In the limit as dr, $d\theta$, and dy tend to zero, the equations of equilibrium become

$$(B\text{-}3)\quad \frac{\partial\sigma_r}{\partial r} + \frac{\partial\tau_{ry}}{\partial y} + \frac{\sigma_r-\sigma_\theta}{r} = 0$$

$$(B\text{-}4)\quad \frac{\partial\tau_{ry}}{\partial r} + \frac{\partial\sigma_y}{\partial y} + \frac{\tau_{ry}}{r} = 0$$

The compatibility equations can be transformed from the rectangular cartesian coordinates to cylindrical coordinates by letting

$$(B\text{-}5)\quad \sigma_x = \sigma_r \cos^2\theta + \sigma_\theta \sin^2\theta$$

$$(B\text{-}6)\quad \sigma_z = \sigma_r \sin^2\theta + \sigma_\theta \cos^2\theta$$

and taking Laplace's operator in cylindrical coordinates as

$$(B\text{-}7)\quad \nabla^2 \equiv \frac{\partial^2}{\partial r^2} + \frac{1}{r}\frac{\partial}{\partial r} + \frac{1}{r^2}\frac{\partial^2}{\partial \theta^2} + \frac{\partial^2}{\partial y^2}$$

Then

$$(B\text{-}8)\quad \nabla^2\sigma_x = \left(\frac{\partial^2}{\partial r^2} + \frac{1}{r}\frac{\partial}{\partial r} + \frac{1}{r^2}\frac{\partial^2}{\partial \theta^2} + \frac{\partial^2}{\partial y^2}\right)(\sigma_r \cos^2\theta + \sigma_\theta \sin^2\theta$$

$$= \left(\frac{\partial^2}{\partial r^2} + \frac{1}{r}\frac{\partial}{\partial r} + \frac{\partial^2}{\partial y^2}\right)(\sigma_r \cos^2\theta + \sigma_\theta \sin^2\theta)$$

$$- \frac{2}{r^2}\cos 2\theta(\sigma_r - \sigma_\theta)$$

$$= \bar{\nabla}^2(\sigma_r \cos^2\theta + \sigma_\theta \sin^2\theta) - \frac{2}{r^2}\cos 2\theta(\sigma_r - \sigma_\theta)$$

where $\bar{\nabla}^2$ is defined as $\frac{\partial^2}{\partial r^2} + \frac{1}{r}\frac{\partial}{\partial r} + \frac{\partial^2}{\partial y^2}$.

Letting Θ be the sum of the three normal components of stress and applying the identity

$$(B\text{-}9)\quad \frac{\partial^2\phi}{\partial x^2} = \frac{\partial^2\phi}{\partial r^2}\cos^2\theta - 2\frac{\partial^2\phi}{\partial\theta\partial r}\frac{\sin\theta\cos\theta}{r} + \frac{\partial\phi}{\partial r}\frac{\sin^2\theta}{r}$$

$$+ 2\frac{\partial\phi}{\partial\theta}\frac{\sin\theta\cos\theta}{r^2} + \frac{\partial^2\phi}{\partial\theta^2}\frac{\sin^2\theta}{r^2}$$

there is obtained for a symmetrical stress distribution

$$(B\text{-}10)\quad \frac{\partial^2\Theta}{\partial x^2} = \frac{\partial^2\Theta}{\partial r^2}\cos^2\theta + \frac{\partial\Theta}{\partial r}\frac{\sin^2\theta}{r}$$

Taking the compatibility equations as developed by Timoshenko (52) to be

$$(B\text{-}11)\quad (1+\nu)\nabla^2\sigma_x + \frac{\partial^2\Theta}{\partial x^2} = 0$$

$$(B\text{-}12)\quad (1+\nu)\nabla^2\sigma_y + \frac{\partial^2\Theta}{\partial y^2} = 0$$

$$(B\text{-}13)\quad (1+\nu)\nabla^2\sigma_z + \frac{\partial^2\Theta}{\partial z^2} = 0$$

$$(B\text{-}14)\quad (1+\nu)\nabla^2\tau_{yz} + \frac{\partial^2\Theta}{\partial y\partial z} = 0$$

$$(B\text{-}15)\quad (1+\nu)\nabla^2\tau_{xz} + \frac{\partial^2\Theta}{\partial x\partial z} = 0$$

$$(B\text{-}16)\quad (1+\nu)\nabla^2\tau_{xy} + \frac{\partial^2\Theta}{\partial x\partial y} = 0$$

and substituting equation (B-9) and (B-10) into (B-11) there results

$$(B\text{-}17)\quad \nabla^2(\sigma_r\cos^2\theta + \sigma_\theta\sin^2\theta) - \frac{2}{r^2}\cos 2\theta(\sigma_r - \sigma_\theta)$$
$$+ \frac{1}{1+\nu}\left(\frac{\partial^2\Theta}{\partial r^2}\cos^2\theta + \frac{\partial\Theta}{\partial r}\frac{\sin^2\theta}{r}\right) = 0$$

Since this equation holds for all values of θ, it must be that

$$(B\text{-}18)\quad \bar{\nabla}^2\sigma_r - \frac{2}{r^2}(\sigma_r - \sigma_\theta) + \frac{1}{1+\nu}\frac{\partial^2\Theta}{\partial r^2} = 0$$

$$(B\text{-}19)\quad \bar{\nabla}^2\sigma_\theta + \frac{2}{r^2}(\sigma_r - \sigma_\theta) + \frac{1}{r}\frac{1}{1+\nu}\frac{\partial\Theta}{\partial r} = 0$$

If the Y-axis is the axis of symmetry, then equation (B-12) will retain the same form in cylindrical coordinates. Also, for the case of a symmetrical deformation, equation (B-13) will give the same result as that obtained by considering equation (B-11); thus, equations (B-18) and (B-19) along with equation (B-12) are sufficient for the components of stress.

For the case of symmetrical deformation, only the shearing stress τ_{ry} remains. The stress components τ_{xy} and τ_{yz}, acting on a plane perpendicular to the Y-axis, are obtained by resolving τ_{ry} into two components parallel to the X- and Z-axes,

$$(B\text{-}20)\quad \tau_{xy} = \tau_{ry}\cos\theta$$

$$(B\text{-}21)\quad \tau_{yz} = \tau_{ry}\sin\theta$$

and

$$(B\text{-}22)\quad \frac{\partial^2\Theta}{\partial x\,\partial y} = \frac{\partial^2\Theta}{\partial r\,\partial y}\cos\theta$$

$$(B\text{-}23)\quad \nabla^2\tau_{xy} = \nabla^2(\tau_{ry}\cos\theta)$$

$$= (\nabla^2\tau_{ry} - \frac{\tau_{ry}}{r^2})\cos\theta$$

substituting into equation (B-16), there results

$$(B\text{-}24)\quad \nabla^2\tau_{ry} - \frac{1}{r^2}\tau_{ry} + \frac{1}{1+\nu}\frac{\partial^2\Theta}{\partial r\partial y} = 0$$

Hence, the compatibility equations in the case of a deformation symmetrical with respect to the Y-axis are in cylindrical coordinates

$$(B\text{-}25)\quad \nabla^2\sigma_r - \frac{2}{r^2}(\sigma_r - \sigma_\theta) + \frac{1}{1+\nu}\frac{\partial^2\Theta}{\partial r^2} = 0$$

$$(B\text{-}26)\quad \nabla^2\sigma_\theta + \frac{2}{r^2}(\sigma_r - \sigma_\theta) + \frac{1}{1+\nu}\frac{1}{r}\frac{\partial\Theta}{\partial r} = 0$$

$$(B\text{-}27)\quad \nabla^2\sigma_y + \frac{1}{1+\nu}\frac{\partial^2\Theta}{\partial z^2} = 0$$

$$(B\text{-}28)\quad \nabla^2\tau_{ry} - \frac{1}{r^2}\tau_{ry} + \frac{1}{1+\nu}\frac{\partial^2\Theta}{\partial r\partial y} = 0$$

If an arbitrary stress function Φ is taken which satisfies the biharmonic equation

$$(B\text{-}29)\quad \nabla^4\Phi = 0$$

then, the compatibility equations (B-25,B-26,B-27,B-28) along with the equations of equilibrium (B-3,B-4) will be satisfied by taking

$$(B\text{-}30)\quad \sigma_r = \frac{\partial}{\partial y}(\nu\nabla^2\Phi - \frac{\partial^2\Phi}{\partial r^2})$$

$$(B\text{-}31)\quad \sigma_\theta = \frac{\partial}{\partial y}(\nu\nabla^2\Phi - \frac{1}{r}\frac{\partial\Phi}{\partial r})$$

$$(B\text{-}32)\quad \sigma_y = \frac{\partial}{\partial y}[(2-\nu)\nabla^2\Phi - \frac{\partial^2\Phi}{\partial y^2}]$$

$$(B\text{-}33) \quad \tau_{ry} = \frac{\partial}{\partial r}[(1-\nu)\nabla^2\Phi - \frac{\partial^2\Phi}{\partial y^2}]$$

With the aid of axial symmetry, the relations between the components of stress and the nonvanishing components of the displacement vector may be written as:

$$(B\text{-}34) \quad \sigma_r = [(\lambda+2G)\frac{\partial}{\partial r} + \frac{\lambda}{r}]u_r + \frac{\partial u_y}{\partial y}$$

$$(B\text{-}35) \quad \sigma_\theta = (\lambda\frac{\partial}{\partial r} + \frac{\lambda+2G}{r})u_r + \frac{\partial u_y}{\partial y}$$

$$(B\text{-}36) \quad \sigma_y = \lambda(\frac{\partial}{\partial r} + \frac{1}{r})u_r + (\lambda+2G)\frac{\partial u_y}{\partial y}$$

$$(B\text{-}37) \quad \tau_{ry} = G(\frac{\partial u_r}{\partial y} + \frac{\partial u_y}{\partial r})$$

where

$$(B\text{-}38) \quad u_r = -\frac{\lambda+G}{G}\frac{\partial^2\Phi}{\partial r\partial y}$$

$$(B\text{-}39) \quad u_y = \frac{\lambda+2G}{G}\nabla^2\Phi - \frac{\lambda+G}{G}\frac{\partial^2\Phi}{\partial y^2}$$

and λ and G are Lame's constants.

The equations for the components of stress reduce to

$$(B\text{-}40) \quad \sigma_r = \lambda\nabla^2(\frac{\partial\Phi}{\partial y} - 2(\lambda+G)\frac{\partial^3\Phi}{\partial r^2\partial y})$$

$$(B\text{-}41) \quad \sigma_y = (3\lambda+4G)\nabla^2(\frac{\partial\Phi}{\partial y} - 2(\lambda+G)\frac{\partial^3\Phi}{\partial y^3})$$

$$(B\text{-}42) \quad \sigma_\theta = \nabla^2(\frac{\partial\Phi}{\partial y}) - \frac{2}{r}(\lambda+G)\frac{\partial^2\Phi}{\partial y\partial r}$$

$$(B\text{-}43) \quad \tau_{ry} = (\lambda+2G)\frac{\partial}{\partial r}\nabla^2\Phi - 2(\lambda+G)\frac{\partial^3\Phi}{\partial y^2\partial r}$$

The equations of equilibrium are satisfied by these expressions and if these expressions are substituted into the compatibility equations, it is found that the compatibility equations are satisfied if the arbitrary function Φ is a solution of the biharmonic equation

$$(B\text{-}44) \quad \nabla^4\phi = 0$$

Thus, the problem reduces to that of finding solutions of the biharmonic equation satisfying the necessary boundary conditions.

Solution of the Equations of Equilibrium

By applying Hankel transforms, the biharmonic equation in r and y can be reduced to a fourth-order, ordinary differential equation in y; the variable r being taken by a parameter. The boundary conditions must then be treated in the same way, so that instead of having relations concerning partial derivatives with respect to r and y, relations are obtained in terms of the derivatives with respect to y of an auxiliary function which depends upon y alone.

Using the idenity[1]

$$(B\text{-}45) \quad \int_0^\infty r\left(\frac{d^2f}{dr^2} + \frac{1}{r}\frac{df}{dr}\right)J_o(\S r)dr = -\S^2\overline{f}(\S)$$

and

$$(B\text{-}46) \quad \nabla^2\phi = \frac{\partial^2\phi}{\partial r^2} + \frac{1}{r}\frac{\partial\phi}{\partial r} + \frac{\partial^2\phi}{\partial y^2}$$

---

[1] See, "Fourier Transforms" by Sneddon, equation (35) page 62.

there results

$$(B\text{-}47)\quad \int_0^\infty r\left(\frac{\partial^2 f}{\partial r^2} + \frac{1}{r}\frac{\partial f}{\partial r} + \frac{\partial^2 f}{\partial y^2}\right)J_o(\S r)\,dr$$

$$= -\S^2 \int_0^\infty rfJ_o(\S r)\,dr + \int_0^\infty r\frac{d^2 f}{dy^2}J_o(\S r)\,dr$$

$$= \left(\frac{d^2}{dy^2} - \S^2\right)\int_0^\infty rfJ_o(\S r)\,dr$$

Replacing f by $\nabla^2\phi$, and repeating the operation, there is obtained

$$(B\text{-}48)\quad \int_0^\infty r\nabla^4\phi J_o(\S r)\,dr = \left(\frac{d^2}{dy^2} - \S^2\right)\int_0^\infty r\left(\frac{d^2\phi}{dr^2} + \frac{1}{r}\frac{d\phi}{dr} + \frac{d^2\phi}{dy^2}\right)J_o(\S r)\,dr$$

$$= \left(\frac{d^2}{dy^2} - \S^2\right)^2 \int_0^\infty r\phi J_o(\S r)\,dr$$

Taking the biharmonic equation

$$(B\text{-}49)\quad \nabla^4\phi = 0$$

and multiplying both sides by $rJ_o(\S r)$ and integrating over the range of r, there results

$$(B\text{-}50)\quad \int_0^\infty r\nabla^4\phi J_o(\S r)\,dr = \left(\frac{d^2}{dy^2} - \S^2\right)^2 \int_0^\infty r\phi J_o(\S r)\,dr$$

$$= \left(\frac{d^2}{dy^2} - \S^2\right)^2 G(\S, y)$$

where $G(\S, y)$ is the zero-order Hankel transform of the

function $\phi(r,y)$ as defined by

$$(B\text{-}51) \quad \bar{f}(\S) = \int_0^\infty xf(x)J_\nu(\S x)dx$$

Making use of the operator notation, equation (B-50) becomes

$$(B\text{-}52) \quad (D^2 - \S^2)^2 G(\S,y) = 0$$

which leads to the auxilary equation

$$(B\text{-}53) \quad (m^2 - \S^2)^2 = 0$$

having the algebraic, repeated roots

$$(B\text{-}54) \quad m = \pm\S, \pm\S$$

To insure that all components tend to 0 as $y \to \infty$, the repeated root $+\S$ must be discarded, and assume the solution to be of the form

$$(B\text{-}55) \quad G(\S,y) = (A + By)\exp(-\S y)$$

where the arbitrary constants, A and B, are to be determined from the boundary conditions and are in general functions of the parameter $\S$.

The determination of the arbitrary constants occuring in this solution may be facilitated by transforming the expressions for the components of stress and displacement into relations involving $G(\S,y)$ and its derivatives with respect to y.

Performing these manipulations, there is obtained

$$(B\text{-}56)\quad u_r = \frac{\lambda+\bar{G}}{\bar{G}} \int_0^\infty \S^2 \frac{dG}{dy} J_1(\S r)\, d\S$$

$$(B\text{-}57)\quad u_y = \int_0^\infty \S \left(\frac{d^2G}{dy^2} - \frac{\lambda+2\bar{G}}{\bar{G}} \S^2 G\right) J_o(\S r)\, d\S$$

$$(B\text{-}58)\quad \sigma_y = \int_0^\infty \S \left[(\lambda+2\bar{G})\frac{d^3G}{dy^2} - (3\lambda+4\bar{G})\S^2 \frac{dG}{dy}\right] J_o(\S r)\, d\S$$

$$(B\text{-}59)\quad \sigma_r = \int_0^\infty \S \left[\frac{d^3G}{dy^3} + (\lambda+2\bar{G})\S^2 \frac{dG}{dy}\right] J_o(\S r)\, d\S$$

$$- \frac{2(\lambda+\bar{G})}{r} \int_0^\infty \S^2 \frac{dG}{dy} J_1(\S r)\, d\S$$

$$(B\text{-}60)\quad \sigma_\theta = \lambda \int_0^\infty \S \left(\frac{d^3G}{dy^3} - \S^2 \frac{dG}{dy}\right) J_o(\S r)\, d\S + \frac{2(\lambda+\bar{G})}{r} \int_0^\infty \left[\S^2 \frac{dG}{dy} J_1(\S r)\, d\S\right]$$

$$(B\text{-}61)\quad \tau_{ry} = \int_0^\infty \S^2 \left[\lambda \frac{d^2G}{dy^2} + (\lambda+2\bar{G})\S^2 G\right] J_1(\S r)\, d\S$$

In the three-dimensional case, it is assumed that the crack is created in the interior of an infinite medium and is circular in shape occupying the region $r^2 = x^2 + z^2 = c^2$ in the plane $y = 0$. If it is further assumed, that the crack is deformed by the application of a constant, axially symmetrical pressure, then at $y = 0$, $\sigma_y = P_o$ for $r < c$.

To determine the values of A and B of equation (B-55), it is necessary to evaluate τ_{ry}, u_y, σ_y on the plane $y = 0$. Expressing Lamé constants in terms of the Young's modulus E and Poisson's ratio ν by

$$(B\text{-}62) \quad \lambda = \frac{E\nu}{(1+\nu)(1-2\nu)}$$

$$(B\text{-}63) \quad \overline{G} = \frac{E}{2(1+\nu)}$$

and differeniating equation (B-55) with respect to y twice and substituting y = 0 into equation (B-61), there results

$$(B\text{-}64) \quad [\tau_{ry}]_{y=0} = \frac{E}{(1+\nu)(1-2\nu)} \int_0^\infty \S^3(A-2\nu B) J_1(\S r)\, d\S$$

Inverting this result by means of the Hankel inversion theorem as defined by

$$(B\text{-}65) \quad f(x) = \int_0^\infty u\overline{f}(u) J_\nu(xu)\, du$$

equation (B-64) becomes

$$(B\text{-}66) \quad \S^2(A-2\nu B) = \frac{(1+\nu)(1-2\nu)}{E} \int_0^\infty r[\tau_{ry}]_{y=0} J_1(\S r)\, d\S$$

If the boundary condition $[\tau_{ry}]_{y=0} = 0$, holds for all values of r, it must be that

$$(B\text{-}67) \quad \S A = 2\nu B$$

Taking the results of equation (B-67) and substituting into equation (B-55) and differeniating equation (B-55) with respect to y and setting y = 0, there is obtained from equations (B-57) and (B-58)

$$(B\text{-}68) \quad [u_y]_{y=0} = - \frac{2(1-\nu)}{1-2\nu} \int_0^\infty \S^2 B J_o(\S r)\, d\S$$

$$(B\text{-}69) \quad [\sigma_y]_{y=0} = \frac{E}{(1+\nu)(1-2\nu)} \int_0^\infty \S^3 B J_o(\S r) d\S$$

Expressing equation (B-55) in the form

$$(B\text{-}70) \quad G = \frac{B(c\S)}{\S}(2\nu+\S y)\exp(-\S y)$$

and letting $\zeta = \S c$ in equations (B-68) and (B-69) there is finally obtained

$$(B\text{-}71) \quad [\sigma_y]_{y=0} = \frac{E}{c^4(1+\nu)(1-2\nu)} \int_0^\infty \zeta f(\zeta) J_o(\rho\zeta) d\zeta$$

$$(B\text{-}72) \quad [u_y]_{y=0} = \frac{-2(1-\nu)}{c^3(1-2\nu)} \int_0^\infty f(\zeta) J_o(\rho\zeta) d\zeta$$

where

$$(B\text{-}73) \quad f(\zeta) = \zeta^2 B(\zeta)$$

and

$$(B\text{-}74) \quad \rho = r/c$$

Taking the boundary conditions $y = 0$, $u_y = 0$ for $r > c$, and $\sigma_y = -P(r)$ for $r < c$, and inserting into equations (B-68) and (B-69) there is obtained the pair of integral equations

$$(B\text{-}75) \quad \int_0^\infty \zeta f(\zeta) J_o(\rho\zeta) d\zeta = g(\rho) \qquad 0 < \rho < 1$$

$$(B\text{-}76) \quad \int_0^\infty f(\zeta) J_o(\rho\zeta) d\zeta = 0 \qquad \rho > 1$$

which can be solved for the determination of the unknown function $f(\zeta)$ and finally the constant $B(c\S)$ of equation

(B-70). Equation (B-75) may be written then as

$$(B\text{-}77) \quad g(\rho) = -\frac{(1+\nu)(1-2\nu)}{E} c^4 P(\rho c)$$

The formal solution of these equations by use of the theory of Mellin transforms was first given by Titchmarsh in his book on Fourier integrals.[2] The solution of these two integral equations can be determined by letting

$$(B\text{-}78) \quad f(\zeta) = \frac{2}{\pi} \int_0^1 \mu \sin(\mu\zeta) d\zeta \int_0^1 \frac{\rho g(\rho\mu)}{(1-\rho^2)^{\frac{1}{2}}} d\rho$$

Substituting from equation (B-77) into equation (B-75) and making use of the result obtained by Watson (53)

$$(B\text{-}79) \quad \int_0^\infty \sin(\mu\zeta) J_o(\rho\zeta) d\zeta = 0 \qquad \rho > \mu$$
$$= (\mu^2 - \rho^2)^{-\frac{1}{2}} \qquad \rho < \mu$$

it is found that when the applied pressure is P(r), the value of the normal component of the surface displacement is given by the equation

$$(B\text{-}80) \quad [u_y]_{y=0} = \frac{4(1-\mu^2)c}{\pi E} \int_0^1 \frac{\mu d\mu}{\rho(\mu^2-\rho^2)^{\frac{1}{2}}} \int_0^1 \frac{xP(x\ c)}{(1-x^2)^{\frac{1}{2}}} dx$$

In the case where the applied pressure P(r) is a constant P_o over the entire surface area $r < c$ of the crack, $P(\rho c)$ may be replaced by P_o; then, there is obtained from

---

[2] Titchmarsh, E. C. (1937): Introduction to the Theory of Fourier Integrals. Oxford, New York, p. 337.

equations (B-77) and (B-78)

$$(B\text{-}81) \quad f(\zeta) = \frac{2P_o c^4(1+\nu)(1-2\nu)}{\pi E} \frac{d}{d\zeta}\left(\frac{\sin\zeta}{\zeta}\right)$$

Substituting this value for $f(\zeta)$ into equation (B-71), it follows that, for the normal component of stress across the plane $y = 0$,

$$(B\text{-}82) \quad [\sigma_y]_{y=0} = \frac{2P_o}{\pi}\left[\int_0^\infty \rho \sin\zeta J_1(\rho\zeta)\,d\zeta - \int_0^\infty \frac{\sin\zeta}{\zeta} J_o(\rho\zeta)\,d\zeta\right]$$

Making use of the relations given by Watson (53)

$$(B\text{-}83) \quad \int_0^\infty \frac{\sin\zeta}{\zeta} J_o(\rho\zeta)\,d\zeta = \sin^{-1}(1/\rho) \qquad \rho > 1$$

$$= \pi/2 \qquad \rho < 1$$

$$(B\text{-}84) \quad \int_0^\infty \rho \sin\zeta J_1(\rho\zeta)\,d\zeta = (\rho^2 - 1)^{-\frac{1}{2}} \qquad \rho > 1$$

$$= 0 \qquad \rho < 1$$

equation (B-82) gives

$$(B\text{-}85) \quad [\sigma_y]_{y=0} = -P_o \qquad \rho < 1$$

and

$$(B\text{-}86) \quad [\sigma_y]_{y=0} = -\frac{2P_o}{\pi}\left[\sin^{-1}(1/\rho) - 1/(\rho^2-1)^{-\frac{1}{2}}\right] \qquad \rho > 1$$

Also, when $\rho \to 1$, the stress $[\sigma_y]_{y=0}$ becomes infinite.

For the values of the other stress components on the plane $y = o$, there is obtained from the equations (B-58) to

(B-61) the expressions

$$(B\text{-}87)\quad (\sigma_r+\sigma_\theta)_{y=0} = (1+2\nu)[\sigma_y]_{y=0}$$

$$(B\text{-}88)\quad (\sigma_r-\sigma_\theta)_{y=0} = \frac{2(1-\nu)P_o}{\pi}\int_0^\infty \zeta J_2(\rho\zeta)\frac{d}{d\zeta}\left(\frac{\sin\zeta}{\zeta}\right)d\zeta$$

$$= \frac{2(1-2\nu)P_o}{\pi}\left[\int_0^\infty J_2(\rho\zeta)\cos\zeta\, d\zeta - \int_0^\infty J_2(\rho\zeta)\frac{\sin\zeta}{\zeta}d\zeta\right]$$

Evaluating the integrals in the square bracket, it is found that the bracket vanishes when $\rho < 1$ and has the value $-(\rho^2-1)^{-\frac{1}{2}}$ when $\rho > 1$. Thus, if $\rho < 1$ and $y = 0$, then

$$(B\text{-}89)\quad \sigma_\theta = \sigma_r = -(\nu+\tfrac{1}{2})P_o \qquad \rho < 1$$

and, for $\rho > 1$, and $y = 0$ it becomes

$$(B\text{-}90)\quad \sigma_r = \frac{2P_o}{\pi}\left[(\rho^2-1)^{-\frac{1}{2}} - (\nu+\tfrac{1}{2})\sin^{-1}(1/\rho)\right]$$

$$(B\text{-}91)\quad \sigma_\theta = \frac{2P_o}{\pi}\left[2\nu(\rho^2-1)^{-\frac{1}{2}} - (\nu+\tfrac{1}{2})\sin^{-1}(1/\rho)\right]$$

To evaluate the stress components in the interior of the medium for $y \neq 0$, the analysis follows that of the Boussinesq problem for a cylinder as developed by Sneddon (46). From equations (B-73) and (B-81), the value of $B(c\S)$ can be determined; and, by substituting equation (B-70) into equations (B-56) and (B-57) there is obtained for the non-vanishing components of the displacement vector

$$(B\text{-}92)\quad u_r = \frac{2P_o c}{\pi E}(1+\nu)\int_0^\infty (1-2\nu-\eta\zeta)\frac{d}{d\zeta}\left(\frac{\sin\zeta}{\zeta}\right)\exp(-\eta\zeta)J_1(\rho\zeta)\,d\zeta$$

$$(B\text{-}93)\quad u_y = -\frac{4P_o c(1-\nu^2)}{\pi E}\int_0^\infty \left(1+\frac{\eta\zeta}{2(1-\nu)}\right)\frac{d}{d\zeta}\left(\frac{\sin\zeta}{\zeta}\right)\exp(-\eta\zeta)J_o(\rho\zeta)\,d\zeta$$

where $\rho = r/c$ and $\eta = y/c$. In the same manner, from equations (B-58) through (B-61), one obtains for the components of stress at a general point in the interior of the elastic solid

$$(B\text{-}94)\quad \sigma_y = \frac{2P_o}{\pi}[C_2^0(\rho,\eta) - S_1^0(\rho,\eta) + C_3^0(\rho,\eta) - \eta S_2^0(\rho,\eta)$$

$$(B\text{-}95)\quad \sigma_r+\sigma_\theta+\sigma_y = \frac{4(1+\nu)P_o}{\pi}[C_2^0(\rho,\eta) - S_1^0(\rho,\eta)]$$

$$(B\text{-}96)\quad \tau_{yr} = \frac{2P_o\eta}{\pi}[C_3^1(\rho,\eta) - S_2^1(\rho,\eta)$$

where C_β^α and S_β^α denote the integrals

$$(B\text{-}97)\quad C_\beta^\alpha(\rho,\eta) = \int_0^\infty \xi^{\alpha-2}\exp(-\rho\xi)J_\beta(\rho\xi)\cos\xi\,d\xi$$

$$(B\text{-}98)\quad S_\beta^\alpha(\rho,\eta) = \int_0^\infty \xi^{\alpha-2}\exp(-\eta\zeta)J_\beta(\rho\xi)\sin\xi\,d\xi$$

The fourth relation needed for the complete determination of all the components of stress can be found by taking the difference of equations (B-60) and (B-59), giving

$$(B\text{-}99)\quad \sigma_\theta-\sigma_r = 2(\lambda+\overline{G})\int_0^\infty \xi^3\,\frac{dG}{dy}\left[\frac{2J_1(\xi r)}{\xi r} - J_o(\xi r)\right]d\xi$$

Letting n = 1 and y = ξr in the recurrence formula

$$(B\text{-}100)\quad J_{n-1}(y) + J_{n+1}(y) = \frac{2n}{y}J_n(y)$$

equation (B-99) becomes

$$(B\text{-}101)\quad \sigma_\theta - \sigma_r = 2(\lambda+\bar{G})\int_0^\infty \S^3 \frac{dG}{dy}J_2(\S r)d\S$$

Using equations (B-62) and (B-63) to express Lame's constants in terms of Young's modulus E and Poisson's ration ν and using the integral relations of equations (B-97) and (B-98), equation (B-101) becomes

$$(B\text{-}102)\quad \sigma_\theta - \sigma_r = \frac{2P_o}{\pi}[(1-2\nu)\{C_2^2(\rho,\eta)-S_1^2(\rho,\eta)-\eta C_3^2(\rho,\eta) - S_2^2(\rho,\eta)\}]$$

Defining the quantity

$$(B\text{-}103)\quad Z_\beta^\alpha(\rho,\eta) = \int_0^\infty p^{\alpha-2}J_\beta(p\rho)\exp(-p\rho)dp$$

the coefficients $C_\beta^\alpha(\rho,\eta)$ and $S_\beta^\alpha(\rho,\eta)$ can be determined by the relation

$$(B\text{-}104)\quad C_\beta^\alpha(\rho,\eta) - iS_\beta^\alpha(\rho,\eta) = Z_\beta^\alpha(\rho,\eta+i)$$

by evaluating $Z_\beta^\alpha(\rho,\eta+i)$ and then separating the real and imaginary parts.

The integral of the Bessel functions with infinite limits can be expressed as

$$(B\text{-}105)\quad J(\nu,p,\mu) \equiv \int_0^\infty J_\nu(at)\exp(-pt)dt(t^\mu)$$

$$= \frac{\Gamma(\mu-\nu+1)}{(a^2+p^2)^{\frac{1}{2}(\mu+1)}} p_\mu^\nu\left[\frac{p}{(a^2+p^2)^{\frac{1}{2}}}\right]$$

where $\Gamma(m)$ denotes the Gamma function and $p_\mu^\nu(z)$ denotes the associated Legendre function of argument z.

As special cases of equation (B-105), there is found

$$(B\text{-}106)\quad \int_0^\infty \exp(-px) J_1(ax) \frac{dx}{x} = \frac{(a^2+p^2)^{\frac{1}{2}} - p}{a}$$

$$(B\text{-}107)\quad \int_0^\infty \exp(-px) J_1(ax)\, dx = \frac{1}{a} - \frac{p}{a(a^2+p^2)^{\frac{1}{2}}}$$

$$(B\text{-}108)\quad \int_0^\infty \exp(-px) J_1(ax)\, x\, dx = a(a^2+p^2)^{-3/2}$$

$$(B\text{-}109)\quad \int_0^\infty \exp(-px) J_o(ax)\, dx = (a^2+p^2)^{-\frac{1}{2}}$$

$$(B\text{-}110)\quad \int_0^\infty \exp(-px) J_o(ax)\, x\, dx = p(a^2+p^2)^{-3/2}$$

Letting $w = \eta + i$, and evaluating equations (B-106) through (B-110), there is obtained

$$(B\text{-}111)\quad Z_2^0(\rho, w) = \int_0^\infty \exp(-pw) J_o(\rho p)\, dp = (\rho^2+w^2)^{-\frac{1}{2}}$$

$$(B\text{-}112)\quad Z_3^0(\rho, w) = \int_0^\infty \exp(-pw) J_o(\rho p)\, p\, dp = w(\rho^2+w^2)^{-3/2}$$

$$(B\text{-}113)\quad Z_1^1(\rho, w) = \int_0^\infty \exp(-pw) J_1(\rho p) \frac{1}{p} dp = \frac{1}{\rho}[(\rho^2+w^2)^{\frac{1}{2}} - w]$$

$$(B\text{-}114)\quad Z_2^1(\rho, w) = \int_0^\infty \exp(-pw) J_1(\rho p)\, dp = \frac{1}{\rho} - \frac{w}{(\rho^2+w^2)}$$

$$(B\text{-}115)\quad Z_3^1(\rho, w) = \int_0^\infty \exp(-pw) J_1(\rho p)\, p\, dp = (\rho^2+w^2)^{-3/2}$$

Making use of the reccurence equation (B-100) expressed in the form

$$(B\text{-}116)\quad Z_n^2 = \frac{2}{\rho}Z_{n-1}^1 - Z_n^0$$

there results

$$(B\text{-}117)\quad Z_3^2(\rho,w) = \frac{2}{\rho}Z_2^1 - Z_2^0$$

$$= \frac{2}{\rho}\left[\frac{1}{\rho} - \frac{w}{\rho(\rho^2+w^2)^{\frac{1}{2}}}\right] - \frac{1}{(\rho^2+w^2)^{\frac{1}{2}}}$$

$$(B\text{-}118)\quad Z_2^2(\rho,w) = \frac{1}{\rho}Z_1^1(\rho,w) - Z_2^0(\rho,w)$$

$$= \frac{1}{\rho^2}\left[(\rho^2+w^2)^{\frac{1}{2}} - w\right] - \frac{1}{(\rho^2+w^2)^{\frac{1}{2}}}$$

The evaluation of $S_1^0(\rho,\eta)$ and $S_1^2(\rho,\eta)$ may be accomplished by integrating the expressions for $Z_1^1(\rho,w)$ and $Z_2^0(\rho,w)$ with respect to w; thus

$$(B\text{-}119)\quad \int_0^\infty\left[\int_0^w \exp(-pw)J_o(\rho p)\,dw\right]dp = \int_0^\infty \frac{1-\exp(-pw)}{\rho}J_o(\rho p)\,dp$$

$$= \ln\left[\frac{(\rho^2+w^2)^{\frac{1}{2}}+w}{\rho}\right]$$

and

$$(B\text{-}120)\quad \int_0^\infty\left[\int_{0\rho}^w \frac{1}{\rho}\exp(-pw)J_1(\rho p)\,dw\right]dp = \int_0^\infty \frac{1-\exp(-pw)}{\rho^2}J_1(\rho p)\,dp$$

$$= \frac{1}{2\rho}\left[w(w^2+\rho^2)^{\frac{1}{2}} - w^2+\rho^2\ln\frac{(\rho^2+w^2)^{\frac{1}{2}}+w}{\rho}\right]$$

Using the recurrence relation

$$(B\text{-}121)\quad J_{n-1}(x) - \frac{2n}{x}J_n(x) + J_{n+1}(x) = 0$$

and expressing $J_2(p\rho)$ in terms of $J_1(p\rho)$ and $J_o(p\rho)$ there is obtained

$$(B\text{-}122)\quad Z_1^2(\rho,\eta) = \int_0^\infty \frac{1-\exp(-pw)}{p} J_2(p,\rho)dp$$

$$= \frac{1}{\rho^2}[w(w^2 + \rho^2) - w^2]$$

$$= \frac{w}{\rho}Z_1^1(\rho,w)$$

putting $w = \eta+i$ and $Z_1^1(\rho,w) = C_1^1(\rho,\eta) - iS_1^1(\rho,\eta)$ in equation (B-120) and equating imaginary parts, there is found

$$(B\text{-}123)\quad S_1^2(\rho,\eta) = \text{Imag}\{\frac{\eta+i}{\rho}[C_1^1(\rho,\eta) - iS_1^1(\rho,\eta)]\}$$

$$= \frac{1}{\rho}[C_1^1(\rho,\eta) - \eta S_1^1(\rho,\eta)]$$

Defining the relations

$$(B\text{-}124)\quad \eta\tan\theta \equiv 1$$

$$(B\text{-}125)\quad r^2 \equiv 1 + \eta^2$$

$$(B\text{-}126)\quad R^2 \equiv (\rho^2 + \eta^2 - 1)^2 + 4\eta^2$$

$$(B\text{-}127)\quad 2\eta\cot\phi \equiv \rho^2 + \eta^2 - 1$$

and equating imaginary parts of equation (B-120) and simplifying

$$(B\text{-}128)\quad S_1^0 = \tan^{-1}\left[\frac{R^{\frac{1}{2}}\sin(\phi/2) + r\sin\phi}{R^{\frac{1}{2}}\cos(\phi/2) + r\cos\theta}\right]$$

In similar manner, by using the relations of equations (B-124) through (B-127) and equating real and imaginary parts after substituting $w = \eta + i$ into the equations (B-111) through (B-115), (B-117), (B-118), and (B-123) and making use of the identity given by equation (B-104), the following results are obtained:

$$(B\text{-}129)\quad C_2^0(\rho,\eta) = R^{-\frac{1}{2}}\cos(\phi/2)$$

$$(B\text{-}130)\quad C_3^0(\rho,\eta) = rR^{-3/2}\cos(3\phi/2 - \theta)$$

$$(B\text{-}131)\quad C_1^1(\rho,\eta) = \frac{1}{\rho}[R^{\frac{1}{2}}\cos(\phi/2) - \eta]$$

$$(B\text{-}132)\quad C_2^1(\rho,\eta) = \frac{1}{\rho}[1 - rR^{-\frac{1}{2}}\cos(\theta - \phi/2)]$$

$$(B\text{-}133)\quad C_3^1(\rho,\eta) = R^{-3/2}\cos(3\phi/2)$$

$$(B\text{-}134)\quad S_2^0(\rho,\eta) = R^{-\frac{1}{2}}\sin(\phi/2)$$

$$(B\text{-}135)\quad S_3^0(\rho,\eta) = rR^{-3/2}\sin(3\phi/2 - \theta)$$

$$(B\text{-}136)\quad S_1^1(\rho,\eta) = \frac{1}{\rho}[1 - R^{\frac{1}{2}}\sin(\phi/2)]$$

$$(B\text{-}137)\quad S_2^1(\rho,\eta) = \frac{r}{\rho}[R^{-\frac{1}{2}}\sin(\theta - \phi/2)$$

$$(B\text{-}138)\quad S_3^1(\rho,\eta) = R^{-3/2}\sin(3\phi/2)$$

$$(B\text{-}139)\quad C_2^2(\rho,\eta) = \frac{2}{\rho^2}[R^{\frac{1}{2}}\cos(\phi/2) - \eta] - R^{-\frac{1}{2}}\cos(\phi/2)$$

$$(B\text{-}140)\quad S_2^2(\rho,\eta) = \frac{2}{\rho^2}[1 - R^{\frac{1}{2}}\sin(\phi/2)] - R^{-\frac{1}{2}}\sin(\phi/2)$$

$$(B\text{-}141)\quad C_3^2(\rho,\eta) = \frac{2}{\rho^2}[1 - rR^{-\frac{1}{2}}\cos(\theta - \phi/2)] - rR^{-3/2}\cos(3\phi/2 - \theta)$$

Finally, the stress components in the interior of the medium for $Y \neq 0$, using the abbreviated notation of C_β^α for $C_\beta^\alpha(\rho,\eta)$ and S_β^α for $S_\beta^\alpha(\rho,\eta)$, can be written

$$(B\text{-}142)\quad \sigma_r = \frac{P_o}{\pi}[(1+2\nu)(C_2^0 - S_1^0) + (C_3^2 - C_3^0 + S_2^0 - S_2^2) + (1-2\nu)(S_1^2 - C_2^2)]$$

$$(B\text{-}143)\quad \sigma_\theta = \frac{P_o}{\pi}[(1+2\nu)(C_2^0 - S_1^0) + \eta(S_2^2 - C_3^2 + S_2^0 - C_3^0) + (1-2\nu)(C_2^2 - S_1^2)]$$

$$(B\text{-}144)\quad \tau_{ry} = \frac{2P_o}{\pi}[C_3^1 - S_2^1]$$

$$(B\text{-}145)\quad \sigma_y = \frac{2P_o}{\pi}[C_2^0 - S_1^2 + (C_3^0 - S_2^0)]$$

where equations (B-143) and (B-144) follow from equations (B-94), (B-95), and (B-102).

APPENDIX C

COMPUTER PROGRAMS FOR THE NUMERICAL CALCULATIONS OF THE STRESS DISTRIBUTION ASSOCIATED WITH THE MATHEMATICAL MODEL

COMPUTER PROGRAM I STRESS ON THE PLANE Y = 0

```
      DIMENSIØN  PØ(26),RHØ(4),RX(4),RRØ(4)
      CX=0.75
      PR=.18
      D1=.5/CX
      PI=3.1415927
      RHØ(1)=D1
      PØ(1)=500.
      DØ 1 N=2,15
      PØ(N)=PØ(N-1)+100.
      PRINT 102, PØ(N)
      PRP=PØ(N)/PI
      P2P=2.*PRP
      YK1=PR+.5
      STR=-YK1*PØ(N)
      STØ=-YK1*PØ(N)
      STY=-PØ(N)
      SRY=0.
      PUNCH 120,STR,STØ,STY,SRY
      PRINT 120,STR,STØ,STY,SRY
      DØ 3 I=2,4
      RHØ(I)=RHØ(I-1)+D1
      RX(I)=RHØ(I)*RHØ(I)
      RRØ(I)=1./RHØ(I)
      YX1=1./SQRTF(RX(I)-1.)
      YX2=RRØ(I)*RRØ(I)
      YX3=YX2*YX2
      ARS=RRØ(I)+RRØ(I)*YX2/6.+(3./40.)*(RRØ(I)*YX3)+(15./33
     16.)*(YX2*RRØ(I))
      STR=P2P*(YX1-YK1+ARS)
      STØ=P2P*((2.*PR)*YX1-YK1*ARS)
      STY=-P2P*(ARS-YX1)
      SRY=0.
      PUNCH 120,STR,STØ,STY,SRY
    3 PRINT 120,STR,STØ,STY,SRY
    1 CØNTINUE
      CALL EXIT
  120 FØRMAT(4F9.3)
  102 FØRMAT(30X,10HPRESSURE =,1F6.0)
      END
```

COMPUTER PROGRAM II STRESS AROUND A CIRCULAR CRACK FOR Y ≠ 0

```
      DIMENSIØN R(6),RHØ(6),RX(6),PØ(26),Y(6),YHØ(6),HEA(6),
     1HA(6),R6(6),TH(6),SIX5(6),RRØ(6),R7(6),R8(6),RR1(6),
     2CØS5(6)
      HA(1)=0.
      R8(1)=0.
      R7(1)=1.
      CX=0.75
      PI=3.1415927
      D1=.5/CX
      PR=.18
      R(1)=.5
      HEA(1)=0.
      RHØ(1)=D1
      RX(1)=D1*D1
      RRØ(1)=1./RHØ(1)
      RR1(1)=2.*RRØ(1)
      PØ(1)=400.
      DØ 1 N=2,26
      PØ(N)=PØ(N-1)+100.
      PRINT 102, PØ(N)
      PRP=PØ(N)/PI
      Y(1)=0.
      P2P=2.*PRP
      XK=2.*PR+1.
      YK=1.-2.*PR
      TH(1)=PI/2.
      R6(1)=1.
      PRINY 100
      DØ 2 I=2,6
      R(I)=R(I-1)+.5
      Y(I)=Y(I-1)+.5
      RHØ(I)=RHØ(I-1)+D1
      HEA(I)=HEA(I-1)+D1
      HA(I)=HEA(I)*HEA(I)
      RA=1./HEA(I)
      RX(I)=RHØ(I)*RHØ(I)
      R6(I)=SQRTF(1.+HA(I))
      TH(I)=ATANF(RA)
      SIX5(I)=SINF(TH(I))
      CØS5(I)=CØSF(TH(I))
      RRØ(I)=1./RHØ(I)
      R7(I)=R6(I)*SIX5(I)
      R8(I)=R6(I)*CØS5(I)
    2 RR1(I)=2.*RRØ(I)
      DØ 5 J=2,5
      DØ 5 I=1,4
      B=(2.*HEA(J))/(RX(I)+HA(J)-1.)
      C=(RX(I)+HA(J)-1.)*(RX(I)+HA(J)-1.)+4.*HA(J)
```

```
      R1=SQRTF(C)
      PH1=ATANF(B)
      IF(B)3,4,4
    3 PH1=PH1+PI
    4 CONTINUE
      R2=SQRTF(R1)
      R3=1./R2
      R4=1./R1
      R5=R3*R4
      PH2=PH1*.5
      PH3=PH1+PH2
      ARG1=PH3-TH(J)
      ARG2=TH(J)-PH2
      CØS1=CØSF(PH2)
      CØS2=CØSF(ARG1)
      CØS3=CØSF(ARG2)
      CØS4=CØSF(PH3)
      SIX1=SINF(PH2)
      SIX2=SINF(ARG1)
      SIX3=SINF(ARG2)
      SIX4=SINF(PH3)
      RS1=R6(J)*SIX1
      RC2=R2*CØS1
      RS2=R2*SIX1
      ARG3=(R7(J)+RS2)/R8(J)+RC2)
      C2Ø=R3*CØS1
      C3Ø=(R6(J)*R5)*CØS2
      C11=RRØ(I)*((R2*CØS1)-HEA(J))
      C21=RRØ(I)*(1.-(R6(J)*R3)*CØS3)
      C31=(RHØ(I)*R5)*CØS4
      S2Ø=R3*SIX1
      S3Ø=(R6(J)*R5)*SIX2
      S11=RRØ(I)*(1.-R2*SIX1)
      S21=((R6(J)*RRØ(I))*R3)*SIX3
      S31=(RHØ(I)*R5)*SIX4
      C22=(RR1(I)*C11)-C2Ø
      S22=(RR1(I)*S11)-S2Ø
      C32=(RR1(I)*C21)-C3Ø
      S12=RRØ(I)*(C11-(HEA(J)*S11))
      S1Ø=ATANF(ARG3)
      IF(R7(J)+RS2)11,21,16
   11 IF(R8(J)+RC2)18,20,21
   16 IF(R8(J)+RC2)18,21,21
   18 S1Ø=S1Ø+PI
      GØ TØ 21
   20 S1Ø+PI
   21 CØNTINUE
      C2S=C2Ø-S1Ø
      C3S=S2Ø-C3Ø
      S2C=S12-C22
      S3C=S22-C32
```

```
      C4S=C22-S12
      C5S=C31-S21
      STR=PRP*(XK*C2S-HEA(J)*(S3C-C3S)+S2C*YK)
      STØ=PRP*(XK*C2S+HEA(J)*(S3C+C3S)+C4S*YK)
      STY=P2P*(C2S-HEA(J)*C3S)
      SRY=P2P*C5S
      STT=((2.*P2P)*(1.+PR)*C2S)
      PUNCH 120,STR,STØ,STY,SRY
    5 PRINT 101,STR,STØ,STY,SRY,STT,S1Ø
    1 CØNTINUE
      CALL EXIT
  100 FØRMAT(6X,8HSTRESS-R,6X,8HSTRESS-T,6X,8HSTRESS-Y,5X,9H
     3STRESS-RY,4X,12HSTRESS-R+T+Y,8X,5HANGLE)
  101 FØRMAT(6F14.2)
  102 FØRMAT(30X,10HPRESSURE +,1F6.0)
  120 FØRMAT(4F9.3)
      END
```

CØMPUTER PRØGRAM III STRESS DUE TØ BIAXIAL LØADING, TRANSFØRMATIØN ØF CØØRDINATES AND DIAGONALIZATIØN TØ QUADRATIC FØRM

```
      DIMENSIØN Z(25),Y(6),TH1(25),PHI(25),R12(25),P1(4),
     1STR1(4,5),STØ1(4,5),STY1(4,5),R(20,20),SRY1(4,5),
     2S(20,20)
      READ 110,((SRY1(I,J),STR1(I,J),STØ1(I,J),STY1(I,J),
     3J=1,5)I=1,4)
      PI=3.1415927
      B=1.78
      P1(1)=PI/3.
      P1(2)=PI/6.
      P1(3)=PI/9.
      P1(4)=PI/12.
      D1=.5
      XM=.18
      XN=2.*XM
      Y(1)=-D1
      PHI(1)=0.
      R11=0.
      N=0
      NØ=0
      M=1
      PØ=2000.
      E1=-1000.
      E2=-500.
C     PØ, E1, AND E2 ARE VARIABLE AND WILL CHANGE THRØUGHØUT
      PRINT 116,PØ,E1,E2
      E12=(E1+E2)/2.
      E21=(E1-E2)/2.
      DØ 64 K=1,4
      R11=R11+d1
```

```
      M=M+6
      NØ=NØ+1
      DØ 64 I=2,6
      L1=I-1
      Y(I)=Y(I-1)+D1
      TH1(1)=-P1(K)
      DØ 64 J=2,M
      L2=J-1
      N=N+1
      YH1(J)=TH1(J-1)+P1(K)
      Z(J)=R11*SINF(YH1(J))
      X1=R11*CØSF(TH1(J))
      X2=Y(I)*Y(I)
      R12(J)=SQRTF(X1*X1+X2)
      IF(X1)62,61,62
61    PHI(J)=PI/2.
      GØ TØ 65
62    PHI(J)=ATANF(Y(I)/X1)
      IF(PHI(J))63,6-,65
63    PHI(J)=PHI(J)+PI
65    CØNTINUE
      ES2=SINF(2.*PHI(J))
      EC2=CØSF(2.*PHI(J))
      S4=(-XM)*(E21*EC2)
      S3=E12-E21*EC2
      S2=E12+E21*EC2
      S1=E21*ES2
      T1=SINF(TH1(J))
      T2=CØSF(TH1(J))
      T3=SINF(PHI(J))
      T4=CØSF(PHI(J))
      T5=T1*T1
      T6=T2*T2
      T7=T3*T3
      T8=T4*T4
      STR2=T6*(T8*S2+T7*S3-2.*(T3*T4)*S1)
      STØ2=T5*(T8*S2+T7*S3-2.*(T3*T4)*S1)
      STY2=T7*S2+T8*S3+2.*(T3*(T4*S1))
      SRØ2=(T2*T1)*(S4-T8*S2-T7*S3+2.*(T3*(T4*S1)))
      SRY2=T4*(T3*(S2-S3)*T4+S1*(T8-T7))
      SØY2=T1*((T3*T4)*(S3-S2)+(T7-T8)*S1)
      STR2=STR2+STR1(K,L1)
      STØ2=STØ2+STØ1(K,L1)
      STY2=STY2+STY1(K,L1)
      SRØ2=SRØ2
      SRY2=SRY2+SRY1(K,L1)
      SØY2=SØY2
66    R(1,1)=STR2
      R(1,2)=SRØ2
      R(1,3)=SRY2
      R(2,1)=SRØ2
      R(2,2)=STØ2
```

```
      R(2,3)=SØY2
      R(3,1)=SRY2
      R(3,2)=SØY2
      R(3,3)=STY2
      CALL JACØBI (R,S,3,1.0E-4)
      PRINT 117
      PRINT 118, (R(LL,LL),LL=1,3)
      PRINT 119
      PRINT 120, ((S(LL,KK),KK=1,3),LL=1,3)
   64 PRINT 115, N,NØ,L1,L2,STR2,STØ2,STY2,SRØ2,SRY2,SØY2
      CALL EXIT
  117 FØRMAT(30X,25HPRINCIPAL STRESSES FØLLØW)
  118 FØRMAT(3F28.1)
  119 FØRMAT(28X,29HCHARACTERISTIC VECTØRS FØLLØW)
  120 FØRMAT(3F28.1)
  115 FØRMAT(I4,2X,2HS(,I1,1H,,I1,1H,,I2,1H),6F9.3)
  116 FØRMAT(10X,10HPRESSURE =,F6.0,5X,10HSTRESS-X =,F7.0,10
     4HSTRESS-Y =,F7.0)
  110 FØRMAT(4F9.3)
      END
```

VITA

The author, William Joseph Kabeiseman, was born April 21, 1933 in Yankton, South Dakota and is the son of Leo and Katherine Kabeiseman. He received his elementary education at the Sacred Heart Catholic School in Yankton and graduated from Yankton High School in May, 1951 after attending the first two years at Trinity High School in Sioux City, Iowa. He attended St. Thomas College in St. Paul, Minnesota from September, 1951 to June, 1954 and received the Bachelor of Arts degree in Physics in June, 1956 and the Master of Arts degree in Physics in August, 1958 from the University of South Dakota at Vermillion. He served as an instructor in Physics from September, 1956 to August, 1961 at the University of South Dakota.

In September, 1961 he moved to Rolla, Missouri where he enrolled as a Ph.D. candidate, at the same time accepting the title of Instructor of Mathematics. During the summer of 1963 he worked as an engineer for Nortronics in Anaheim, California and during the summer of 1964 he worked as a scientist for Sinclair Research in Tulsa, Oklahoma.

He is married to the former Rose Burgi and is the father of two children: Michael and Kathleen.